

**Density functional theory calculations and electrochemistry  
of octahedral  $M(L,L'\text{-}BID)_3$  complexes, L and L' = N and/or O  
and M = selected transition metals.**

Hendrik Ferreira

Submitted in fulfilment of the requirements for the degree

**Philosophiae Doctor**

in the

**Faculty of Natural and Agricultural Sciences**

**Department of Chemistry**

at the

**University of the Free State**

Promoter: Prof. Jeanet Conradie

Co-promoter: Dr. Marrigje Marianne Conradie

January 2019



## Declaration

---

It is hereby declared that the thesis submitted for the degree Philosophiae Doctor (Chemistry) at the University of the Free State is the independent work of the undersigned and has not previously been submitted to/at another university or faculty. Copyright of this thesis is hereby ceded in favour of the University of the Free State.

---

Hendrik Ferreira

---

Date

Department of Chemistry

Faculty of Natural and Agricultural Sciences

University of the Free State

South Africa





## Abstract

---

In this thesis “Density functional theory calculations and electrochemistry of octahedral  $M(L,L'-\text{BID})_3$  complexes, L and L' = N and/or O and M = selected transition metals” the focus is on density functional theory (DFT) calculations and electrochemistry of octahedral  $M(N,N,N)_2^{2+}$  and  $M(N,N)_3^{2+}$  complexes with M = Co or Fe and N,N,N = the tridentate terpyridine(tpy) ligand (with three N donor atoms) and N,N = bipyridine (bpy), phenanthroline (phen) or substituted bpy and phen ligands (with two N donor atoms). Many linear correlations were obtained between the experimentally measured redox potentials and DFT calculated energies of the different series of complexes. DFT may thus assist to decrease research time and cost in the lab through the use of these correlations to design related complexes with the desired redox potential as needed for mediators and dyes in dye sensitized solar cells (DSSC). The results obtained on the ligands and complexes investigated, are presented in four main publications, namely on (i) phenanthroline and substituted phen ligands, (ii)  $\text{Co}(\text{phen})_3^{2+}$  where phen = phenanthroline and substituted phen ligands, (iii) polypyridine ligands (tpy, bpy or substituted bpy ligands) and Co(II)-polypyridine complexes and (iv) a series of Fe(II) complexes containing tpy, bpy, phen and substituted bpy and phen ligands.

The correlations made between the experimentally determined reduction potentials of the uncoordinated, substituted phenanthrolines as well as the density functional theory calculated energies and properties of the ligands (both the neutral and reduced phenanthrolines) are presented first. The electrochemical study shows irreversible reduction of the uncoordinated free phenanthrolines. Chloride substituents, which are electron withdrawing, on the 4 and 7 positions of the phenanthrolines, increase the measured reduction potential by 0.3 V and the methyl substituents, which are electron donating, lead to the decrease, or lowering, of the reducing potential when compared with the unsubstituted 1,10-phenanthroline. Linear correlations are obtained between the DFT calculated properties and energies when compared with the experimental reduction potentials of phenanthrolines containing non-aromatic substituents. Non-aromatic substituents affect the electron density across the phenanthroline ring system solely via  $\sigma$ -induction effects. Phenyl substituents on the phenanthroline ring system donate electron density through both  $\sigma$ -induction and  $\pi$ -resonance effects, which leads to a deviation from the trends observed. These dual donation effects, allow the phenanthroline system to more easily accept electrons at less negative, or higher, potentials than expected. Comparison between the reduction potential of metal coordinated phenanthroline complexes (M = Fe, Ru and Cu) and the reduction potential of unbound ligands, provided linear correlations.

Electrochemical studies of a series of phenanthrolines coordinated to a Co(II) metal center are presented and illustrate 3 redox events in each of the investigated series (containing both substituted and unsubstituted phenanthrolines). An electrochemically and chemically reversible Co(III/II) couple is observed as well as a Co(II/I) couple, also reversible in both respects. A ligand based reduction is also observed at potentials lower than the potentials observed for both of the metal centered redox events. The electron withdrawing or donating capability of the substituents on the coordinated phenanthroline ligands influences the density of electrons on the Co metallic center similarly to those results obtained in the electrochemical and DFT study of the uncoordinated, free ligands, leading to linear correlations between the different redox couples and calculated theoretical energies.

The next material presented is an investigation into the properties of a series of bipyridines that are coordinated to the Co(II) metal center. The density functional theory (DFT) calculations focussed on the structure of the Co(II) complexes, as well as the oxidized Co(III) and reduced Co(I) complexes, also identifying the locus of the experimentally observed redox processes. Low spin DFT calculations of the Co(II)-bpy complexes showed shorter equatorial and longer axial Co-N bonds which is classified as elongation Jahn-Teller distortion. The Co(II)-tpy complex is shown to possess four longer distal Co-N bonds and two shorter axial Co-N bonds which is classified as compression Jahn-Teller distortion. Similar trends were observed in the calculations performed of the high spin Co(II) complexes. The electrochemical investigation showed three redox couples, that are both electrochemically and chemically reversible, which are the Co(III/II) couple, Co(II/I) couple as well as the ligand based reduction (at lower potentials than the potentials of the metal centered redox processes), similar to the results obtained for the series of Co-phen complexes. Comparison of the free, uncoordinated ligand's reduction potential with the results from this study, shows a reduction potential 0.5 V more negative than the reduction potential observed for the reduction of the coordinated ligand in the associated Co(I) complex.

Lastly a comparative investigation of the oxidation of an Fe(II) metal center coordinated series of phenanthrolines, bipyridines and terpyridine are presented. The electrochemical results showed the Fe(II/III) oxidation range varies from 0.363 V up to 0.894 V with tris(3,6-dimethoxybipyridyl)Fe<sup>2+</sup> exhibiting the lowest and tris(5-nitrophenanthroline)Fe<sup>2+</sup> the highest oxidation potential. Also noted from this study is the role of the substituent's position on the coordinating ligand on the electrochemical properties of the Fe(II) complexes, i.e. the oxidation potential is 0.669 V for the complex containing a methyl substituent on the 5-phen position (on the inner phenanthroline ring) and 0.613 V for the complex containing a methyl substituent on the 4-phen position (on the outer

phenanthroline ring). Density functional theory calculations, performed on the oxidized, reduced and neutral complexes provided optimized electronic energies for each state allowing for correlations between the calculated energies and the experimentally determined results. Considerations between closely related complexes, which allows for linear correlations, showed good correlations for the two considered series (bipyridine and phenanthroline), with  $R^2 > 0.9$ . Renderings of the molecular orbitals (HOMO and LUMO) illustrate that the top three HOMOs are metal-centric, with the directional transfer of the charge during UV/vis excitation to the six lowest LUMOs, which are ligand-centric.

Key words: dye-sensitized solar cell (DSSC), polypyridyl, density functional theory (DFT), octahedral, electrochemistry, molecular orbitals, linear correlations, redox, ligand, substituent.



## Table of Contents

---

Abstract.....	v
Acknowledgements.....	xi
Chapter 1 : Introduction.....	1
Chapter 2 : Electrochemical and DFT study of the reduction of substituted phenanthrolines.....	3
Chapter 3 : Electrochemical properties of a series of Co(II) complexes, containing substituted phenanthrolines, Data in Brief.....	13
Chapter 4 : Electrochemical and electronic properties of a series of substituted polypyridine ligands and their Co(II) complexes, Data in Brief.....	41
Chapter 5 : Electronic properties of Fe charge transfer complexes - A combined experimental and theoretical approach.....	63
Chapter 6 : Conclusions.....	73
Appendix A : Author Copyright Permissions.....	75



## Acknowledgements

---

- Thanks must go to our Lord God as well as His Son Jesus Christ, for always being with me as well as continuing to provide me with strength, stamina and guidance.
- A very large thank you to my promoters, Prof. Jeanet Conradie and Dr. Marianne Conradie, for their patience, motivation, guidance and wisdom during the course of my studies.
- My late father, Willem Hendrik Ferreira, who was always steadfast, brave, a provider and protector of his family.
- My mother, Elizabeth Ann Ferreira, for her unwavering and unconditional love and faith.
- My sister, Alida Ferreira, for her love and support during my studies.
- The entire Physical Chemistry research group and all my friends for all of the support, conversations, laughs and day to day distractions that help to remind us that we deserve a break every now and then.
- The Chemistry department of the University of the Free State (UFS) for the use of their facilities.
- The University of the Free State and the National Research Foundation (NRF) for the financial support.





# Chapter 1

## Introduction

---

Renewable energy such as wind and solar energy, has gained attraction within mainstream news the last few years due to potential future supply concerns of exhaustible fossil fuels. Solar cells, converting sunlight energy into electric current, have the shortcoming that it cannot store energy. In 1991 the Grätzel cell, a solar cell with a regenerative battery, was patented, known as the dye-sensitized solar cells (DSSC).<sup>1</sup> To generate the current, the Grätzel cell uses a porous layer of titanium dioxide nanoparticles, covered with a molecular dye that absorbs sunlight, accompanied by an iodide/triiodide redox couple which functions as the electron-transfer mediator.<sup>2</sup> Platinum group metals complexed with polypyridyl ligands are mostly used within solar cells,<sup>3</sup> however due to their scarcity and high cost, alternative complexing metals are being investigated for use as potential mediators within solar cells, with the focus of the present research placed on the transition metals iron and cobalt. To determine if polypyridyl complexes of iron and cobalt qualify as possible applications as potential mediators and dyes in DSSC, their experimental redox and UV/Vis-absorbance properties are important. Computational chemistry density functional theory (DFT) calculations were used to compliment experimental findings.

Firstly the characteristics and properties, mainly focussed on the electrochemical and computed properties, of a series of substituted free phenanthroline(Chapter 1),<sup>4</sup> bipyridine and terpyridine<sup>5,6</sup> ligands were investigated. These ligands were then complexed to cobalt and iron.

Research on Co-polypyridine complexes as potential mediators in electrochemical solar cells has previously been published,<sup>7</sup> however the published material, especially with respect to bis-terpyridyl-cobalt, focussed primarily on the Co(III/II) redox couple. A detailed investigation into the redox properties of both the Co(III/II) and Co(II/I) redox couples of a series of substituted Co-phenanthroline complexes led to various linear relationships between the experimental values and DFT calculated energies, for use in the determination and design of new, customized substituted phenanthroline-Co(II) complexes with selected redox properties, as desired for application as a redox mediator for use within dye-sensitized solar cells (Chapter 2).<sup>8,9</sup>

The study of the properties of substituted bipyridine and terpyridine ligands and their Co-polypyridyl compounds showed that the polypyridine ligand is reduced more than 0.5 V more negative than the reduction of the coordinated ligand in these polypyridine-Co(I) complexes. DFT calculations were

used to confirm the locus of the different redox processes observed, namely metal based Co(II/III) oxidation, metal based Co(II/I) reduction and ligand based Co(I) reduction. DFT calculations further showed that, due to the Jahn-Teller distortion illustrated in the calculated geometries, the substituted  $[\text{Co}(\text{2,2'}\text{-bipyridine})_3]^{2+}$  complexes, have four shorter equatorial and two longer axial Co-N bonds (elongation Jahn-Teller), while  $[\text{Co}(\text{terpyridine})_2]^{2+}$ , in contrast, has four longer distal Co-N bonds and two shorter central (axial) Co-N bonds (compression Jahn-Teller). This is due to the distal Co-N bonds being more flexible than the Co-N axial bonds in the rigid structure of the tridentate terpyridine ligand. (Chapter 3).<sup>5,6</sup>

A detailed investigation correlation between experimentally measured redox and spectral properties of synthesized Fe-polypyridine complexes and quantum computational data showed that DFT calculations could be used to assist in the design and tailoring of complexes within solar cell research (Chapter 4).<sup>10</sup>

1. B.O'Regan; M. Grätzel. *Nature* 1991, 335, 737.
2. M. Grätzel, Solar energy conversion by dye-sensitized photovoltaic cells, *Inorganic Chemistry*, 44 (2005) 6841–6851.
3. N. Robertson, Optimizing dyes for dye-sensitized solar cells. *Angewandte Chemie International*, 45 (2006) 2338–2345.
4. H. Ferreira, M.M. Conradie, K.G. von Eschwege, J. Conradie, Electrochemical and DFT study of the reduction of substituted phenanthrolines, *Polyhedron*, 122 (2017) 147-154. DOI: 10.1016/j.poly.2016.11.018 <http://www.journals.elsevier.com/polyhedron/>
5. H. Ferreira, M.M. Conradie, J. Conradie, Electrochemical and electronic properties of a series of substituted polypyridine ligands and their Co(II) complexes, *Inorg. Chim. Acta* 486 (2019) 26-35. DOI 10.1016/j.ica.2018.10.020
6. H. Ferreira, M.M. Conradie, J. Conradie, Cyclic voltammetry data of polypyridine ligands and Co(II)-polypyridine complexes, *Data in Brief*, 22 (2019) 436–445 DOI: 10.1016/j.dib.2018.12.043 <https://www.journals.elsevier.com/data-in-brief>
7. a) Z. Yu, N. Vlachopoulos, M. Gorlov, L. Kloo, Liquid electrolytes for dye-sensitized solar cells, *J. Chem. Soc., Dalton Trans.* 40 (2011) 10289-10303, b) A. K.C. Mengel, W. Cho, A. Breivogel, K. Char, Y.S. Kang, K. Heinze, A bis(tridentate)cobalt polypyridine complex as mediator in dye-sensitized solar cells, *Eur. J. Inorg. Chem.* (2015) 3299-3306, c) F. Gajardo, B. Loeb, Spectroscopic and electrochemical properties of a series of substituted polypyridine Co(II)/Co(III) couples and their potentiality as mediators for solar cells, *J. Chil. Chem. Soc.* 56 (2) (2011) 697-701,
8. H. Ferreira, M.M. Conradie, J. Conradie, Electrochemical properties of a series of Co(II) complexes, containing substituted phenanthrolines, *Electrochimica Acta*. 292 (2018) 489-501, DOI 10.1016/j.electacta.2018.09.151. <http://dx.doi.org/10.1016/j.electacta.2018.09.151>.
9. H. Ferreira, M.M. Conradie, J. Conradie, Electrochemical data of Co(II) complexes containing phenanthroline functionalized ligands, *Data in Brief*, 21 (2018) 866–877 DOI 10.1016/j.dib.2018.10.046 <https://www.journals.elsevier.com/data-in-brief>
10. H. Ferreira, K.G. von Eschwege, J. Conradie, Electronic Properties of Fe Charge Transfer Complexes - a Combined Experimental and Theoretical Approach. *Electrochimica Acta* 216 (2016) 339-346. DOI 10.1016/j.electacta.2016.09.034 <http://www.journals.elsevier.com/electrochimica-acta/>

# Chapter 2

---

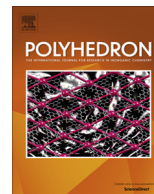
## **Electrochemical and DFT study of the reduction of substituted phenanthrolines**

Hendrik Ferreira, Murrigje M. Conradie, Karel G. von Eschwege, Jeanet Conradie

Published by Polyhedron

DOI: 10.1016/j.poly.2016.11.018





# Electrochemical and DFT study of the reduction of substituted phenanthrolines



Hendrik Ferreira, Marrigje M. Conradie, Karel G. von Eschwege, Jeanet Conradie \*

Department of Chemistry, University of the Free State, PO Box 339, Bloemfontein 9300, South Africa

## ARTICLE INFO

### Article history:

Received 30 September 2016

Accepted 10 November 2016

Available online 19 November 2016

### Keywords:

Phenanthroline  
Reduction potential  
Cyclic voltammetry  
DFT  
Exp-DFT relationships

## ABSTRACT

The irreversible electrochemical reduction data of a series of free uncoordinated differently substituted phenanthrolines is presented. Electron withdrawing chloride substituents in the 4,7 ring positions increase the reduction potential by 0.3 V, while electron donating methyl substituents lead to a lowering of reduction potential relative to unsubstituted 1,10-phenanthroline. Linear relationships are obtained between the reduction potential of free uncoordinated differently substituted phenanthrolines and density functional theory (DFT) calculated LUMO (lowest unoccupied molecular orbital) energies, electron affinities, global electrophilicity indexes and Mulliken electronegativities. The reduction potential of 4,7-diphenyl-1,10-phenanthroline deviates slightly from the linear trend, since the phenyl groups donate electron density to the phenanthroline ring system through both  $\pi$ -resonance and  $\sigma$ -inductive effects. This enables the phenanthroline ring system to more readily accept an electron at a higher, less negative potential than is otherwise the case. On the contrary, the non-aromatic substituents (e.g. Me, NH<sub>2</sub> and Cl) withdraw/donate electron density from/to the phenanthroline ring system through  $\sigma$ -inductive effects only. Linear relationships are also obtained between the reduction potential of the series of phenanthroline free ligands and the formal reduction potential of corresponding metal-phenanthroline complexes.

© 2016 Elsevier Ltd. All rights reserved.

## 1. Introduction

Phenanthroline (phen) is a heterocyclic organic compound that is often used as a ligand in coordination chemistry, forming complexes with most metal ions. A variety of coordination spheres are reported for these complexes, i.e. square-antiprismatic [Ca<sup>II</sup>(phen)<sub>4</sub>]<sup>2+</sup> [1], octahedral [Fe<sup>II</sup>(phen)<sub>3</sub>]<sup>2+</sup> [2] and [Ni<sup>II</sup>(phen)<sub>3</sub>]<sup>2+</sup> [3], pseudotetrahedral [Cu<sup>I</sup>(phen)<sub>2</sub>]<sup>+</sup>, pseudotrigonal [Cu<sup>I</sup>Cl(phen)] [4], as well as the 10-coordinated [Ba<sup>II</sup>(phen)<sub>4</sub>]<sup>2+</sup> complex [5]. These metal-phenanthroline complexes have applications in many fields such as analytical chemistry [6], catalysis [7] and biochemistry [8]. Complexes with different substituents on the 1,10-phenanthroline ligands exhibit altered physical properties. As a result variations in electrochemical properties (substituted 1,10-phenanthroline complexes of iron [9]), UV-Vis absorption maxima and luminescence (substituted 1,10-phenanthroline complexes of copper [10] and ruthenium [11]), rates of exchange. Substitution and oxidation kinetics (substituted 1,10-phenanthroline complexes of rhodium [12], iridium and iron [13]), etc., were

observed. Bis(2,9-dimethyl-1,10-phenanthroline)copper(I/II) [14] and tris(1,10-phenanthroline)cobalt(II/III) [15] showed promising results as redox mediators in dye-sensitized solar cells (DSSC's).

Finding a way to predict the reactivity of metal complexes containing substituted 1,10-phenanthroline ligands even before synthesis, should therefore be of great value. In continuation of our interest in finding cost-effective theoretical ways to predict experimental reduction potentials by relating experimental reduction potentials to theoretically calculated energies [16–26], we now present a combined reduction potential and density functional study of a series of substituted uncoordinated 1,10-phenanthrolines (see Fig. 1). We also compare the experimental order of reduction potentials of the series of 1,10-phenanthroline free ligands with altered substituents with the order of reduction potentials of its corresponding metal-phenanthroline complexes.

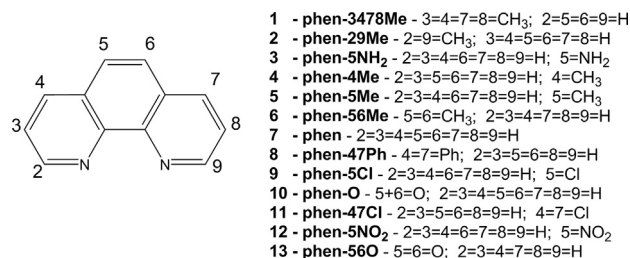
## 2. Experimental

### 2.1. General

The series of phenanthrolines were obtained from Sigma Aldrich and used without further purification.

\* Corresponding author. Tel.: 27 51 4012194; fax: 27 51 4017295.

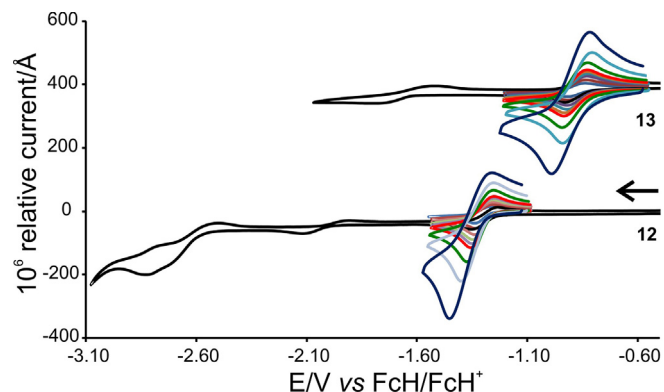
E-mail address: [conradj@ufs.ac.za](mailto:conradj@ufs.ac.za) (J. Conradie).



**Fig. 1.** Chemically altered 1,10-phenanthrolines employed in this study. Both ring and ligand numbers are indicated.

## 2.2. Theoretical approach

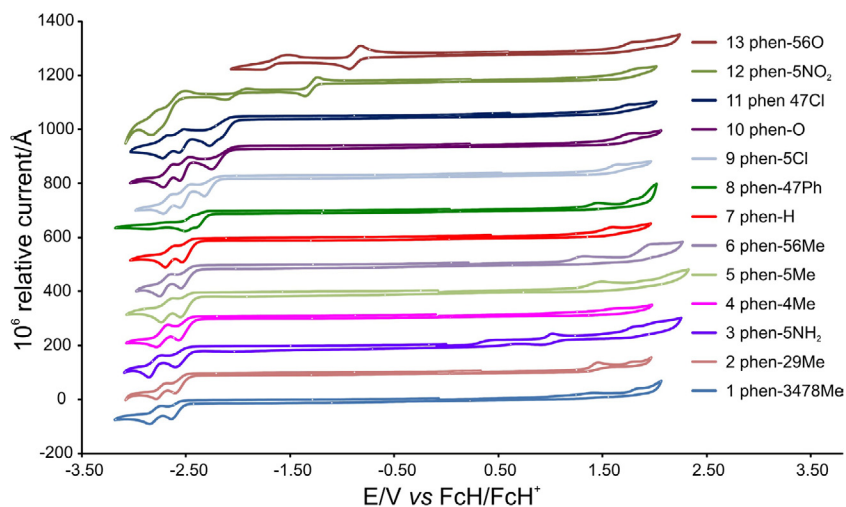
Density functional theory (DFT) calculations were performed, using the GGA functional BP86 [27,28] with the TZP (Triple  $\zeta$  polarized) basis set, as implemented in the Amsterdam Density Functional (ADF2014) [29]. Geometry relaxed (adiabatic) energies of the compounds ( $N$  electron system), with the corresponding  $N - 1$  (reduced) and  $N + 1$  (oxidized) electron systems, were calculated to determine the following values of the compounds: electron affinity (EA), ionization potential (IP), global electrophilicity



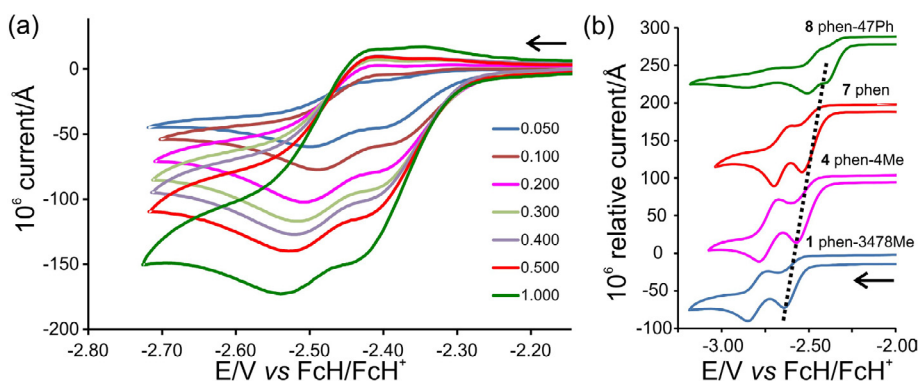
**Fig. 4.** Cyclic voltammograms of ca 0.002 mol dm<sup>-3</sup> or saturated solutions of phenanthrolines **12** (bottom) and **13** (top), in CH<sub>3</sub>CN/0.1 mol dm<sup>-3</sup> [n(Bu<sub>4</sub>)N][PF<sub>6</sub>], on a glassy carbon-working electrode, at scan rates of 0.05 (smallest peak current), 0.10, 0.20, 0.30, 0.40, 0.50, 1.0, 2.0 and 5.0 (largest peak current) V s<sup>-1</sup>, indicating the additional first reversible reduction process, which is located at NO<sub>2</sub> and the two oxygens respectively. The wider scan in black is obtained at 0.10 V s<sup>-1</sup>. Scans were initiated in the negative direction, as indicated by the arrow.

index ( $\omega$ ) and Mulliken electronegativity ( $\chi$ ) by application of the following formulas [30–33]:

$$EA(\text{compound}) = E(\text{reduced compound}) - E(\text{compound})$$



**Fig. 2.** Cyclic voltammograms of ca 0.002 mol dm<sup>-3</sup> or saturated solutions of phenanthrolines **1–13**, in CH<sub>3</sub>CN/0.1 mol dm<sup>-3</sup> [n(Bu<sub>4</sub>)N][PF<sub>6</sub>], on a glassy carbon-working electrode, at a scan rate of 0.100 V s<sup>-1</sup>, indicating the shift observed in the reduction potential of these phenanthrolines, depending on the type and amount of substituents. Scans were initiated in the positive direction from ca -0.2 V.



**Fig. 3.** Cyclic voltammograms of the reduction peak of ca 0.002 mol dm<sup>-3</sup> or saturated solutions of (a) phenanthroline **8** substituted with aromatic phenyl groups at scan rates of 0.05–1.0 V s<sup>-1</sup>, indicating the re-oxidation peak which increases as the scan rate increases, and (b) **1**, **4**, **7** and **8** at 0.100 V s<sup>-1</sup>. CVs obtained in CH<sub>3</sub>CN/0.1 mol dm<sup>-3</sup> [n(Bu<sub>4</sub>)N][PF<sub>6</sub>], on a glassy carbon-working electrode. Scans were initiated in the negative direction as indicated by the arrows.

$$IP(\text{compound}) = E(\text{oxidized compound}) - E(\text{compound})$$

$$\omega = (\mu^2/2\eta)$$

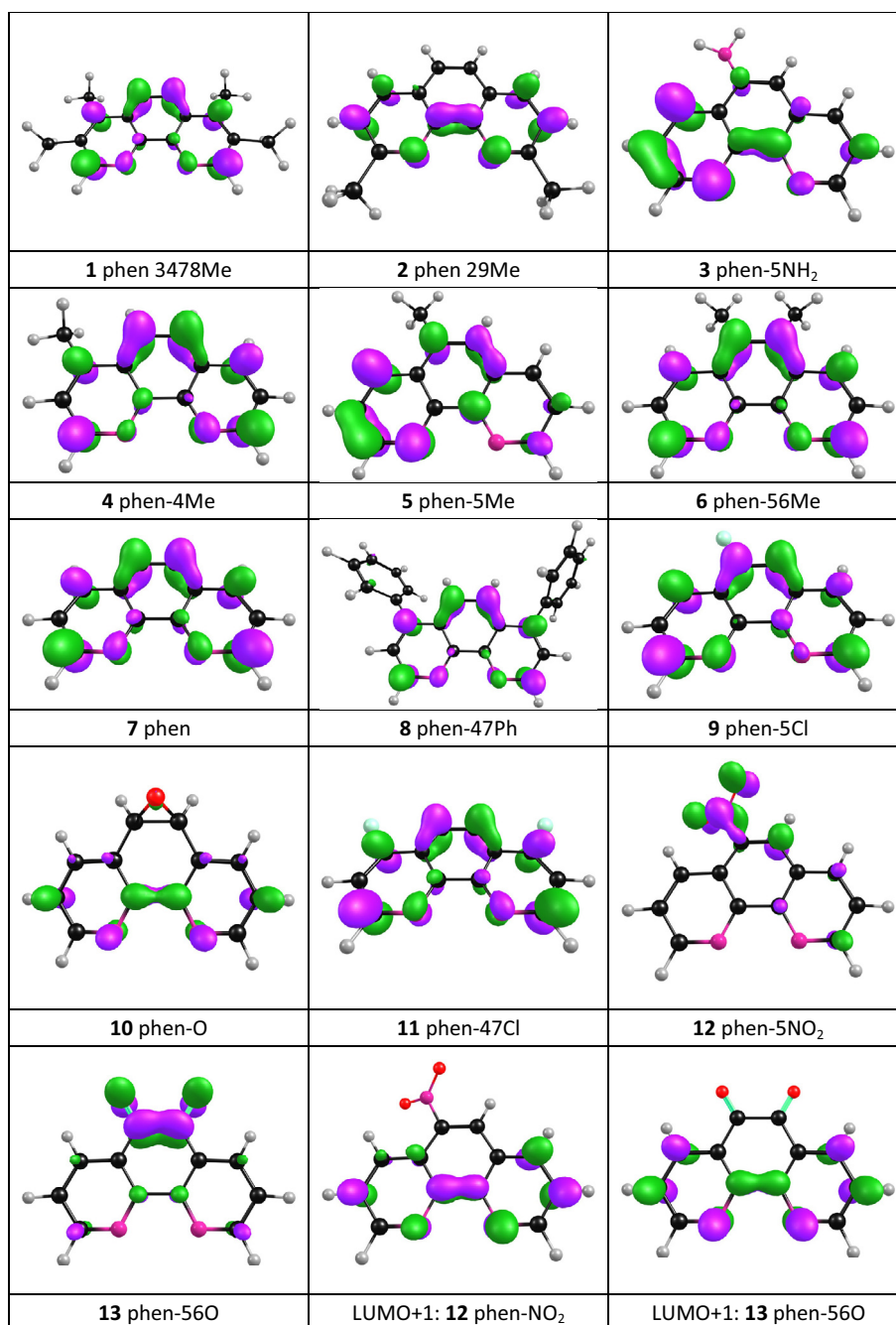
$$\text{where } \mu = -(IP + EA)/2 \text{ and } \eta = IP - EA$$

$$\chi = (IP + EA)/2$$

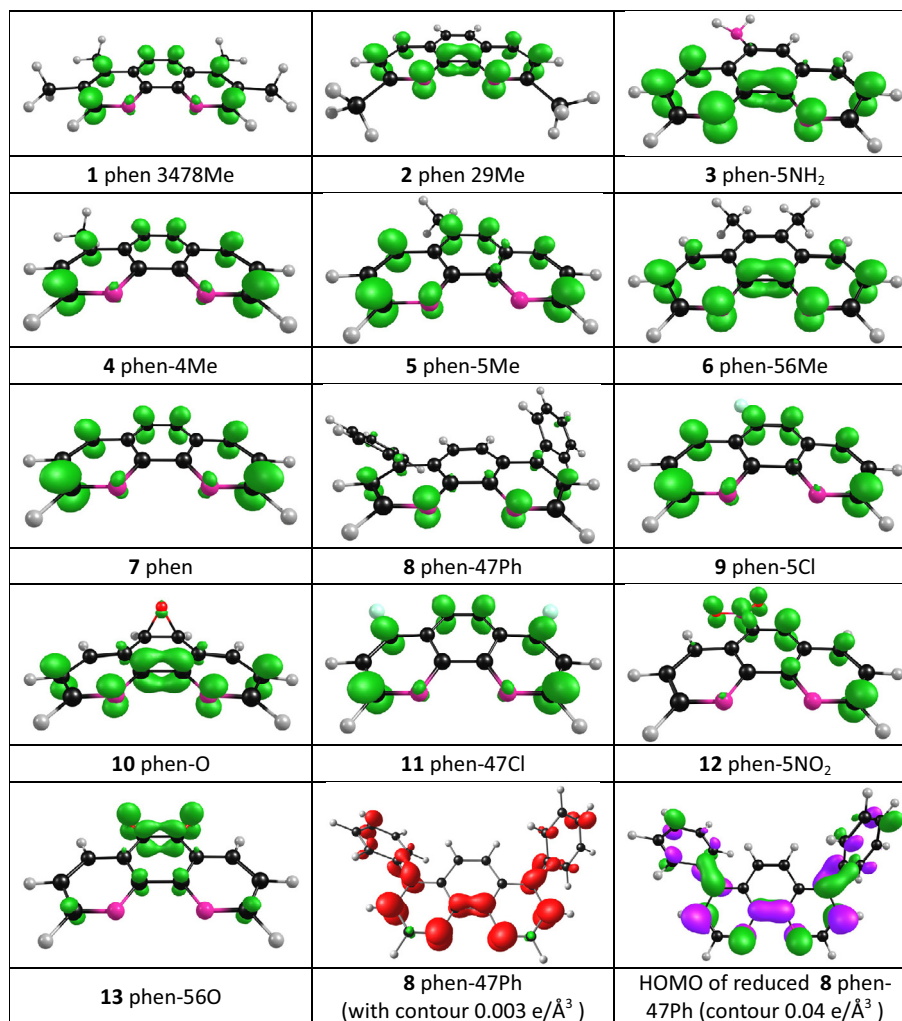
### 2.3. Electrochemistry

Electrochemical studies by means of cyclic voltammetry were performed on 0.002 mol dm<sup>-3</sup> or saturated solutions of a series of thirteen free uncoordinated differently substituted phenanthrolines, in dry acetonitrile, containing 0.1 mol dm<sup>-3</sup> tetra-*n*-butylam-

monium hexafluorophosphate ([<sup>n</sup>(Bu<sub>4</sub>)N][PF<sub>6</sub>]) as supporting electrolyte, under a blanket of purified argon at 25 °C, utilizing a BAS 100B/W electrochemical analyzer. A three-electrode cell, with a glassy carbon (surface area 7.07 × 10<sup>-6</sup> m<sup>2</sup>) working electrode, Pt auxiliary electrode and a Ag/Ag<sup>+</sup> (10 mmol dm<sup>-3</sup> AgNO<sub>3</sub> in CH<sub>3</sub>CN) reference electrode [34], mounted on a Luggin capillary, was used [35]. Scan rates were 0.050–5.000 V s<sup>-1</sup>. Successive experiments under the same experimental conditions showed that all oxidation and formal reduction potentials were reproducible within 0.010 V. All cited potentials were referenced against the FcH/FcH<sup>+</sup> couple, as suggested by IUPAC [36]. Ferrocene (Fc) exhibited peak separation, Δ*E*<sub>p</sub> = *E*<sub>pa</sub> – *E*<sub>pc</sub> = 0.070 V and *i*<sub>pc</sub>/*i*<sub>pa</sub> = 1.00 under our experimental conditions, where *E*<sub>pa</sub> (*E*<sub>pc</sub>) = anodic (cathodic) peak potential and *i*<sub>pa</sub> (*i*<sub>pc</sub>) = anodic (cathodic) peak current.



**Fig. 5.** BP86/TZP DFT calculated LUMO plots of phenanthrolines 1–13, as well as the LUMO + 1 plots of phenanthrolines 12 and 13 (bottom middle and right). A contour of 0.07 e/Å<sup>3</sup> was used for the orbital plots.



**Fig. 6.** BP86/TZP DFT calculated spin density plots of the reduced phenanthrolines **1–13** and HOMO of reduced **8**. A contour of  $0.008 \text{ e}/\text{\AA}^3$  was used for the spin plots, except for the spin plot (contour  $0.003 \text{ e}/\text{\AA}^3$ ) and HOMO (contour  $0.04 \text{ e}/\text{\AA}^3$ ) of reduced **8** (bottom middle and right).

### 3. Results and discussion

#### 3.1. Cyclic voltammetry

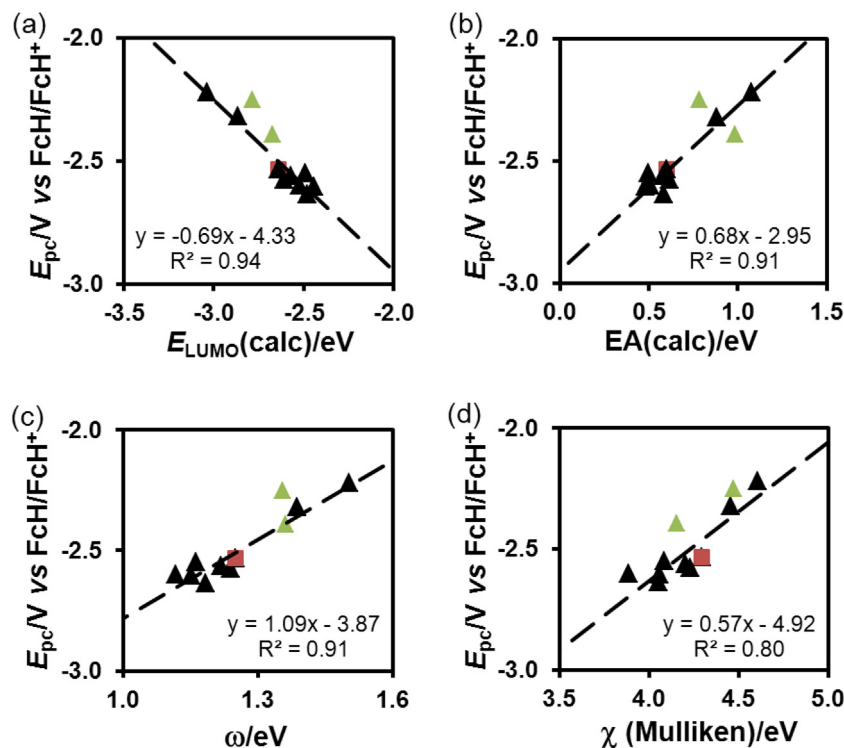
Fig. 2 shows the  $0.100 \text{ V s}^{-1}$  cyclic voltammetry scans for the series of differently substituted uncoordinated 1,10-phenanthrolines **1–13** (see [Electronic Supporting Information](#) for the cyclic voltammetry scans and data of scan rates  $0.05\text{--}5.0 \text{ V s}^{-1}$ ) with selected data summarized in [Table 1](#). Phenanthrolines **1–11** show two or more reduction processes at a potential below  $-2 \text{ V}$  vs  $\text{FcH}/\text{FcH}^+$ . The first, less negative, reduction process observed for phenanthrolines **1–11** is irreversible at all scan rates up to  $5 \text{ V s}^{-1}$ , except for phenanthroline **8**, namely 4,7-diphenyl-1,10-phenanthroline. The cyclic voltammogram of compound **8** in [Fig. 2](#) shows a re-oxidation peak, which increases as the scan rate increases, see [Fig. 3a](#). This implies that the lifetime of some of the short-lived reduced species of **8** is long enough to be re-oxidized at higher scan rates. The electron density on the reduced species of **8** is stabilized through  $\pi$ -conjugation between the phenyl rings and the aromatic phenanthroline rings (as described below in more detail), making a second reduction easier. The first two reduction processes of **8** at  $E^{0'} = -2.36$  and  $-2.46 \text{ V}$  with  $\Delta E = 0.07$  and  $0.08 \text{ eV}$  respectively, are thus closely overlapping.

Fig. 4 shows the  $0.100 \text{ V s}^{-1}$  scans of phenanthrolines **12** and **13**, namely 5-nitro-1,10-phenanthroline and 1,10-phenanthroline-5,6-dione. These phenanthrolines show an additional reversible reduc-

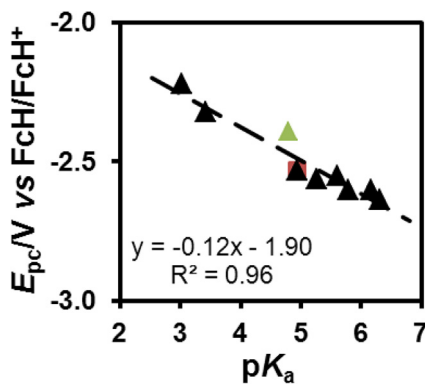
tion process, with  $E^{0'} = -1.295 \text{ V}$  and  $-0.876 \text{ V}$  respectively, which are more than  $1 \text{ V}$  more positive than the first reduction waves seen in phenanthrolines **1–11**. The DFT computational study presented in the next section here below will confirm that the first reversible reductions observed for **12** and **13** are located on  $\text{NO}_2$  and the two oxygens respectively, instead of being distributed on the aromatic rings of the phenanthroline, as is the case for **1–11**. Earlier studies showed that a series of *para*-nitrobenzenes,  $\text{R-C}_6\text{H}_4\text{-NO}_2$ , exhibit a reversible redox couple in the potential range  $-1.0 \text{ V}$  to  $-1.7 \text{ V}$  vs ferrocene [16]. The reduction potential  $E^{0'} = -1.295 \text{ V}$  of **12**, namely 5-nitro-1,10-phenanthroline, falls well within this range.

From [Fig. 2](#) it is clear that the different substituents have an influence on the ease of reduction of the corresponding phenanthroline. For example, the 3,4,7,8-tetramethyl-1,10-phenanthroline (**1**) is being reduced at  $-2.635 \text{ V}$  vs ferrocene, which is  $0.414 \text{ V}$  more negative than the 4,7-dichloro-1,10-phenanthroline (**11**), which reduces at  $-2.221 \text{ V}$ . This observed shift in the reduction potential of the phenanthrolines depends on the amount of substituents, the electron-donating/withdrawing properties of the substituents, the position, as well as the inductive effect of the substituent(s). Electron donating substituents on phenanthroline, like methyl and amine, decrease the reduction potential, while electron withdrawing substituents like chloride, increase the reduction potential relative to unsubstituted 1,10-phenanthroline (**7**). This is expected, since when electron density is drawn from





**Fig. 7.** Linear correlation graphs of experimental reduction potentials ( $E_{pc}$ ) vs corresponding calculated (a) LUMO energy ( $E_{LUMO}$ ), (b) electron affinity (EA), (c) global electrophilicity index ( $\omega$ ) and (d) Mulliken electronegativity ( $\chi$ ) of phenanthrolines 1–7, 9 and 11. The value of the unsubstituted 1,10-phenanthroline, 7, is indicated in brown. Phenanthrolines 8 and 10 (green) in some correlations deviate slightly from the observed trend. (Colour online.)



**Fig. 8.** Linear correlation graphs of experimental reduction potentials ( $E_{pc}$ ) vs  $pK_a$  of phenanthrolines 1–7, 9 and 11. The value of unsubstituted 7 is indicated in brown. Phenanthroline 8 (green) deviates slightly from the observed linear trend. (Color online.)

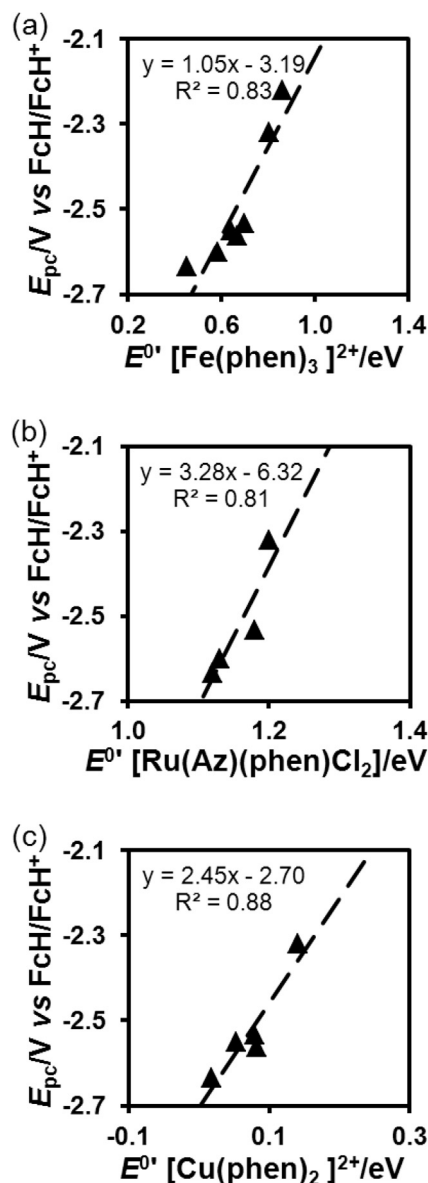
the phenanthroline aromatic ring system towards the substituents, an electron can more readily be added to the ring system during the reduction process, as is the case with the chloride substituted phenanthrolines 9 and 11. A methyl substituent on position 5 and/or 6, i.e. on the central ligand ring of 1,10-phenanthroline, shifts the reduction potential with less than 0.030 V relative to unsubstituted 1,10-phenanthroline (7), while a methyl substituent in position 4, i.e. on the outer ring of 1,10-phenanthroline has a slightly larger influence on the reduction potential. Methyl substituents in the 2,9 positions of 1,10-phenanthroline (phenanthroline 2) have a marked shift of 0.070 V relative to unsubstituted 1,10-phenanthroline (7), while the 3,4,7,8-tetramethyl substituents (in phenanthroline 1) shift the reduction potential 0.102 V more negative from that of unsubstituted 1,10-phenanthroline (7). This suggests that substituents on the pyridine rings

of the phenanthroline (positions 2, 3, 4, 7, 8, 9) have a larger influence on the reduction potential than substituents on the inner ring (positions 5 and 6) of phenanthroline. The same is true for the positive shift in reduction potential due to electron withdrawing chloride substituents on position 5 (phenanthroline 9, shift = ca 0.2 V) or positions 4,7 (phenanthroline 11, shift = ca 0.3 V), relative to unsubstituted 1,10-phenanthroline.

The 4,7-di-phenyl substituted 1,10-phenanthroline (8) is reduced at 0.100 V higher than that of unsubstituted 1,10-phenanthroline (7), while the reduction potentials of the 4-methyl (4) and 3,4,7,8-tetramethyl substituted 1,10-phenanthroline (1) are respectively 0.044 and 0.100 V lower than that of unsubstituted 1,10-phenanthroline (7), see Fig. 3(b). The combined e-donating strength of the four methyl groups on (1) thus lead to a much lower reduction potential for (1) than for (8) with only two e-donating phenyl groups. The higher reduction potential of (8) is further explained in terms of the increase in effective conjugation length through the compound, as described in the computational study here below.

### 3.2. Computational chemistry

Reduction of compounds viewed at molecular level involves addition of an electron into the lowest unoccupied molecular orbital (LUMO) of the neutral compound. The character of the reduction center of a compound can thus be identified by evaluating the nature of the LUMO. However, sometimes a reorganisation of the molecular orbitals occurs after reduction, leading to the reduction of a higher unoccupied orbital [37]. Therefore, when evaluating reduction centers of molecules it is good practice to inspect the characters of both the LUMO of the neutral compound and the HOMO of the reduced compound. If the molecule is diamagnetic, the spin density profile of the reduced compound shows the distribution of the added unpaired electron.



**Fig. 9.** Relationships between reduction potentials  $E_{pc}$  of the differently substituted phenanthroline series and corresponding experimental formal reduction potentials of (a)  $Fe^{II/III}$  in  $[FeL_3]^{2+}$ , (b)  $Ru^{II/III}$  in  $trans-[Ru(II)(Az)(L)Cl_2]$  (where Az:  $C_6H_5N=NC(COCH_3)=NC_6H_5$ ) and (c)  $Cu^{II/I}$  in  $[CuL_2]^{2+}$ . L = substituted 1,10-phenanthroline indicated as “phen” in the figure above. Data in Table 1.

DFT calculations were performed on both the neutral ( $q = 0$ ,  $S = 0$ ) and reduced ( $q = -1$ ,  $S = \frac{1}{2}$ ) phenanthrolines **1–13**. The BP86/TZP LUMOs of phenanthrolines **1–13** are shown in Fig. 5, while spin density plots of added unpaired electrons are shown in Fig. 6. For phenanthrolines **1–11**, the LUMOs are of aromatic  $\pi$ -character, distributed over the entire phenanthroline ring system. The LUMOs of phenanthrolines **12** and **13** are located on the  $NO_2$  group and O atoms respectively. LUMO + 1 of phenanthrolines **12** and **13** (Fig. 5, bottom right) are similar in aromatic  $\pi$ -character distributed over the phenanthroline ring atoms to the LUMOs of phenanthrolines **1–11**. This suggests that the first reduction of phenanthrolines **1–11** will lead to the formation of a radical, with the added electron distributed over the three phenanthroline rings, as shown by the spin density plots of the reduced species ( $q = -1$ ,  $S = \frac{1}{2}$ ) in Fig. 6. However, in this case frontier orbital arguments

suggest that first reductions in phenanthrolines **12** and **13** are located on the  $NO_2$  group and O atoms respectively, as again seen in the spin density plots of the reduced species, see Fig. 6.

Although group electronegativities [38] of phenyl ( $\chi_{Ph} = 2.21$  [39]) and methyl ( $\chi_{Me} = 2.34$  [40]) groups are rather similar, the aromatic  $\pi$ -character of the LUMOs of the neutral compounds explains why the phenyl substituents in phenanthroline **8** with substituents on the 4 and 7 positions, do not have the same influence on the reduction potential of the corresponding phenanthroline than methyl substituents. The methyl groups on phenanthroline donate electron density through  $\sigma$  induction, while phenyl groups exhibit both  $\sigma$  and  $\pi$  induction interaction. The group electronegativity of a group is a description of its  $\sigma$  donation property. In reduced phenanthroline **8**, 67.5% electron density resides on the aromatic phenanthroline rings and 32.5% on the phenyl ring substituents (see spin density plot of **8** in Fig. 6, bottom middle), while in the methyl substituted phenanthrolines (**1**, **2**, **4**, **5** and **6**), more than 94% electron density resides on the aromatic phenanthroline rings itself. The increase in effective conjugation length of reduced **8** is visualized by the HOMO of reduced **8** that is of aromatic  $\pi$ -character (Fig. 6 bottom, right).

### 3.3. Relationships

Due to the role of the LUMO in the reduction of phenanthroline, it is expected that the energy of the LUMO ( $E_{LUMO}$ ) will be related to the experimentally measured reduction potential  $E_{pc}$ . This relationship is shown in Fig. 7a. Also shown is the relationship between  $E_{pc}$  and the DFT calculated electron affinity (EA) of the phenanthrolines (Fig. 7b). Both these graphs illustrate a higher less negative reduction potential being associated with a lower LUMO energy (the electron is therefore added more readily to the LUMO) and a higher EA (the reduction center is more electron hungry and thus reduces at a higher more positive potential). As expected, and for reasons already mentioned, data obtained for **8** deviates from this trend. The same is observed for phenanthroline **10** (phen-O). This may be explained in terms of the absence of aromatic bonds between the two outer rings of 5,6-epoxy-5,6-dihydro-1,10-phenanthroline, which consequently limits the  $\sigma$ -inductive effect of the 5,6-epoxy-5,6-dihydro substituent on the phenanthroline ring system.

Linear trends with  $R^2$  values of 0.91 and 0.80 also exist between experimental  $E_{pc}$  and the DFT calculated global electrophilicity index ( $\omega$ ) and Mulliken electronegativity ( $\chi$ ) of the substituted phenanthrolines (Fig. 7c and d). The four relationships in Fig. 7 complement each other and can thus be used in combination with each other for the purpose of predicting  $E_{pc}$  of other substituted phenanthrolines.

The  $\sigma$ -donor ability of the different substituents on a phenanthroline molecule is generally expressed in terms of corresponding  $pK_a$  values [41]. The relationship between the reduction potential of phenanthrolines **1–7**, **9** and **11** and their corresponding  $pK_a$  values follows a good linear trend, with a  $R^2 = 0.96$ , see Fig. 8. Again, due to the additional  $\pi$ -induction influence of the phenyl substituents on the reduction potential of phenanthroline **8**, this data point does not closely fit the series. No  $pK_a$  value of phenanthroline **10** (phen-O) could be found in literature (see Table 1).

In Fig. 9, reduction potentials obtained for the series of substituted 1,10-phenanthrolines of this study are correlated with published formal reduction potential data of selected related metal-phenanthroline complexes, i.e.  $[FeL_3]^{2+}$  (L – bidentate phenanthroline ligands) [42],  $trans-[Ru(II)(Az)(L)Cl_2]$  (where Az:  $C_6H_5N=NC(COCH_3)=NC_6H_5$ ) [43] and  $[CuL_2]^{2+}$  [44]. Fig. 9a–c shows the expected linear trend between the reduction potentials of the

**Table 1**

Electrochemical and DFT calculated data of the series of substituted 1,10-phenanthrolines, including  $pK_a$  values and formal reduction potentials of selected metal-phenanthroline complexes.

No	$E_{pc}/V$	$E_{LUMO}/eV$	EA/eV	IP/eV	$\eta/eV$	$\omega/eV$	$\chi/eV$	$pK_a^a$	$E^0$ of metal/ $V^{b,c}$		
									[FeL <sub>3</sub> ] <sup>2+</sup>	[Ru(Az)(L)Cl <sub>2</sub> ]	[CuL <sub>2</sub> ] <sup>2+</sup>
1	−2.635	−2.477	0.58	7.52	6.938	1.18	4.05	6.31	0.452		0.018
2	−2.603	−2.442	0.48	7.64	7.157	1.15	4.06	6.17			
3	−2.600	−2.521	0.51	7.26	6.749	1.12	3.88	5.78	0.585		
4	−2.577	−2.607	0.62	7.85	7.232	1.24	4.23				
5	−2.562	−2.573	0.58	7.83	7.258	1.22	4.20	5.27	0.669	−0.302	0.082
6	−2.550	−2.490	0.50	7.67	7.176	1.16	4.08	5.6	0.64	−0.384	0.053
7	−2.533	−2.640	0.60	7.99	7.390	1.25	4.30	4.93	0.698	−0.284	0.08
8	−2.393	−2.670	0.98	7.32	6.339	1.36	4.15	4.80			0.083
9	−2.321	−2.864	0.88	8.03	7.152	1.39	4.46	3.43	0.802	−0.225	0.141
10	−2.252	−2.784	0.78	8.16	7.377	1.35	4.47		0.802		
11	−2.221	−3.037	1.08	8.13	7.056	1.50	4.61	3.03	0.860		
12	−1.348	−3.935	1.95	8.37	6.423	2.07	5.16		0.894		0.147
13	−0.925	−4.545	2.40	8.48	6.080	2.43	5.44			−0.168	

<sup>a</sup>  $pK_a$  from Ref. [41] (phenanthrolines **1**, **2**, **5**, **6**, **7** and **8**), [45] (phen-5NH<sub>2</sub>, phenanthroline **3**), [46] (phen-5Cl, phenanthroline **9**) and [47] (phen-47Cl, phenanthroline **11**).

<sup>b</sup>  $E^0$  from Ref. [42–44]

<sup>c</sup> L = substituted 1,10-phenanthroline.

uncoordinated 1,10-phenanthroline series and that of corresponding metal-centered Fe<sup>2+</sup>, Ru<sup>2+</sup> and Cu<sup>2+</sup> complexes. The apparent absence of published cyclic voltammetry data on more metals limits the present correlation to only the named three metals.

Available experimental reduction potential data of a series of substituted 1,10-phenanthrolines, in combination with the redox potential data of only the unsubstituted metal-phenanthroline complex, may therefore enable determination of suitable substituents for desired redox tuning of its metal complexes. This may be particularly relevant during redox indicator and dye design for solar cell applications, both being of huge practical benefit and in active areas of research.

#### 4. Conclusion

The reduction potential of the series of derivatized uncoordinated 1,10-phenanthrolines relate linearly to corresponding DFT calculated LUMO energies, electron affinities, global electrophilicity index and Mulliken electronegativities, as well as the formal reduction potentials of its corresponding metal-phenanthroline complexes. This is the result of  $\sigma$ -inductive effects supported by effective electronic communication between the substituents and the phenanthroline ring system through to the metal. Phenanthrolines containing aromatic substituents, like phenyl groups, deviate slightly from the trend, since the aromatic substituents on the phenanthrolines also exhibit  $\pi$ -resonance communication with the phenanthroline ring system in addition to  $\sigma$ -induction. This leads to an increase in the reduction potential and stabilisation of the reduced phenanthroline.

#### Acknowledgements

This work has received support from the South African National Research Foundation and the Central Research Fund of the University of the Free State, Bloemfontein, South Africa. The High Performance Computing facility of the UFS is acknowledged for computer time.

#### Appendix A. Supplementary data

Optimised coordinates of the DFT calculations and electrochemical graphs and data are given in the Supporting Information. Supplementary data associated with this article can be found, in the online version, at <http://dx.doi.org/10.1016/j.poly.2016.11.018>.

#### References

- X.-S. Tai, J. Yin, M.-Y. Hao, Tetrakis(1,10-phenanthroline)calcium(II)bis(perchlorate) 4-(dimethylamino)benz-aldehyde disolvate, Acta Crystallogr. A E63 (2007) m1827, <http://dx.doi.org/10.1107/S1600536807027055>.
- V.C.R. Payne, R.T. Stibran, A.A. Holder, Synthesis and Crystal Structure of Tris (1,10-phenanthroline)iron(II) perchlorate ethanol monosolvate hemihydrate, Anal. Sci.: X-Ray Struct. Anal. Online 23 (2007) 23, <http://dx.doi.org/10.2116/analsci.23.x169>, x169.
- (a) Sethu Ramakrishnan, Eringadothi Suresh, Anvarbarcha Riyasdeen, Mohamad Abdulkadhar Akbarsha, Mallayan Palaniandavar, Interaction of  $\text{rac-[M(diimine)}_3\text{]}^{2+}$  (M = Co, Ni) complexes with CT DNA: role of 5,6-dmp ligand on DNA binding and cleavage and cytotoxicity, Dalton Trans. 40 (2011) 3245, <http://dx.doi.org/10.1039/C0DT01360A>;  
(b) P. Thuéry, Interlocked aromatic species: crystal structure and Hirshfeld surface analysis of the uranyl ion complex of 3-(pyrimidin-2-yl)benzoate with Ni(phen)<sub>3</sub><sup>2+</sup> counter-ions, Inorg. Chem. Commun. 59 (2015) 25, <http://dx.doi.org/10.1016/j.inoche.2015.06.022>.
- A.J. Pallenberg, K.S. Koenig, D.M. Barnhart, Synthesis and characterization of some copper(I) phenanthroline complexes, Inorg. Chem. 34 (1995) 2833, <http://dx.doi.org/10.1021/jc00115a009>.
- B.W. Skelton, A.F. Waters, A.H. White, Synthesis and structural systematics of nitrogen base adducts of group 2 salts. VII. Some complexes of group 2 metal halides with aromatic N,N'-bidentate ligands, Aust. J. Chem. 49 (1996) 99, <http://dx.doi.org/10.1071/CH9960099>.
- (a) S.J. Chalk, J.F. Tyson, Comparison of the maximum sensitivity of different flow-injection manifold configurations – alternating variable search optimization of the iron(II) 1,10-phenanthroline system, Anal. Chem. 66 (1994) 660, <http://dx.doi.org/10.1021/ac00077a013>;  
(b) N.V. Mudasir, N. Yoshioka, H. Inoue, Ion-paired chromatographic separation of iron(II) complexes of 1,10-phenanthroline and its derivatives, Anal. Lett. 29 (1996) 2239, <http://dx.doi.org/10.1080/00032719608002245>;  
(c) N.V. Mudasir, N. Yoshioka, H. Inoue, Ion paired chromatography of iron(II, III), nickel(II) and copper(II) as their 4,7-Diphenyl-1,10-phenanthroline chelates, Talanta 44 (1997) 1195, [http://dx.doi.org/10.1016/S0039-9140\(96\)02156-X](http://dx.doi.org/10.1016/S0039-9140(96)02156-X);  
(d) N.V. Mudasir, M. Arai, N. Yoshioka, H. Inoue, Reversed-phase high-performance liquid chromatography of iron(II) and copper(II) chelates with 4,7-diphenyl-1,10-phenanthroline disulfonate, J. Chromatogr. 799 (1998) 171, [http://dx.doi.org/10.1016/S0021-9673\(97\)01094-7](http://dx.doi.org/10.1016/S0021-9673(97)01094-7).
- (a) R. Sario, L. Farias, S.A. Moya, Complexes with heterocyclic nitrogen ligands – IV: complexes of ruthenium(II) and applications in catalysis, Polyhedron 16 (1997) 3847, [http://dx.doi.org/10.1016/S0277-5387\(97\)00130-7](http://dx.doi.org/10.1016/S0277-5387(97)00130-7);  
(b) P.B. Samnani, P.K. Bhattacharya, P.A. Ganeshpure, V.J. Koshy, S. Satish, Mixed ligand complexes of chromium(III) and iron(III): synthesis and evaluation as catalysts for oxidation of olefins, J. Mol. Catal. 110 (1996) 89, [http://dx.doi.org/10.1016/1381-1169\(95\)00299-5](http://dx.doi.org/10.1016/1381-1169(95)00299-5).
- (a) T.W. Johann, J.K. Barton, Recognition of DNA by octahedral coordination complexes, Philos. Trans. R. Soc. Lond. A 354 (1996) 299, <http://dx.doi.org/10.1098/rsta.1996.0010>;  
(b) C.S. Chow, F.M. Bogdan, A Structural Basis for RNA-Ligand Interactions, Chemical;  
(c) P.G. Sammes, G. Yahsioglu, 1,10-Phenanthroline: a versatile ligand, Chem. Soc. Rev. 23 (1994) 327, <http://dx.doi.org/10.1039/CS9942300327>;  
(d) N.V. Mudasir, N. Yoshioka, H. Inoue, Iron(II) and nickel(II) mixed-ligand complexes containing 1,10-phenanthroline and 4,7-diphenyl-1,10-phenanthroline, Transition Met. Chem. 24 (1999) 210, <http://dx.doi.org/>

- 10.1023/A:1006906208569;
- (e) B. Nordén, F. Tjerner, Binding of inert metal complexes to deoxyribonucleic acid detected by linear dichroism, *Fed. Eur. Biochem. Soc. Lett.* 67 (1976) 368, [http://dx.doi.org/10.1016/0014-5793\(76\)80566-2](http://dx.doi.org/10.1016/0014-5793(76)80566-2);
- (f) T. Hård, B. Nordén, Enantioselective interactions of inversion-labile trigonal iron(II) complexes upon binding to DNA, *Biopolymers* 25 (1986) 1209, <http://dx.doi.org/10.1002/bip.360250704>;
- (g) T. Hård, C. Hiort, B. Nordén, On the use of chiral compounds for probing the dna handedness: Z to B conversion in poly(dGm<sup>5</sup>dC) upon binding of Fe(phen)<sub>3</sub><sup>3+</sup> and Ru(phen)<sub>3</sub><sup>3+</sup>, *J. Biomol. Struct. Dyn.* 5 (1987) 89, <http://dx.doi.org/10.1080/07391102.1987.10506377>;
- (h) A. Yamagishi, Electric dichroism evidence for stereospecific binding of optically active tris chelated complexes to DNA, *J. Phys. Chem.* 88 (1984) 5709, <http://dx.doi.org/10.1021/j150667a050>.
- [9] (a) G. Bellé, R. Lente, I. Fábián, Central role of phenanthroline mono-N-oxide in the decomposition reactions of tris(1,10-phenanthroline)iron(II) and -iron(III) Complexes, *Inorg. Chem.* 49 (2010) 3968, <http://dx.doi.org/10.1021/ic902554b>;
- (b) W.W. Brandt, G.F. Smith, Polysubstituted 1,10-phenanthrolines and bipyridines as multiple range redox indicators, *Anal. Chem.* 21 (1949) 1313, <http://dx.doi.org/10.1021/ac60035a003>;
- (c) G.F. Smith, F.P. Richter, Substituted 1,10-phenanthroline ferrous complex oxidation–reduction indicators potential determinations as a function of acid concentration, *Ind. Eng. Chem. Anal. Ed.* 16 (1944) 580, <http://dx.doi.org/10.1021/i560133a014>.
- [10] N. Armaroli, Photoactive mono- and polynuclear Cu(I)-phenanthrolines. A viable alternative to Ru(II)-polypyridines?, *Chem Soc. Rev.* 30 (2001) 113, <http://dx.doi.org/10.1039/b000703j>.
- [11] A.N. Hidayatullah, E. Wachter, D.K. Heidary, S. Parkin, E.C. Glazer, Photoactive Ru(II) complexes with dioxinophenanthroline ligands are potent cytotoxic agents, *Inorg. Chem.* 53 (2014) 10030, <http://dx.doi.org/10.1021/ic5017164>.
- [12] (a) C.G. Robb, W. Nicholson, Kinetics of the exchange reactions of ethylenediamine with a series of cationic rhodium(I) complexes, *S. Afr. J. Chem.* 31 (1978) 1, [http://hdl.handle.net/10520/AJ03794350\\_812](http://hdl.handle.net/10520/AJ03794350_812);
- (b) J.G. Leipoldt, G.J. Lamprecht, E.C. Steynberg, Kinetics of the substitution of acetylacetonate in acetylacetonato-1,5-cyclooctadienerhodium(I) by derivatives of 1,10-phenanthroline and 2,2'-dipyridyl, *J. Organomet. Chem.* 402 (1991) 259, [http://dx.doi.org/10.1016/0022-328X\(91\)83069-G](http://dx.doi.org/10.1016/0022-328X(91)83069-G).
- [13] J.G. Leipoldt, S.S. Basson, G.J. van Zyl, G.J.J. Steyn, Kinetics of the substitution reactions of  $\beta$ -diketonato-1,5-cyclo-octadiene iridium(I) complexes with derivatives of 1,10-phenanthroline and 2,2'-dipyridyl, *J. Organomet. Chem.* 418 (1991) 241, [http://dx.doi.org/10.1016/0022-328X\(91\)86370-6](http://dx.doi.org/10.1016/0022-328X(91)86370-6).
- [14] (a) M. Freitag, F. Giordano, W. Yang, M. Pazoki, Y. Hao, B. Zietz, M. Grätzel, A. Hagfeldt, G. Boschloo, Copper phenanthroline as a fast and high-performance redox mediator for dye-sensitized solar cells, *J. Phys. Chem. C* 120 (2016) 9595, <http://dx.doi.org/10.1021/acs.jpcc.6b01658>;
- (b) M. Freitag, Q. Daniel, M. Pazoki, K. Sveinbjörnsson, J. Zhang, L. Sun, A. Hagfeldt, G. Boschloo, High-efficiency dye-sensitized solar cells with molecular copper phenanthroline as solid hole conductor, *Energy Environ. Sci.* 8 (2015) 2634, <http://dx.doi.org/10.1039/C5EE01204J>.
- [15] S.M. Feldt, E.A. Gibson, E. Gabriellsson, L. Sun, G. Boschloo, A. Hagfeldt, Design of organic dyes and cobalt polypyridine redox mediators for high-efficiency dye-sensitized solar cells, *J. Am. Chem. Soc.* 132 (2010) 16714, <http://dx.doi.org/10.1021/ja1088869>.
- [16] A. Kuhn, K.G. von Eschwege, J. Conradie, Reduction potentials of para-substituted nitrobenzenes – an infrared, nuclear magnetic resonance, and density functional theory study, *J. Phys. Org. Chem.* 25 (2011) 58, <http://dx.doi.org/10.1002/poc.1868>.
- [17] A. Kuhn, K.G. von Eschwege, J. Conradie, Electrochemical and density functional theory modeled reduction of enolized 1,3-diketones, *Electrochim. Acta* 56 (2011) 6211, <http://dx.doi.org/10.1016/j.electacta.2011.03.083>.
- [18] K.G. von Eschwege, Oxidation resilient dithiones – synthesis, cyclic voltammetry and DFT perspectives, *Polyhedron* 39 (2012) 99, <http://dx.doi.org/10.1016/j.poly.2012.03.028>.
- [19] J. Conradie, Density Functional Theory Calculations of Rh- $\beta$ -diketonato complexes, *J. Chem. Soc., Dalton Trans.* 44 (2015) 1503, <http://dx.doi.org/10.1039/C4DT02268H>.
- [20] M.M. Conradie, J. Conradie, Electrochemical behaviour of tris( $\beta$ -diketonato) iron(III) complexes: a DFT and experimental study, *Electrochim. Acta* 152 (2015) 512, <http://dx.doi.org/10.1016/j.electacta.2014.11.128>.
- [21] R. Freitag, J. Conradie, Electrochemical and computational chemistry study of Mn( $\beta$ -diketonato)<sub>3</sub> complexes, *Electrochim. Acta* 158 (2015) 418, <http://dx.doi.org/10.1016/j.electacta.2015.01.147>.
- [22] R. Liu, J. Conradie, Tris( $\beta$ -diketonato)chromium(III) complexes: effect of the  $\beta$ -diketonate ligand on the redox properties, *Electrochim. Acta* 185 (2015) 288, <http://dx.doi.org/10.1016/j.electacta.2015.10.116>.
- [23] J.J.C. Erasmus, J. Conradie, Chemical and electrochemical oxidation of [Rh( $\beta$ -diketonato)(CO)(P(OCH<sub>2</sub>)<sub>3</sub>CCH<sub>3</sub>)]: an experimental and DFT study, *Dalton Trans.* 42 (2013) 8655, <http://dx.doi.org/10.1039/C3DT50310K>.
- [24] A. Kuhn, J. Conradie, Electrochemical and DFT study of octahedral bis( $\beta$ -diketonato)-titanium(IV) complexes, *Inorg. Chim. Acta* 453 (2016) 247, <http://dx.doi.org/10.1016/j.ica.2016.08.010>.
- [25] J. Conradie, Oxidation potential of [Rh( $\beta$ -diketonato)(P(OPh)<sub>3</sub>)<sub>2</sub>] complexes – relationships with experimental, electronic and calculated parameters, *Electrochim. Acta* 110 (2013) 718, <http://dx.doi.org/10.1016/j.electacta.2013.01.021>.
- [26] K.G. von Eschwege, J. Conradie, Redox potentials of ligands and complexes – a DFT approach, *S. Afr. J. Chem.* 64 (2011) 203.
- [27] A.D. Becke, Density-functional exchange-energy approximation with correct asymptotic behavior, *Phys. Rev. A* 38 (1988) 3098, <http://dx.doi.org/10.1103/PhysRevA.38.3098>.
- [28] J.P. Perdew, Density-functional approximation for the correlation energy of the inhomogeneous electron gas, *Phys. Rev. B* 33 (1986) 8822, Erratum: J.P. Perdew, *Phys. Rev. B* 34 (1986) 7406, doi:10.1103/PhysRevB.33.8822.
- [29] The ADF program system was obtained from Scientific Computing and Modeling, Amsterdam (<http://www.scm.com/>). For a description of the methods used in ADF, see: G. te Velde, F.M. Bickelhaupt, E.J. Baerends, C.F. Guerra, S.J.A. van Gisbergen, J.G. Snijders, T.J. Ziegler, Chemistry with ADF, *J. Comput. Chem.* 22 (2001) 931–967, doi:<http://dx.doi.org/10.1002/jcc.1056>.
- [30] R.S. Mulliken, A new electroaffinity scale; together with data on valence states and on valence ionization potentials and electron affinities, *J. Chem. Phys.* 2 (1934) 782, <http://dx.doi.org/10.1063/1.1749394>.
- [31] M.V. Putz, N. Russo, E. Sicilia, About the Mulliken electronegativity in DFT, *Theor. Chem. Acc.* 114 (2005) 38, <http://dx.doi.org/10.1007/s00214-005-0641-4>.
- [32] F. De Proft, W. Langenaeker, P. Geerlings, Ab initio determination of substituent constants in a density functional theory formalism: calculation of intrinsic group electronegativity, Hardness, and Softness, *J. Phys. Chem.* 97 (1993) 1826, <http://dx.doi.org/10.1021/j100111a018>.
- [33] R.G. Parr, L. von Szentpály, S. Liu, Electrophilicity index, *J. Am. Chem. Soc.* 121 (1999) 1922, <http://dx.doi.org/10.1021/ja983494x>.
- [34] D.T. Sawyer, J.L. Roberts Jr., *Experimental Electrochemistry for Chemists*, John Wiley & Sons, New York, 1974, p. 54.
- [35] D.H. Evans, K.M. O'Connell, R.A. Peterson, M.J. Kelly, *Cyclic voltammetry*, *J. Chem. Educ.* 60 (1983) 290.
- [36] G. Gritzner, J. Kuta, Recommendations on reporting electrode potentials in nonaqueous solvents, *Pure Appl. Chem.* 56 (1984) 461, <http://dx.doi.org/10.1351/pac198456040461>.
- [37] J. Ferrando-Soria, O. Fabelo, M. Castellano, J. Cano, S. Fordham, H.-C. Zhou, Multielectron oxidation in a ferromagnetically coupled dinickel(II) triple mesocate, *Chem. Commun.* 51 (2015) 13381, <http://dx.doi.org/10.1039/C5CC03544A>.
- [38] Gordy scale group electronegativities,  $\chi_R$ , are empirical numbers that express the combined tendency of not only one atom, but a group of atoms, like R = CF<sub>3</sub> or CH<sub>3</sub>, to attract electrons (including those in a covalent bond) as a function of the number of valence electrons, n, and the covalent radius, r (in Å), of groups as discussed in P.R. Wells, in: *Progress in Physical Organic Chemistry*, vol. 6, John Wiley & Sons Inc., New York, 1968, pp. 111–145.
- [39] W.C. du Plessis, T.G. Vosloo, J.C. Swarts,  $\beta$ -Diketones containing a ferrocenyl group: synthesis, structural aspects,  $pK_a$  values, group electronegativities and complexation with rhodium(I), *J. Chem. Soc., Dalton Trans.* 15 (1998) 2507, <http://dx.doi.org/10.1039/A802398K>.
- [40] R.E. Kagarie, Relation between the electronegativities of adjacent substituents and the stretching frequency of the carbonyl group, *J. Am. Chem. Soc.* 77 (1955) 1377, <http://dx.doi.org/10.1021/ja01610a093>.
- [41] L. Gasque, G. Medina, L. Ruiz-Ramírez, R. Moreno-Esparza, Cu–O stretching frequency correlation with phenanthroline  $pK_a$  values in mixed copper complexes, *Inorg. Chim. Acta* 288 (1999) 106, [http://dx.doi.org/10.1016/S0020-1693\(99\)00034-1](http://dx.doi.org/10.1016/S0020-1693(99)00034-1).
- [42] H. Ferreira, K.G. von Eschwege, J. Conradie, Electronic properties of Fe charge transfer complexes – a combined experimental and theoretical approach, *Electrochim. Acta* (2016), <http://dx.doi.org/10.1016/j.electacta.2016.09.034>.
- [43] M. Al-Noaimi, M. El-Khateeb, S.F. Haddad, M. Sunjuk, R.J. Crutchley, Synthesis, structural characterization, and DFT investigation of azoimine–ruthenium complexes containing aromatic–nitrogen ligands, *Polyhedron* 27 (2008) 3239, <http://dx.doi.org/10.1016/j.poly.2008.07.033>.
- [44] G. Sanna, M.I. Pilo, M.A. Zoroddu, R. Seeber, Electrochemical and spectroelectrochemical study of copper complexes with 1,10-phenanthrolines, *Inorg. Chim. Acta* 208 (1993) 153, [http://dx.doi.org/10.1016/S0020-1693\(00\)85115-4](http://dx.doi.org/10.1016/S0020-1693(00)85115-4).
- [45] V. Ramírez-Delgado, M. Cruz-Ramírez, L.F. Hernández-Ayala, Y. Reyes-Vidal, R. Patakalvi, J.C. García-Ramos, F.J. Tenorio, L. Ruiz-Azuara, L. Ortiz-Frade, The role of the  $\pi$  acceptor character of polypyridine ligands on the electrochemical response of Co(II) complexes and its effect on the homogenous electron transfer rate constant with the enzyme glucose oxidase, *J. Mex. Chem. Soc.* 59 (2015) 282.
- [46] M.T. Ramírez-Silva, M. Gómez-Hernández, M.deL. Pacheco-Hernández, A. Rojas-Hernández, L. Galicia, Spectroscopy study of 5-amino-1,10-phenanthroline, *Spectrochim. Acta Part A* 60 (2004) 781.
- [47] A.A. Schilt, G.F. Smith, Acid dissociation constants of substituted 1,10-phenanthrolines, *J. Phys. Chem.* 60 (1956) 1546, <http://dx.doi.org/10.1021/j150545a017>.

## Chapter 3

---

### **Electrochemical properties of a series of Co(II) complexes, containing substituted phenanthrolines**

Hendrik Ferreira, Marrigje M. Conradie, Jeanet Conradie

Published by Electrochimica Acta

DOI: 10.1016/j.electacta.2018.09.151

### **Electrochemical data of Co(II) complexes containing phenanthroline functionalized ligands**

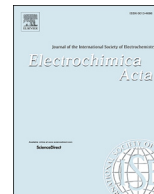
Hendrik Ferreira, Marrigje M. Conradie, Jeanet Conradie

Data in Brief

DOI: 10.1016/j.dib.2018.10.046







# Electrochemical properties of a series of Co(II) complexes, containing substituted phenanthrolines

Hendrik Ferreira, M. Conradie, Jeanet Conradie\*

Department of Chemistry, PO Box 339, University of the Free State, Bloemfontein, 9300, South Africa

## ARTICLE INFO

### Article history:

Received 22 June 2018

Received in revised form

14 August 2018

Accepted 22 September 2018

Available online 26 September 2018

### Keywords:

Cobalt

Reduction potential

Substituent effect

Exp-DFT relationships

N-donor

## ABSTRACT

Electrochemical studies of a series of substituted phenanthroline-Co(II) complexes all show generally similar behaviour, namely a chemically and electrochemically reversible  $\text{Co}^{\text{III/II}}$  redox couple, as well as a chemically and electrochemically reversible  $\text{Co}^{\text{II}}$  redox couple, followed by a ligand-based reduction. Electron donating- or -withdrawing substituents on the phenanthroline ligands which are coordinated to the Co metal, directly influence the electron density on the Co metal, due to good communication between these substituents and the Co metal via the aromatic rings of the heterocyclic substituted phenanthroline-Co(II) complexes, leading to either more negative (for electron donating groups) or more positive (for electron withdrawing groups) redox potentials respectively. Linear relationships relating  $E^\circ(\text{Co}^{\text{III/II}})$  oxidation and  $E^\circ(\text{Co}^{\text{II}})$  reduction to various experimental and empirical values, as well as to theoretically calculated energies, show that the electron density on Co is linearly influenced by the electronic properties of the ligands attached to the Co metal. All these established relationships can be used in the design of new substituted phenanthroline-Co(II) complexes with specific customized redox properties as required, for example, for the application of such Co(II) complexes as redox mediator for dye-sensitized solar cells.

© 2018 Elsevier Ltd. All rights reserved.

## 1. Introduction

1,10-Phenanthroline (phen) is a heterocyclic organic compound with nitrogen donor atoms which can coordinate to most metal ions. It was found that the irreversible electrochemical reduction potential of a series of differently substituted phenanthrolines relate linearly to density functional theory (DFT) calculated energies, such as LUMO (lowest unoccupied molecular orbital) energies, as well as to electron affinities, global electrophilicity indexes and Mulliken electronegativities of the various substituted phenanthrolines [1]. This is due to the effective electronic communication between the substituents and the phenanthroline ring system. Phenanthroline coordinates bidentately to most metals (e.g. Mn, Fe [2], Co, Ni, Cu, Zn [3]). This complexation leads to various octahedral  $\text{M}(\text{phen})_3^{n+}$  complexes. A direct relationship was found between the electronic influence of different substituents on the free phenanthroline ligands (as measured by the reduction potential of the free ligand), and the electronic influence of

different phenanthroline-substituents on the metal of the corresponding metal-phenanthroline complexes (as measured by the metal redox potential), for the following metals: Fe, Ru and Cu [1]. It is reported that terpyridine ligand functionalization in bis-terpyridyl-cobalt complexes allows tuning of the redox potentials for redox couples  $\text{Co}^{\text{III/II}}$ /Co(II), Co(II)/Co(I), and Co(I)/Co(I)(tpy) $^{\bullet-}$  couples, over a range of 1 V [4]. However, previous reports on the electrochemical behaviour of tris-phenanthroline-cobalt complexes in non-aqueous solvents, mostly focused only on the  $\text{Co}^{\text{III/II}}$ /Co(II) redox couple of tris-phenanthroline-cobalt, containing the unsubstituted phenanthroline ligand. Few reports described more than one Co redox couple and only some reports exist on the electrochemical behaviour of tris-phenanthroline-cobalt complexes containing substituted phenanthroline ligands, see Table 1. In this contribution we therefore for the first time describe the electrochemical behaviour of at least three observed redox events of a series of eight tris-phenanthroline-cobalt complexes, containing both the unsubstituted, as well as substituted phenanthrolines as ligands, see Fig. 1.

Different polypyridine Co(II) and Co(III) complexes showed promising properties as potential mediators [5–7] for photo-electrochemical solar cells. In dye-sensitized solar cells (DSSCs),

\* Corresponding author.

E-mail address: [conradj@ufs.ac.za](mailto:conradj@ufs.ac.za) (J. Conradie).

**Table 1**  
Experimental electrochemical data of synthesized  $[\text{Co}^{\text{II}}(\text{L})_3]^{2+}$  complexes **1–8** from this study, as well as additional data obtained from literature, for a variety of solvents and/or reference electrodes. L = differently substituted phenanthrolines as ligands, as shown in Fig. 1.

Complex number	Ligand L	Reference electrode <sup>a</sup>	Solvent	$[\text{Co}^{\text{III}}(\text{L})_3]^{3+}/[\text{Co}^{\text{II}}(\text{L})_3]^{2+}$		$[\text{Co}^{\text{II}}(\text{L})_3]^{2+}/[\text{Co}^{\text{I}}(\text{L})_3]^{1+}$		$[\text{Co}^{\text{I}}(\text{L})_3]^{1+}/[\text{Co}^{\text{I}}(\text{L})_2(\text{L}^-)]^0$		Reference
				reported	vs Fc/Fc <sup>+</sup>	reported	vs Fc/Fc <sup>+</sup>	reported	vs Fc/Fc <sup>+</sup>	
<b>1</b>	5-NO <sub>2</sub> -phen	Fc/Fc <sup>+</sup>	CH <sub>3</sub> CN		0.190		−0.960 <sup>b</sup>			this study
<b>2</b>	4,7-di-Cl-phen	Fc/Fc <sup>+</sup>	CH <sub>3</sub> CN		0.135		−1.160		−1.77 <sup>c</sup>	this study
<b>2</b>	4,7-di-Cl-phen	NHE	CH <sub>3</sub> CN	0.770	0.110					[32]
<b>3</b>	5-Cl-phen	Fc/Fc <sup>+</sup>	CH <sub>3</sub> CN		0.077		−1.256		−1.96 <sup>c</sup>	this study
<b>4</b>	phen	Fc/Fc <sup>+</sup>	CH <sub>3</sub> CN		−0.036		−1.366		−2.070	this study
<b>4</b>	phen	Ag/Ag <sup>+</sup>	CH <sub>3</sub> CN			−1.38	−1.46			[33]
<b>4</b>	phen	Ag/Ag <sup>+</sup>	CH <sub>3</sub> CN	0.12	0.04	−1.33	−1.41	−1.99	−2.07	[34]
<b>4</b>	phen	SCE	CH <sub>3</sub> CN	0.38	−0.04					[35]
<b>4</b>	phen	NHE	CH <sub>3</sub> CN	0.638	−0.022					[5]
<b>5</b>	5-Me-phen	Fc/Fc <sup>+</sup>	CH <sub>3</sub> CN		−0.079		−1.381		−2.094	this study
<b>6</b>	5,6-di-Me-phen	Fc/Fc <sup>+</sup>	CH <sub>3</sub> CN		−0.151		−1.395		−2.110	this study
<b>7</b>	5-NH <sub>2</sub> -phen	Fc/Fc <sup>+</sup>	CH <sub>3</sub> CN		−0.170		−1.438		−2.130	this study
<b>7</b>	5-NH <sub>2</sub> -phen	NHE	CH <sub>3</sub> CN	0.494	−0.166					[5]
<b>8</b>	3,4,7,8-Me-phen	Fc/Fc <sup>+</sup>	CH <sub>3</sub> CN		−0.263		−1.581		−2.250	this study
<b>8</b>	3,4,7,8-Me-phen	NHE	CH <sub>3</sub> CN	0.384	−0.276					[5]

<sup>a</sup> In order to convert to potential vs Fc/Fc<sup>+</sup> for comparative reasons, the following values have been used:  $E^\circ(\text{Fc}/\text{Fc}^+) = 0.66(5) \text{ V}$  vs NHE in  $[\text{t}(\text{Bu}_4)\text{N}][\text{PF}_6]/\text{CH}_3\text{CN}$  [36]; Saturated calomel (SCE) = 0.2444 V vs NHE;  $\text{Ag}/\text{Ag}^+$  (0.010 mol dm<sup>−3</sup> AgNO<sub>3</sub> in CH<sub>3</sub>CN) = 0.080 V vs Fc/Fc<sup>+</sup>.

<sup>b</sup> Reduction of  $\text{Co}(\text{NO}_2\text{-phen})_3^{3+}$ , complex **1**, is NO<sub>2</sub> ligand based, therefore not a  $\text{Co}^{\text{II/I}}$  redox process.

<sup>c</sup> Irreversible reduction.

**Table 2**  
Experimental, Electrochemical and DFT calculated data of  $\text{Co}(\text{II})$  complexes **1–8** obtained from this study and from literature; also including electrochemical data from a previous study [2], for the  $\text{Fe}^{\text{III/II}}$  redox couple corresponding to the  $\text{Co}^{\text{III/II}}$  redox couple, containing the same ligand.

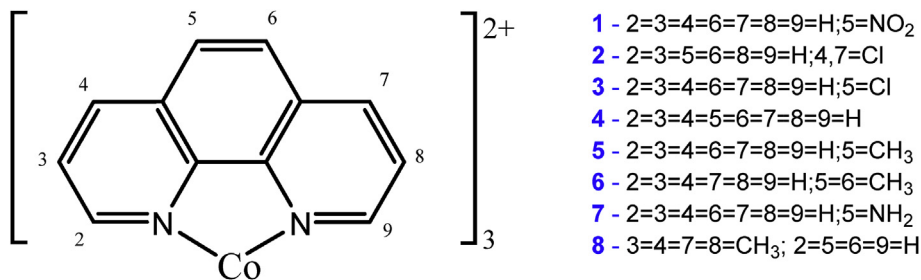
No	Ligand	$E^\circ(\text{Co}^{\text{III/II}})/\text{V}$	$E^\circ(\text{Co}^{\text{II/I}})/\text{V}$	$E^\circ(\text{Fe}^{\text{III/II}})/\text{V}^a$	$E_{\text{pc}}(\text{ligand})/\text{V}^b$	$\text{pK}_a(\text{ligand})^c$	$E_{\text{HOMO}}/\text{eV}$	$E_{\text{LUMO}}/\text{eV}$	EA/eV	IP/eV	$\omega/\text{eV}$	$\chi/\text{eV}$
<b>1</b>	5-NO <sub>2</sub> -phen	0.190	−0.960	0.894	−1.295 <sup>d</sup>	3.57	−14.208	−12.844	8.00	11.37	13.90	9.68
<b>2</b>	4,7-di-Cl-phen	0.135	−1.160	0.860	−2.221	3.03	−14.187	−12.207	7.60	10.83	13.14	9.21
<b>3</b>	5-Cl-phen	0.077	−1.256	0.802	−2.321	3.43	−9.671	−8.819	7.53	10.92	12.56	9.23
<b>4</b>	phen	−0.036	−1.366	0.698	−2.533	4.93	−9.319	−8.873	7.42	10.75	12.38	9.08
<b>5</b>	5-Me-phen	−0.079	−1.381	0.669	−2.562	5.27	−9.338	−8.491	7.17	10.58	11.57	8.88
<b>6</b>	5,6-di-Me-phen	−0.151	−1.395	0.640	−2.550	5.6	−9.146	−8.311	7.02	10.37	11.29	8.69
<b>7</b>	5-NH <sub>2</sub> -phen	−0.170	−1.438	0.585	−2.600	5.78	−9.139	−8.213	6.96	10.34	11.09	8.65
<b>8</b>	3,4,7,8-Me-phen	−0.263	−1.581	0.452	−2.635	6.31	−8.722	−7.861	6.63	9.85	10.53	8.24

<sup>a</sup>  $E^\circ(\text{Fe}^{\text{III/II}})$  from Ref. [2], for the  $\text{Fe}^{\text{III/II}}$  redox couple corresponding to the  $\text{Co}^{\text{III/II}}$  redox couple, with the same ligand.

<sup>b</sup>  $E_{\text{pc}}(\text{ligand})$  from Ref. [1] for the free ligand.

<sup>c</sup>  $\text{pK}_a$  from Ref. [50] (5Cl-phen), [51] (3,4,7,8-Me-phen, 5-Me-phen, 5,6-di-Me-phen, phen) and [52] (5-NH<sub>2</sub>-phen), [53] (phen-47Cl, phenanthroline), [54] (phen-5NO<sub>2</sub>).

<sup>d</sup> Reversible reduction process of **1** located on group NO<sub>2</sub>, instead of being distributed on the aromatic rings of the phenanthroline, as for **2–8** [1].



**Fig. 1.** The series of  $\text{Co}(\text{L})_3^{2+}$  complexes employed in this study, with L = differently substituted phenanthrolines as ligands.

the redox mediator plays the important role of regenerating the oxidized dye and transporting the hole towards the cathode, where the oxidized electrolyte is regenerated, thereby closing the circuit [8,9]. The redox-couples of redox mediators therefore play an extremely important role in dye-sensitized solar cells (DSSCs). Knowledge of the redox properties of the  $\text{Co}(\text{II/III})$  redox couple of differently substituted polypyridine  $\text{Co}(\text{II})$  complexes, is therefore vital for finding the best redox mediator most suitable for a certain

DSSC [10]. Finding relationships between experimental redox data and quantum computational energies, may assist in the design of redox mediators with specific customized properties. In continuation of our ongoing interest with obtaining relationships between experimentally measured redox potentials and computational chemistry calculated energies [11–13], we hereby present the results obtained for the series of substituted phenanthroline ligands coordinated to  $\text{Co}(\text{II})$  shown in Fig. 1.



## 2. Experimental

### 2.1. General

The phenanthroline ligands were obtained from Sigma Aldrich and used without further purification. UV–visible spectra of dilute methanol solutions of complexes **1–8** in quartz cuvettes, were recorded on a Shimadzu UV-2550 spectrometer. Infrared stretching frequencies were measured on a Bruker Tensor 27 FTIR spectrophotometer.

### 2.2. Synthesis

All eight Co(II) complexes (with  $(\text{NO}_3)_2$  as anion) were synthesized through the following method, using the literature method as a guide [14]:  $\text{Co}(\text{NO}_3)_2 \cdot 6\text{H}_2\text{O}$  was dissolved in a minimum of absolute ethanol. The desired ligand (3.3 eq) for each of the eight complexes was also dissolved in a minimum of absolute ethanol. The  $\text{Co}(\text{NO}_3)_2 \cdot 6\text{H}_2\text{O}$  solution was added dropwise to the respective ligand solution whilst stirring. The mixture was left to stir for 6 h. A precipitate formed in each case, the mixture was then filtered and the precipitate left to dry overnight in air. All these complexes are paramagnetic [15,16]. Electrochemical and other data for complexes **2**, **4**, **7** and **8** has been reported previously, while the electrochemical data for complexes **1**, **3**, **5** and **6** is reported here for the first time.

#### 2.2.1. Characterization *tris*(5-nitro-1,10-phenanthroline)*Cobalt*(II) nitrate, $[\text{Co}(\text{5-NO}_2\text{-phen})_3](\text{NO}_3)_2$ (**1**)

Yield 54.8%. Colour: light yellow. Melting point  $>245^\circ\text{C}$ .  $\lambda_{\text{max}}$  (methanol) = 269 nm;  $\nu_{\text{C-N}}$  =  $1327\text{ cm}^{-1}$ .

#### 2.2.2. Characterization *tris*(4,7-dichloro-1,10-phenanthroline)*Cobalt*(II) nitrate, $[\text{Co}(\text{4,7-di-Cl-phen})_3](\text{NO}_3)_2$ (**2**)

Yield 88.2%. Colour: light yellow. Melting point  $>245^\circ\text{C}$ .  $\lambda_{\text{max}}$  (methanol) = 271 nm;  $\nu_{\text{C-N}}$  =  $1322\text{ cm}^{-1}$ .

#### 2.2.3. Characterization *tris*(5-chloro-1,10-phenanthroline)*Cobalt*(II) nitrate, $[\text{Co}(\text{5-Cl-phen})_3](\text{NO}_3)_2$ (**3**)

Yield 88.2%. Colour: light yellow. Melting point  $205^\circ\text{C}$ .  $\lambda_{\text{max}}$  (methanol) = 271 nm;  $\nu_{\text{C-N}}$  =  $1326\text{ cm}^{-1}$ .

#### 2.2.4. Characterization *tris*(1,10-phenanthroline)*Cobalt*(II) nitrate, $[\text{Co}(\text{phen})_3](\text{NO}_3)_2$ (**4**)

Yield 87.1%. Colour: light yellow. Melting point  $>245^\circ\text{C}$ .  $\lambda_{\text{max}}$  (methanol) = 267 nm;  $\nu_{\text{C-N}}$  =  $1330\text{ cm}^{-1}$ .

#### 2.2.5. Characterization *tris*(5-methyl-1,10-phenanthroline)*Cobalt*(II) nitrate, $[\text{Co}(\text{5-Me-phen})_3](\text{NO}_3)_2$ (**5**)

Yield 54.2%. Colour: light yellow. Melting point  $>245^\circ\text{C}$ .  $\lambda_{\text{max}}$  (methanol) = 272 nm;  $\nu_{\text{C-N}}$  =  $1326\text{ cm}^{-1}$ .

#### 2.2.6. Characterization *tris*(5,6-dimethyl-1,10-phenanthroline)*Cobalt*(II) nitrate, $[\text{Co}(\text{5,6-di-Me-phen})_3](\text{NO}_3)_2$ (**6**)

Yield 73.6%. Colour: light yellow. Melting point  $>245^\circ\text{C}$ .  $\lambda_{\text{max}}$  (methanol) = 275 nm;  $\nu_{\text{C-N}}$  =  $1329\text{ cm}^{-1}$ .

#### 2.2.7. Characterization *tris*(1,10-phenanthroline-5-amine)*Cobalt*(II) nitrate, $[\text{Co}(\text{5-NH}_2\text{-phen})_3](\text{NO}_3)_2$ (**7**)

Yield 97.1%. Colour: light yellow. Melting point  $>245^\circ\text{C}$ .  $\nu_{\text{C-N}}$  =  $1311\text{ cm}^{-1}$ .

#### 2.2.8. Characterization *tris*(3,4,7,8-tetramethyl-1,10-phenanthroline)*Cobalt*(II) nitrate, $[\text{Co}(\text{3,4,7,8-Me-phen})_3](\text{NO}_3)_2$ (**8**)

Yield 82.3%. Colour: light yellow. Melting point  $>245^\circ\text{C}$ .

$$\lambda_{\text{max}}(\text{methanol}) = 274\text{ nm}; \nu_{\text{C-N}} = 1333\text{ cm}^{-1}.$$

### 2.3. Theoretical calculations

Density functional theory (DFT) calculations were performed on all 8 complexes, using the Amsterdam Density Functional program (ADF2014 and updates) [17]. The GGA functional BP86 [18,19] with the TZP (Triple  $\zeta$  polarized) basis set was used. All complexes were computed both in the gas phase, as well as in solvents dichloromethane (DCM) and acetonitrile ( $\text{CH}_3\text{CN}$ ), using the COSMO (Conductor like Screening Model) model of solvation [20–22], as implemented in ADF. Complexes were computed spin unrestricted, with spin  $S = 1/2$  for Co(II) [15,16], and  $S = 1$  for Co(I) (reduced form), and spin restricted with  $S = 0$  for Co(III) (oxidized form) [23]. The BP86 functional was also used to calculate the geometry relaxed (adiabatic) energies of the Co(II), Co(I) (reduced) and Co(III) (oxidized) complexes, in order to determine the following parameters: electron affinity (EA), ionization potential (IP), global electrophilicity index ( $\omega$ ) and Mulliken electronegativity ( $\chi$ ), according to the following formulae [24–27]:

$$\text{EA}(\text{compound}) = E(\text{reduced compound}) - E(\text{compound})$$

$$\text{IP}(\text{compound}) = E(\text{oxidized compound}) - E(\text{compound})$$

$$\omega = \left( \mu^2 / 2\eta \right); \text{ where } \mu = -(\text{IP} + \text{EA})/2 \text{ and } \eta = \text{IP} - \text{EA}$$

$$\chi = (\text{IP} + \text{EA})/2$$

### 2.4. Electrochemistry

Electrochemical studies by means of cyclic voltammetry (CV) were performed on  $0.002\text{ mol dm}^{-3}$  or on saturated compound solutions of complexes **1–8** in dry acetonitrile, containing  $0.1\text{ mol dm}^{-3}$  tetra-*n*-butylammoniumhexafluorophosphate ( $[\text{t}^{\text{Bu}}_4\text{N}][\text{PF}_6]$ ) as supporting electrolyte, under a blanket of purified argon, at  $25^\circ\text{C}$ , utilizing a BAS 100 B/W electrochemical analyzer. A three-electrode cell was used, with a glassy carbon (surface area  $7.07 \times 10^{-6}\text{ m}^2$ ) working electrode, Pt auxiliary electrode and a  $\text{Ag}/\text{Ag}^+$  ( $0.010\text{ mol dm}^{-3}$   $\text{AgNO}_3$  in  $\text{CH}_3\text{CN}$ ) reference electrode [28], mounted on a Luggin capillary [29]. Scan rates for the CVs were  $0.05\text{--}5.00\text{ V s}^{-1}$ . Successive experiments under the same experimental conditions showed that all oxidation and reduction potentials were reproducible within  $0.010\text{ V}$ . All cited potentials were referenced against the  $\text{Fc}/\text{Fc}^+$  couple, as suggested by IUPAC [30]. Ferrocene (Fc) exhibited a peak separation of  $\Delta E_p = E_{\text{pa}} - E_{\text{pc}} = 0.070\text{ V}$  and ratio  $i_{\text{pc}}/i_{\text{pa}} = 1.00$  under our experimental conditions, where  $E_{\text{pa}}$  ( $E_{\text{pc}}$ ) = anodic (cathodic) peak potential and  $i_{\text{pa}}$  ( $i_{\text{pc}}$ ) = anodic (cathodic) peak current. The formal reduction potential is determined by  $E^{\circ'} = (E_{\text{pa}} - E_{\text{pc}})/2$  for an electrochemically reversible process [29]; where values for the peak separation  $\Delta E_p$  up to  $0.090\text{ V}$ , will be considered to be electrochemically reversible.

## 3. Results and discussion

### 3.1. Computational chemistry understanding of redox process

This computational section is presented for better understanding of the character of the different redox processes that are presented in the electrochemistry section. Reduction and oxidation of complexes generally involve either the addition or removal of an

electron to or from the frontier orbitals of the complex respectively. For example, reduction of the closed shell singlet Co(III) complex, involves the addition of an electron to the lowest unoccupied molecular orbital (LUMO) of the initial Co(III) complex. This LUMO orbital will then become the highest occupied molecular orbital (HOMO) of the reduced complex, while a spin plot of the reduced complex will show the distribution of the added electron, based either on the metal or the ligand. These orbitals and spin plots, as shown in Fig. 2 for complex 4, namely  $\text{Co}(\text{phen})_3^{3+}$  (with  $n = 2$  or  $3$ ), clearly indicate that the Co(III) reduction is metal based, i.e. the reduction is a  $\text{Co}^{\text{III/II}}$  redox process; since the spin plot of  $\text{Co}(\text{phen})_3^{2+}$  (4) shows that the added unpaired electron is of  $d_{z^2}$  character on the Co-metal. Similarly, the spin plots of the other Co(II) complexes 1–3, 5–8 also indicate that the  $\text{Co}^{\text{III/II}}$  reduction is Co-metal based (see Fig. 4 for complex 1 as example). This assignment of the added electron to the Co-metal is in agreement with the experimental electrochemical Co(III) reduction process, as measured by cyclic voltammetry, which will be discussed in the next section.

Reduction of the spin =  $\frac{1}{2}$  Co(II) complex involves the addition of an electron to the lowest unoccupied molecular orbital (LUMO) of the Co(II) complex. The spin plot of the reduced complex will show the distribution of the added electron. Both the LUMO of Co(II) and the spin plot of Co(I), as shown in Fig. 3 for complex 4,

namely  $\text{Co}(\text{phen})_3^{2+}$  (where  $n = 1$  or  $2$ ), again clearly indicate that the Co(II) reduction is metal based, i.e. the reduction is a  $\text{Co}^{\text{II/I}}$  redox process. The spin plot of  $\text{Co}(\text{phen})_3^{1+}$  shows that both unpaired electrons are based on the Co-metal. Similarly, the LUMOs of Co(II) for the other complexes 2–3, 5–8 also indicate that the Co(II) reduction is Co-metal based. There is however one exception, since the Co(II) LUMO of  $\text{Co}(\text{NO}_2\text{-phen})_3^{2+}$ , complex 1, is located on a  $\text{NO}_2$  group (Fig. 4) instead of on the Co-metal, suggesting that the reduction of  $\text{Co}(\text{NO}_2\text{-phen})_3^{2+}$ , complex 1, is  $\text{NO}_2$  ligand based instead, i.e. not also a  $\text{Co}^{\text{II/I}}$  redox process (as for the other complexes 2–8). For further evidence of the character of the reduced complex 1, the spin density plots of complex 1,  $\text{Co}(\text{5-NO}_2\text{-phen})_3^{2+}$ , as well as of the reduced complex 1, are also given in Fig. 4. The Co(II) spin plot of  $\text{Co}(\text{5-NO}_2\text{-phen})_3^{2+}$ , complex 1, shows that the unpaired electron is of  $d_{z^2}$  character on the Co-metal. This was also found for the other complexes 2–8. However, the Co(I) spin plot of the reduced complex 1 shows that one of the unpaired electrons is based on the Co-metal, while the other unpaired electron is distributed over the  $\text{NO}_2$  groups of the ligand, thereby forming an unstable reduced complex.

On the other hand, the LUMO of Co(I), also shown in Fig. 3 for the reduced complex 4,  $\text{Co}(\text{phen})_3^{1+}$ , is based on the phenantroline-ligand instead, therefore the reduction of the Co(I) of the other complexes 2–8 will also involve the phenantroline-ligands. These

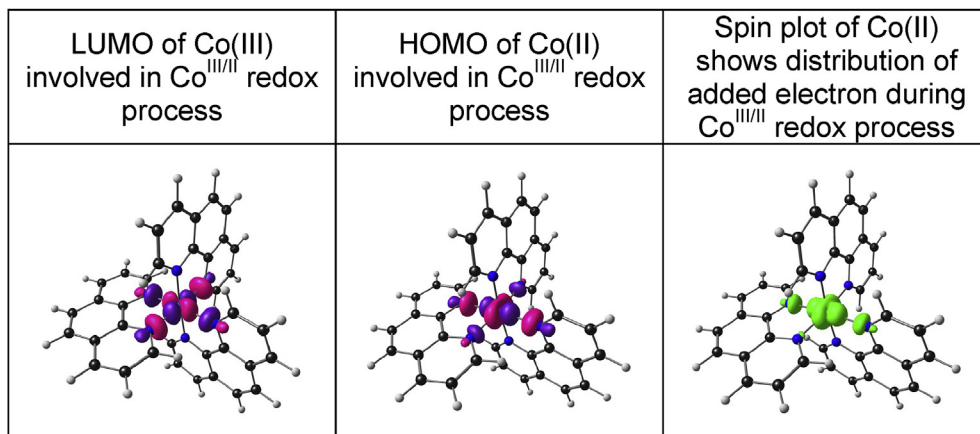


Fig. 2. DFT calculated BP86/TZP frontier orbitals of  $\text{Co}(\text{phen})_3^{n+}$  (with  $n = 2, 3$ ), which are involved in the  $\text{Co}^{\text{III/II}}$  redox process. The spin plot of the reduced Co(II) complex is also shown. A contour of 0.06 and 0.006  $\text{e}/\text{\AA}^3$  was used for the orbital and spin plots respectively.

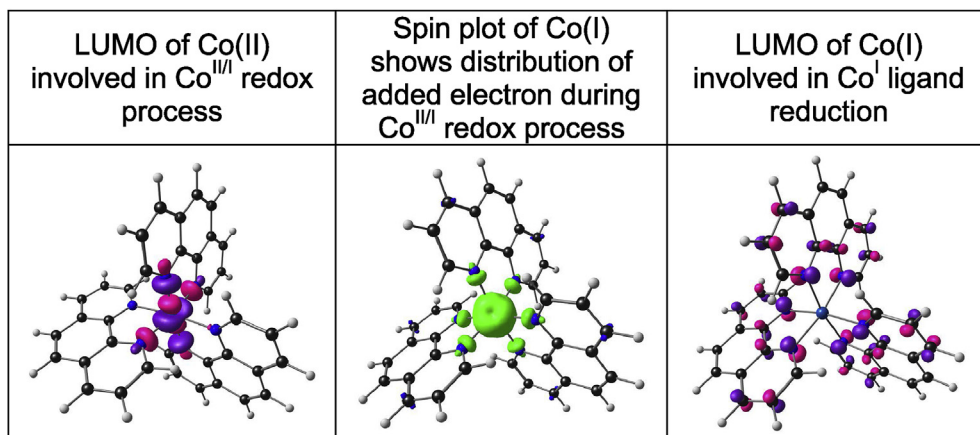
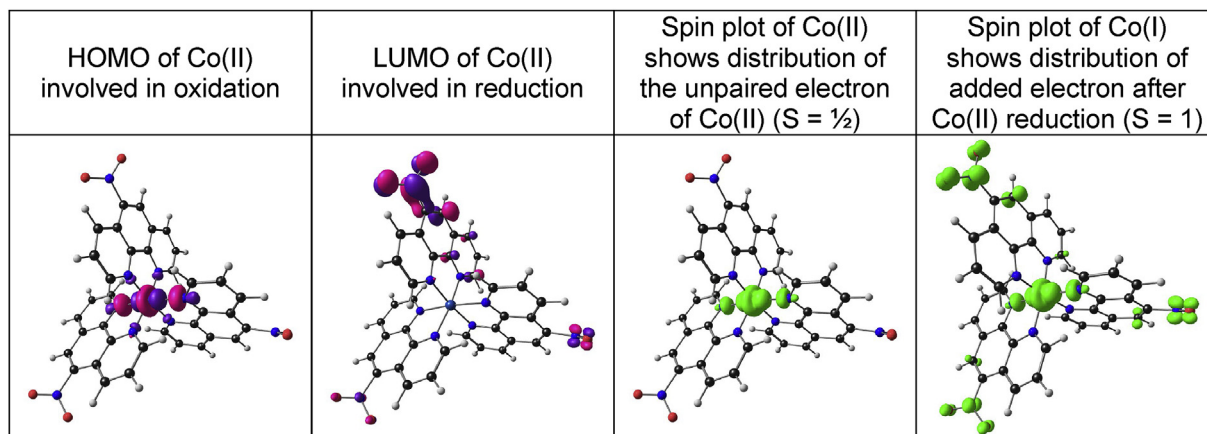


Fig. 3. DFT calculated BP86/TZP LUMO of  $\text{Co}(\text{phen})_3^{2+}$  which are involved in the  $\text{Co}^{\text{II/I}}$  redox process. The LUMO of  $\text{Co}(\text{phen})_3^{1+}$ , which is involved in the  $\text{Co}^{\text{I}}$  ligand reduction and the spin plot of  $\text{Co}(\text{phen})_3^{1+}$ , are also shown. A contour of 0.06 and 0.006  $\text{e}/\text{\AA}^3$  was used for the orbital and spin plots respectively.



**Fig. 4.** DFT calculated BP86/TZP HOMO and LUMO (calculated in  $\text{CH}_3\text{CN}$  as solvent) of  $\text{Co}(\text{NO}_2\text{-phen})_3^{2+}$ , complex **1**, which are involved in the oxidation and reduction of complex **1**, respectively. A contour of 0.06 and 0.006  $\text{e}/\text{\AA}^3$  was used for the orbital and spin plots respectively.

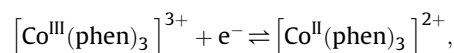
assignments are in agreement with the experimentally observed electrochemical Co(II) and Co(I) reduction processes, as measured by cyclic voltammetry, which are presented in the next section.

### 3.2. Electrochemistry

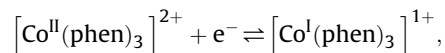
Fig. 5 shows the cyclic voltammetry scans for  $[\text{Co}(\text{phen})_3](\text{NO}_3)_2$ , complex **4**, of this study, at different scan rates (0.05–5.00  $\text{V s}^{-1}$ ) over different potential ranges. Three chemically and electrochemically reversible redox couples were observed in the solvent window for  $\text{CH}_3\text{CN}$ , as well as a few irreversible oxidation or reduction peaks. Firstly, the irreversible oxidation peak at ca. 1.63 V vs  $\text{Fc}/\text{Fc}^+$ , is ascribed to anionic nitrate oxidation. Secondly, the chemically and electrochemically reversible redox couple at  $-0.036$  V vs  $\text{Fc}/\text{Fc}^+$  ( $\Delta E = 0.084$  V at  $0.100$   $\text{V s}^{-1}$ ), is ascribed to the  $\text{Co}^{\text{III/II}}$  redox couple, while the other chemically and electrochemically reversible redox couple at  $-1.366$  V vs  $\text{Fc}/\text{Fc}^+$  ( $\Delta E = 0.076$  V at  $0.100$   $\text{V s}^{-1}$ ), is attributed to the  $\text{Co}^{\text{II/I}}$  redox couple. Further, the chemically and electrochemically reversible peak at  $-2.070$  V vs  $\text{Fc}/\text{Fc}^+$  ( $\Delta E = 0.088$  V at  $0.100$   $\text{V s}^{-1}$ ) is ascribed to ligand reduction, i.e.  $[\text{Co}^{\text{I}}(\text{phen})_3]^+ / [\text{Co}^{\text{I}}(\text{phen})_2(\text{phen}^-)]^0$  reduction. The next reduction peak at  $-2.44$  V vs  $\text{Fc}/\text{Fc}^+$ , is ascribed to a second ligand based reduction, i.e.  $[\text{Co}^{\text{I}}(\text{phen})_2(\text{phen}^-)]^0 / [\text{Co}^{\text{I}}(\text{phen})(\text{phen}^-)_2]^-$  [31]. This

assignment is in agreement with reported electrochemical data on  $[\text{Co}(\text{phen})_3]^{2+}$  and  $[\text{Co}(\text{phen})_3]^{3+}$  (see Table 1), as well as with the DFT computational chemistry study presented above.

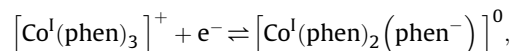
CVs obtained over different potential ranges for  $[\text{Co}(\text{phen})_3](\text{NO}_3)_2$ , complex **4**, are shown in Fig. 5. The  $\text{Co}^{\text{III/II}}$  redox couple was scanned alone, then the  $\text{Co}^{\text{III/II}}$  and  $\text{Co}^{\text{II/I}}$  redox couples together and then all three redox couples in the same scan. It can clearly be seen that not one redox process influences the reversibility of the other two, when obtained in the same potential scan. Only when the scan is reversed, after the irreversible ligand-based reductions below  $-2.5$  V, re-oxidation of the  $\text{Co}^{\text{II/I}}$  redox couple is no longer observed. A linear response of peak currents vs the square root of the scan rate is obtained for the three reversible redox events in the CV of complex **4**, namely the oxidation of  $[\text{Co}^{\text{II}}(\text{phen})_3]^{2+}$  to  $[\text{Co}^{\text{III}}(\text{phen})_3]^{3+}$ , the reduction of  $[\text{Co}^{\text{II}}(\text{phen})_3]^{2+}$  to  $[\text{Co}^{\text{I}}(\text{phen})_3]^{1+}$ , as well as for the reduction of  $[\text{Co}^{\text{I}}(\text{phen})_3]^+$  to  $[\text{Co}^{\text{I}}(\text{phen})_2(\text{phen}^-)]^0$ . These linear responses, as described by the Randles-Sevcik equation, indicate diffusion-controlled electrochemical processes for all three reversible redox events of  $[\text{Co}(\text{phen})_3](\text{NO}_3)_2$ , complex **4**. The first three cell reactions observed can be written as:



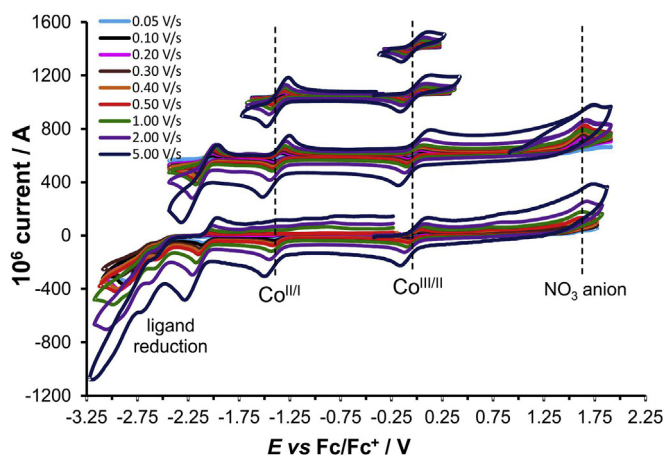
$$\text{with } E^0(\text{vs } \text{Fc}/\text{Fc}^+) = -0.036 \text{ V}$$



$$\text{with } E^0(\text{vs } \text{Fc}/\text{Fc}^+) = -1.366 \text{ V}$$



$$\text{with } E^0(\text{vs } \text{Fc}/\text{Fc}^+) = -2.070 \text{ V}$$



**Fig. 5.** Cyclic voltammograms of a  $0.002 \text{ mol dm}^{-3}$  solution of  $[\text{Co}(\text{phen})_3](\text{NO}_3)_2$  (complex **4**), in  $\text{CH}_3\text{CN}$  as solvent and  $0.1 \text{ mol dm}^{-3}$   $[\text{n}(\text{Bu}_4)\text{N}][\text{PF}_6]$  as supporting electrolyte, on a glassy carbon-working electrode, at different scan rates (0.05–5.00  $\text{V s}^{-1}$ ) over different potential ranges.

Fig. 6 shows the  $0.100 \text{ V s}^{-1}$  cyclic voltammetry scans for the Co(II) complexes **1–8** of this study, focusing on the electrochemical processes between  $-2.5$  and  $0.5$  V vs  $\text{Fc}/\text{Fc}^+$ , namely: (i) the chemically and electrochemically reversible  $\text{Co}^{\text{III/II}}$  redox couple between  $-0.3$  and  $0.2$  V (complexes **1–8**), (ii) the chemically and

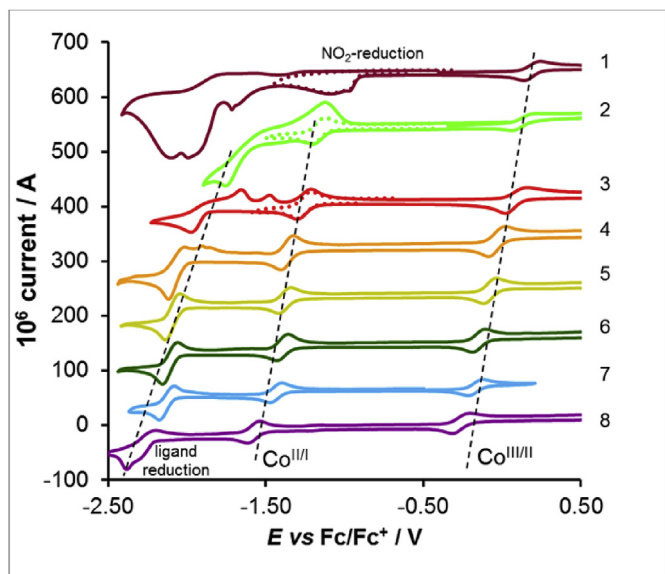


Fig. 6. Cyclic voltammograms of ca. 0.002 mol dm<sup>-3</sup>, or of saturated solutions of Co(II) complexes **1–8**, in solvent CH<sub>3</sub>CN/0.1 mol dm<sup>-3</sup> [n(Bu<sub>4</sub>)N][PF<sub>6</sub>], on a glassy carbon-working electrode, at a scan rate of 0.100 V s<sup>-1</sup>.

electrochemically reversible Co<sup>II/I</sup> redox couple between  $-1.6$  and  $-1.0$  V (for complexes **2–8**), and (iii) the ligand reduction below  $-2$  V. The exception is complex **1**, where the irreversible reduction of Co(NO<sub>2</sub>-phen)<sub>3</sub><sup>2+</sup>, complex **1**, at  $-0.960$  V vs Fc/Fc<sup>+</sup>, is assigned to a NO<sub>2</sub> ligand based reduction instead of a Co<sup>II/I</sup> redox process, as was observed for the other complexes **2–8**. This assignment is in agreement with the character of the LUMO of Co(NO<sub>2</sub>-phen)<sub>3</sub><sup>2+</sup>, complex **1**, in Fig. 4, as well as with the fact that the first reduction of the uncoordinated free NO<sub>2</sub>-phenanthroline ligand, observed at  $E^0 = -1.295$  V vs Fc/Fc<sup>+</sup>, is located on the substituted NO<sub>2</sub> groups of the ligand, instead of being distributed over the aromatic rings of the phenanthroline ligand, as was observed for the uncoordinated free phenanthroline ligands of complexes **2–8** [1].

Table 1 gives selected electrochemical data of complexes **1–8**, including reported electrochemical data on some of the complexes. From Table 1 it is clear that the electrochemical redox data, obtained in this study with solvent CH<sub>3</sub>CN, agrees well with published redox data obtained under various experimental conditions (varying solvents, scan rates and supporting electrolytes). The electrochemical data for complexes **1, 3, 5** and **6** is reported here for the first time. For complexes **2, 7** and **8**, only the Co<sup>II/I</sup> and the Co<sup>I</sup> ligand based redox processes are reported here for the first time.

The oxidation of Co(5-X'-phen)<sub>3</sub><sup>2+</sup> complexes with substituents X' = NO<sub>2</sub> (**1**), Cl (**3**), H (**4**), Me (**5**) or NH<sub>2</sub> (**7**), show that the redox potential for  $E^0(\text{Co}^{\text{III/II}})$  increases as follows: NH<sub>2</sub> (**7**) < Me (**5**) < H (**4**) < Cl (**3**) < NO<sub>2</sub> (**1**). The nitro group NO<sub>2</sub> in complex **1** is therefore most electron withdrawing, leading to a more positive redox potential for Co(5-NO<sub>2</sub>-phen)<sub>3</sub><sup>2+</sup>, complex **1**, in the series of complexes (**1**)–(**8**). The reduction of the Co(5-X'-phen)<sub>3</sub><sup>2+</sup> complexes with substituents X' = NO<sub>2</sub> (**1**), Cl (**3**), H (**4**), Me (**5**) or NH<sub>2</sub> (**7**), increases as follows: NH<sub>2</sub> (**7**) < Me (**5**) < H (**4**) < Cl (**3**) < NO<sub>2</sub> (**1**). However, the reduction of complexes **3–4, 5, 7** is Co-metal based, while the reduction of complex **1**, containing the strongly electron-withdrawing nitro substituent groups, is NO<sub>2</sub>-based instead.

The electron donating effect of the Me group is cumulative; for example, complex **8** with four Me groups on each phenanthroline ligand, has lower (more negative) redox potentials for both the  $E^0(\text{Co}^{\text{III/II}})$  and  $E^0(\text{Co}^{\text{II/I}})$  redox couples, as well as for the reversible

Co<sup>I</sup>-ligand based reduction, than complex **6** with only two Me groups on each phenanthroline ligand, or complex **5** with one Me group on each phenanthroline ligand, or than Co(phen)<sub>3</sub><sup>2+</sup>, complex **4**, with no Me group on the phenanthroline ligands. Complex **8** with four electron donating Me groups on each phenanthroline ligand, is therefore reduced at the lowest potential of all the complexes (**1**)–(**8**).

Similarly, the electron withdrawing effect of the Cl group, is also cumulative. The  $E^0(\text{Co}^{\text{III/II}})$  and  $E^0(\text{Co}^{\text{II/I}})$  redox processes, as well as the irreversible Co<sup>I</sup>-ligand based reduction of complex **3**, containing only one Cl group on each phenanthroline ligand, are lower (more negative) than that of complex **2** with two Cl groups on each phenanthroline ligand. Further, the different redox processes of complex **2** (two Cl groups on each phenanthroline ligand) and of complex **3** (one Cl group on each phenanthroline ligand) are all at a higher potential than that of Co(phen)<sub>3</sub><sup>2+</sup>, complex **4**, with no Cl group on the phenanthroline ligands.

### 3.3. Relationships

Although some electrochemical data for some of the complexes has been reported previously, this report is the first comprehensive study, reporting all three redox couples of a series of eight Co(phen)<sub>3</sub><sup>2+</sup> complexes containing substituted phenanthroline ligands, each obtained under the same experimental conditions. We have previously shown that the electrochemical data of a series of related complexes can be linearly related to various experimental and electronic parameters, as well as to theoretically calculated energies [1,37,38]. The electrochemical data obtained experimentally in this study for complexes **1–8**, should therefore also be compared to similar experimental data obtained for other related complexes, as well as to theoretically calculated energies of these same complexes **1–8**.

#### 3.3.1. Relationships with experimental values

Fig. 7 displays the relationships between the redox potential  $E^0$  of the Co<sup>III/II</sup> redox couple with other experimental values, namely with the pK<sub>a</sub> of the free uncoordinated ligand (Fig. 7a) and the reduction potential  $E_{\text{pc}}$  of the free uncoordinated ligand [1] (Fig. 7b), as well as with published results for the redox potential  $E^0$  of the corresponding Fe<sup>III/II</sup> redox couple of the related Fe(L)<sub>3</sub><sup>2+</sup> complexes [2], containing the same substituted phenanthroline ligands L as the Co(L)<sub>3</sub><sup>2+</sup> complex (Fig. 7c). The relationship between  $E^0$  of the Co<sup>III/II</sup> redox couple and the pK<sub>a</sub> of the free uncoordinated ligand is shown in (Fig. 7d). The relationship predicting the redox potential  $E^0(\text{Co}^{\text{III/II}})$  from the various experimental values are:

$$E^0(\text{Co}^{\text{III/II}}) = -0.12(1)\text{pK}_a(\text{free ligand}) + (0.55(7)) \quad R^2 = 0.93$$

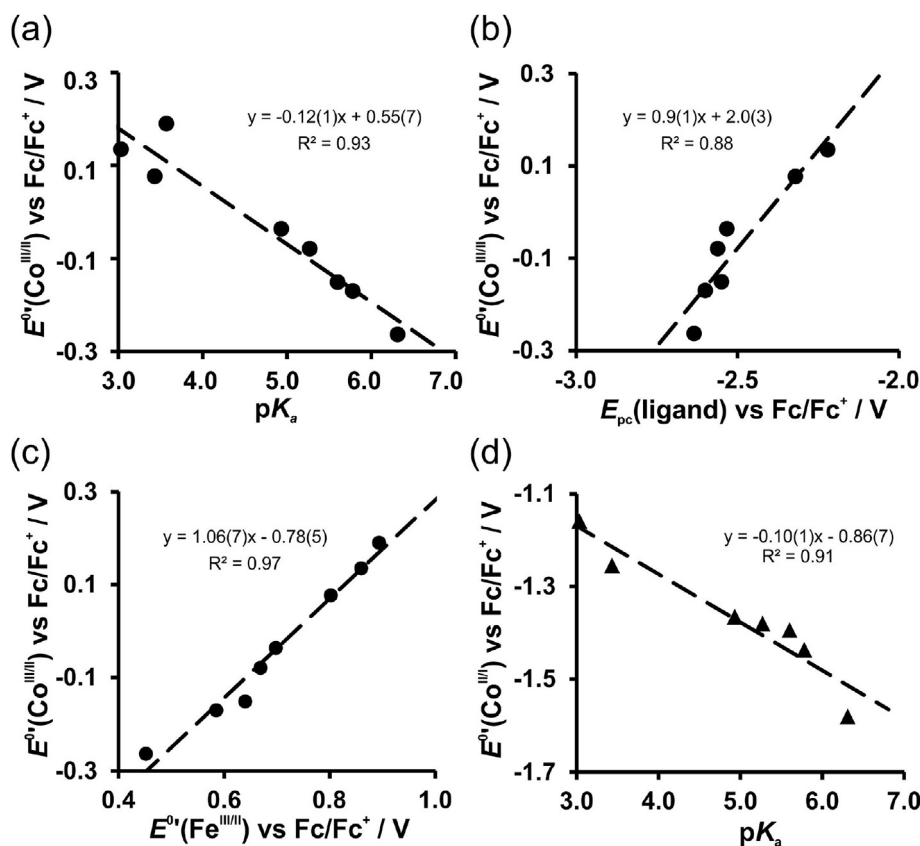
$$E^0(\text{Co}^{\text{II/I}}) = -0.10(1)\text{pK}_a(\text{free ligand}) - (0.86(7)) \quad R^2 = 0.91$$

$$E^0(\text{Co}^{\text{III/II}}) = -0.9(1)E_{\text{pc}}(\text{free ligand}) - (2.0(3)) \quad R^2 = 0.88$$

$$E^0(\text{Co}^{\text{III/II}}) = -1.06(7)E^0(\text{Fe}^{\text{III/II}}) - (0.78(5)) \quad R^2 = 0.97$$

A multilinear regression of the dependence of  $E^0(\text{Co}^{\text{III/II}})$  on all three of the above mentioned experimental values (Fig. 7a–c) for complexes **1–6** gives:





**Fig. 7.** Relationships obtained between the redox potential  $E^\circ$  (vs  $\text{Fc}/\text{Fc}^+$ ) of the  $\text{Co}^{\text{III/II}}$  redox couple of the  $\text{Co}(\text{II})$  complexes **1–8** of this study, and (a) the  $\text{pK}_a$  of the free ligand of each, (b) with the reduction potential  $E_{\text{pc}}$  of the free ligand, (c) with the redox potential  $E^\circ$  (vs  $\text{Fc}/\text{Fc}^+$ ) of the corresponding  $\text{Fe}^{\text{III/II}}$  redox couple and (d) between the redox potential  $E^\circ$  (vs  $\text{Fc}/\text{Fc}^+$ ) of the  $\text{Co}^{\text{II/I}}$  redox couple and the  $\text{pK}_a$  of the corresponding free ligand of the  $\text{Co}(\text{II})$  complexes **2–8** of this study. Data is given in Table 2.

$$\begin{aligned}
 E^\circ(\text{Co}^{\text{III/II}}) &= -0.16(2)\text{pK}_a(\text{free ligand}) \\
 &\quad - 0.8(1)E_{\text{pc}}(\text{free ligand}) + 0.33(7)E^\circ(\text{Fe}^{\text{III/II}}) \\
 &\quad - 1.4(2) \quad R^2 \\
 &= 1.00
 \end{aligned}$$

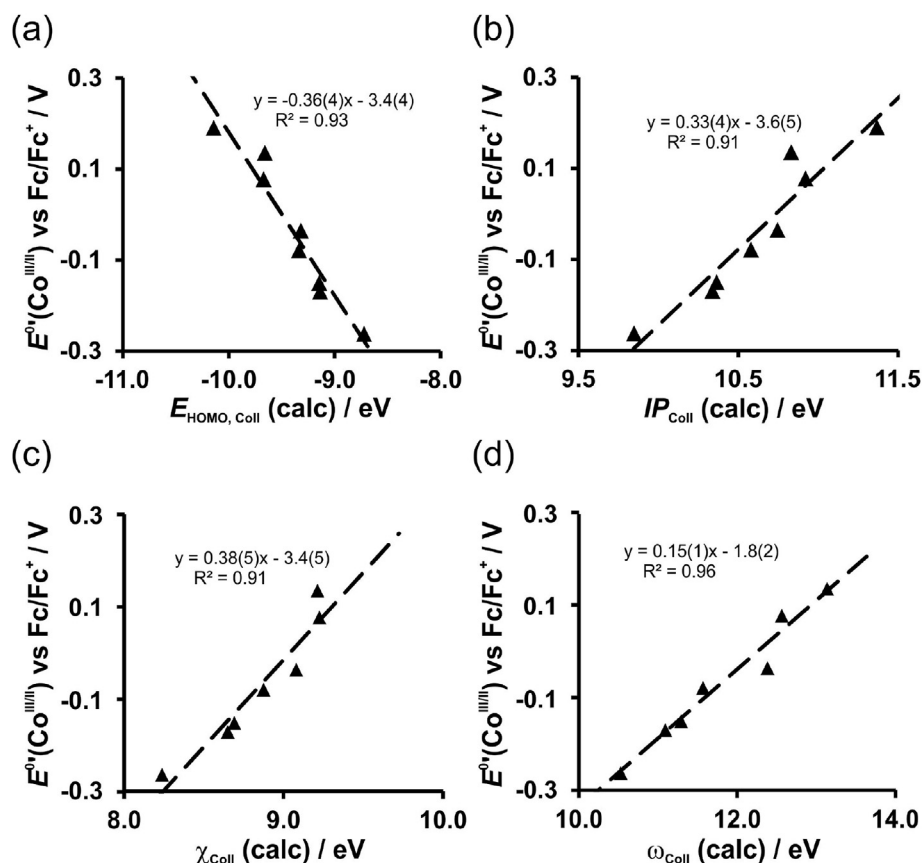
The relationship between the reversible redox potential  $E^\circ(\text{Co}^{\text{III/II}})$  that is Co-metal based, and the irreversible reduction potential of the free ligand ( $E_{\text{pc}}$ ) that is ligand based, shows a regular curved line; we however recommend applying a linear approximation, which also gives acceptable results (Fig. 7 b), especially for our purpose, where the aim is to evaluate redox potentials of analogous species. The slope of the graph between redox couple  $E^\circ(\text{Co}^{\text{III/II}})$  and the  $\text{pK}_a$  of the free uncoordinated ligand (Fig. 7a) and the other redox couple  $E^\circ(\text{Co}^{\text{II/I}})$  and the same  $\text{pK}_a$  of the free uncoordinated ligand (Fig. 7d) is very similar, according to expectation, due to the same influence of the ligands on the electron density of  $\text{Co}^{\text{II}}$  in complexes **1–8**. Since the reduction of complex **1** does not involve Co, but is  $\text{NO}_2$  ligand based instead (see Section 3.2), data of complex **1** is not used when considering relationships involving  $E^\circ(\text{Co}^{\text{II/I}})$ .

The linear relationships between both the redox potentials  $E^\circ(\text{Co}^{\text{III/II}})$  and  $E^\circ(\text{Fe}^{\text{III/II}})$  in Fig. 7(c), show that the electronic influence of the differently substituted phenantrolines on the different metals which they are coordinated to (Co or Fe), is very similar for both metals. The relationship obtained between the redox values  $E^\circ(\text{Co}^{\text{III/II}})$  and  $E^\circ(\text{Fe}^{\text{III/II}})$ , for the same ligands complexed to different metals, can be used to forecast the experimental

redox potential data for any new customized  $\text{Co}(\text{L})_3^{2+}$  or  $\text{Fe}(\text{L})_3^{2+}$  complexes, enabling the identification of suitable groups to be substituted on analogous phenantrolines L for desired redox tuning of their metal complexes. Both the  $\text{Co}(\text{phen})_3^{2+}$  and  $\text{Fe}(\text{phen})_3^{2+}$  complexes have potential applications as potential mediators and dyes in DSSC (solar cells) respectively, and the relationships obtained here in Fig. 7 (as well as with theoretically calculated energies, in Fig. 8) can be used in the customized design of suitable dyes and mediators of DSSCs. The iodide/triiodide ( $\text{I}_3^-/\text{I}^-$ ) redox couple has been the preferred redox couple since the initial development of dye-sensitized solar cells, DSSC [39]. An average value obtained for  $E^\circ(\text{I}_3^-/\text{I}^-)$  in acetonitrile, is  $-0.34 \pm 0.02 \text{ V}$  vs  $\text{Fc}/\text{Fc}^+$  [40]. In order to be considered for DSSC application, alternative redox mediators may have redox potentials up to 0.5 V more positive than that of iodide/triiodide [39], implying that complexes **2–8** may qualify as possible redox mediators. However, the election of a redox couple as successful mediator, will also depend on the electronic properties of the specific dye in a given cell [5].

### 3.3.2. Relationships with calculated values

The oxidation potential of a molecule is generally related to its ionization potential (IP), since the oxidation potential is the energy needed to move an electron from the HOMO of the solution species into the electrode, while the IP is the amount of energy required to remove a HOMO electron from an isolated gaseous molecule to form a cation. From the Koopmans' theorem [41], also applicable to the Kohn-Sham orbital energies of DFT calculations [42–44], it follows that the lowest ionization energy (IP) of a molecular system is related to the negative of the energy of its HOMO ( $-E_{\text{HOMO}}$ ). The



**Fig. 8.** Relationships obtained between the redox potential  $E^\circ$  (vs  $\text{Fc/Fc}^+$ ) of the  $\text{Co}^{\text{III/II}}$  redox couple of complexes **1–8** of this study and the gas phase BP86/TZP (a) calculated HOMO energies ( $E_{\text{HOMO}}$ ), (b) calculated ionization potential (IP), (c) calculated Mulliken electronegativity ( $\chi$ ) and (d) the calculated global electrophilicity index ( $\omega$ ). Data is given in Table 2.

theorem was later extended to also relate electron affinity (EA) to the energy of the LUMO ( $-E_{\text{LUMO}}$ ) [45,46]. Thus oxidation potential, ionization potential and HOMO energies are all related. Similarly, reduction potential, electron affinity and LUMO energies also are related. The relationship between both the experimental  $E^\circ(\text{Co}^{\text{III/II}})$  and  $E^\circ(\text{Co}^{\text{II/I}})$  potentials of complexes **1–8** and the theoretically calculated energies, are shown in Figs. 8 and 9 respectively. During oxidation, an electron will be removed more easily from a higher energy HOMO, i.e. it will be oxidized more easily at a lower, less positive (more negative) redox potential. Similarly, during reduction, an electron will be added with more difficulty to a higher energy LUMO, i.e. it will be more difficult to be reduced at a less positive (more negative) redox potential. The relationship between the  $E^\circ(\text{Co}^{\text{III/II}})$  oxidation and the energy of the HOMO of  $\text{Co}(\text{II})$ , is shown in Fig. 8(a), while the relationship between the  $E^\circ(\text{Co}^{\text{II/I}})$  reduction and the energy of the LUMO of  $\text{Co}(\text{II})$ , is shown in Fig. 9(a), while Fig. 9(e) shows the relationship of the  $E^\circ(\text{Co}^{\text{II/I}})$  reduction with the energy of the HOMO of  $\text{Co}(\text{I})$ . These three relationships result in the following linear mathematical relationships:

$$E^\circ(\text{Co}^{\text{III/II}}) = -0.36(4)E_{\text{HOMO}}(\text{Co}^{\text{II}}) - 3.4(4) \quad R^2 = 0.93$$

$$E^\circ(\text{Co}^{\text{II/I}}) = -0.30(8)E_{\text{LUMO}}(\text{Co}^{\text{II}}) - 4.0(7) \quad R^2 = 0.75$$

$$E^\circ(\text{Co}^{\text{II/I}}) = -0.42(3)E_{\text{HOMO}}(\text{Co}^{\text{I}}) - 3.9(2) \quad R^2 = 0.97$$

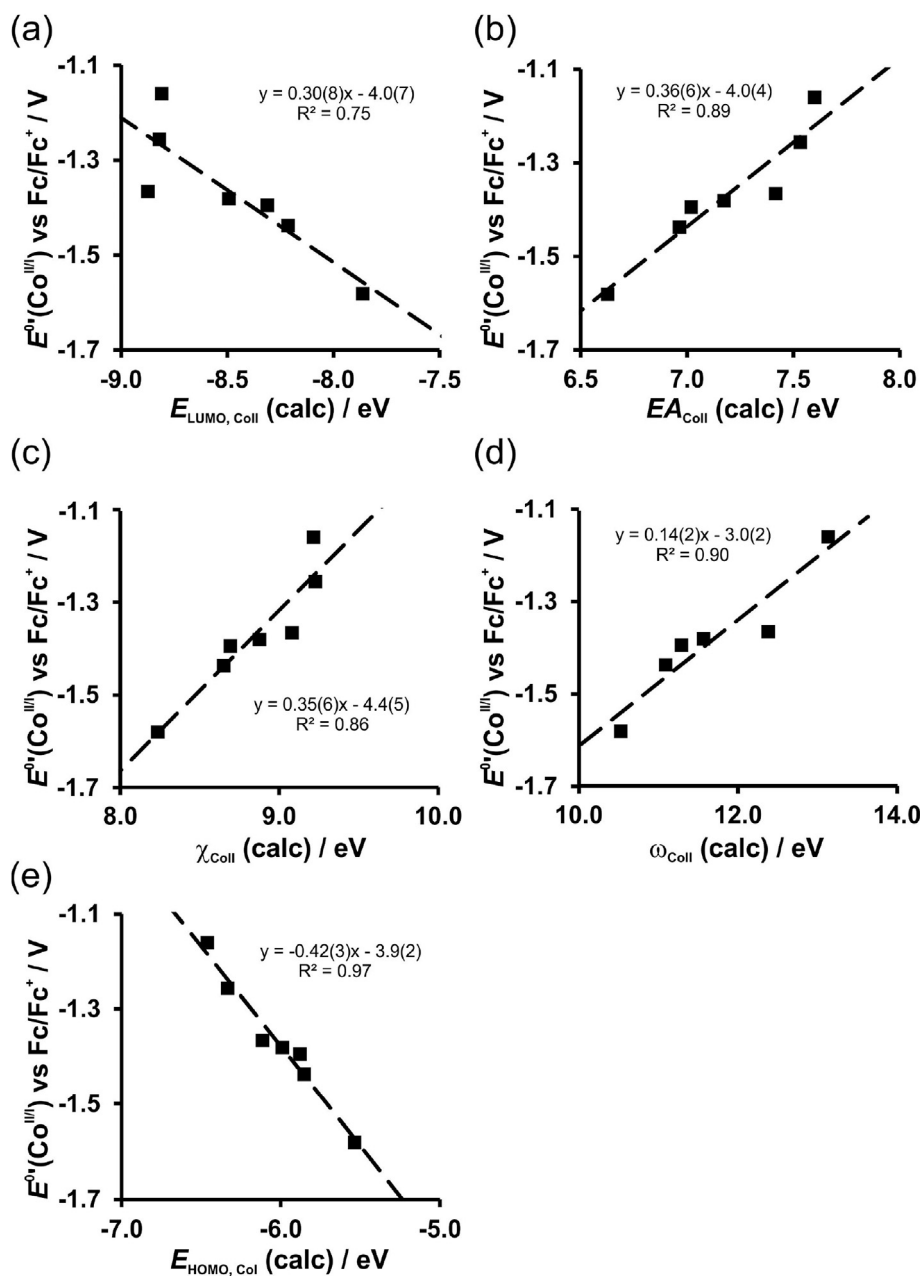
Oxidation or reduction of the  $\text{Co}(\text{phen})_3^{2+}$  complexes **1–8**, are

also linearly related to either the gas phase calculated adiabatic ionization potential ( $\text{IP}_{\text{calc}}$  for oxidation) or to the adiabatic electron affinity ( $\text{EA}_{\text{calc}}$  for reduction), as shown in Figs. 8(b) and 9(b) respectively, namely:

$$E^\circ(\text{Co}^{\text{III/II}}) = 0.33(4)\text{IP}(\text{Co}^{\text{II}}) - 3.6(5) \quad R^2 = 0.91$$

$$E^\circ(\text{Co}^{\text{II/I}}) = 0.36(6)\text{EA}(\text{Co}^{\text{II}}) - 4.0(4) \quad R^2 = 0.89$$

To obtain either the  $\text{IP}_{\text{calc}}$  or the  $\text{EA}_{\text{calc}}$  values, the oxidized  $\text{Co}(\text{phen})_3^{3+}$  complexes (for  $\text{IP}_{\text{calc}}$ ,  $\text{Coll}$ ), or the reduced  $\text{Co}(\text{phen})_3^{+}$  complexes (for  $\text{EA}_{\text{calc}}$ ,  $\text{Coll} = \text{IP}_{\text{calc}}$ ,  $\text{Coll}$ ) were also optimized, for all complexes **1–8**. Further calculations from these calculated EA and IP values produce the Mulliken electronegativity ( $\chi$ , a measure of the tendency of an atom or molecule to attract electrons [24]) and the global electrophilicity index ( $\omega$ , a measure of the electrophilic power of atoms and molecules) of the  $\text{Co}(\text{II})$  complexes. Relationships between the experimental  $E^\circ(\text{Co}^{\text{III/II}})$  and  $E^\circ(\text{Co}^{\text{II/I}})$  values with these calculated  $\chi_{\text{calc}}$  and  $\omega_{\text{calc}}$  values, are shown in Fig. 8(c) and (d) for the  $E^\circ(\text{Co}^{\text{III/II}})$  redox couple, and in Fig. 9(c) and (d) for the  $E^\circ(\text{Co}^{\text{II/I}})$  redox couple. Linear fits (with  $R^2$  values  $> 0.91$ ) are obtained for relationships involving  $E^\circ(\text{Co}^{\text{III/II}})$ , while relationships involving  $E^\circ(\text{Co}^{\text{II/I}})$  are slightly less accurate (with  $R^2$  values  $> 0.75$ ). A better fit ( $R^2 = 0.97$ ) is obtained between  $E^\circ(\text{Co}^{\text{II/I}})$  and the energy of the HOMO of  $\text{Co}(\text{I})$  (the MO from where the electron is removed upon  $E^\circ(\text{Co}^{\text{II/I}})$  oxidation), than between  $E^\circ(\text{Co}^{\text{II/I}})$  and the energy of the LUMO of  $\text{Co}(\text{II})$  (the MO where the electron is added upon  $E^\circ(\text{Co}^{\text{II/I}})$  reduction) with ( $R^2 = 0.75$ ). The  $R^2$  value of the latter increases slightly when a solvent is taken into account during the



**Fig. 9.** Relationships obtained between the redox potential  $E^\circ$  (vs Fc/Fc<sup>+</sup>) of the Co<sup>III/II</sup> redox couple of complexes **2–8** of this study and the gas phase BP86/TZP (a) calculated LUMO energies of Co<sup>II</sup> ( $E_{\text{LUMO}}$ ), (b) calculated electron affinity (EA), (c) calculated Mulliken electronegativity ( $\chi$ ), (d) the calculated global electrophilicity index ( $\omega$ ) and (e) calculated HOMO energies of Co<sup>I</sup> ( $E_{\text{HOMO}}$ ). Data is given in Table 2.

DFT calculations, see section 3.3.3 below.

For the Co<sup>III/II</sup> redox couple, a multilinear regression of the dependence of  $E^\circ(\text{Co}^{\text{III/II}})$  on the three DFT calculated energies  $E_{\text{HOMO}}(\text{Co}^{\text{II}})$ ,  $\text{IP}(\text{Co}^{\text{II}})$  and  $\text{EA}(\text{Co}^{\text{II}})$  for all complexes **1–8**, results in the following equation:

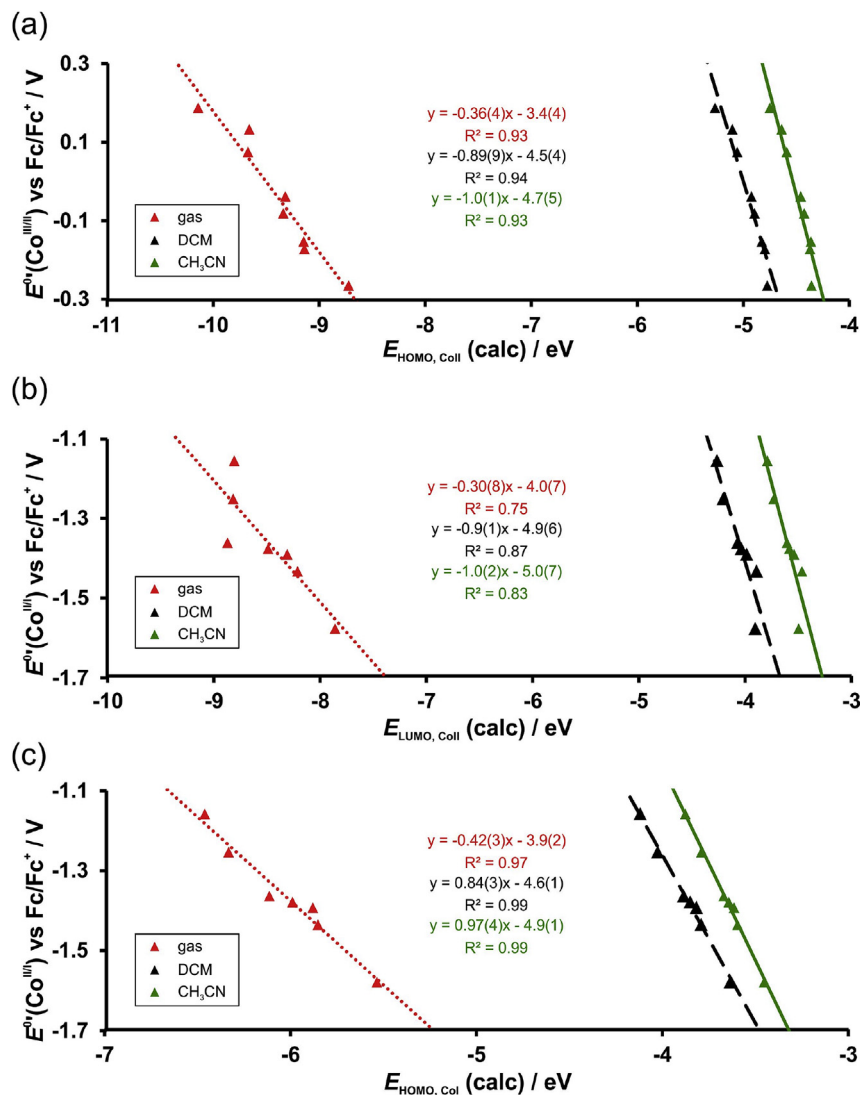
$$E^\circ(\text{Co}^{\text{III/II}}) = -0.34(6)E_{\text{HOMO}}(\text{Co}^{\text{II}}) + 0.43(7)\text{IP}(\text{Co}^{\text{II}}) + 0.53(7)\text{EA}(\text{Co}^{\text{II}}) - 2.5(2) \quad R^2 = 1.00$$

Similarly for the Co<sup>III/I</sup> redox couple, a multilinear regression of the dependence of  $E^\circ(\text{Co}^{\text{III/I}})$  on the DFT calculated  $E_{\text{LUMO}}(\text{Co}^{\text{II}})$  and  $\text{EA}(\text{Co}^{\text{II}})$  energies, as well as of  $E^\circ(\text{Co}^{\text{III/I}})$  on the DFT calculated

$E_{\text{HOMO}}(\text{Co}^{\text{I}})$  and  $\text{IP}(\text{Co}^{\text{I}})$  (which is the same as  $\text{EA}(\text{Co}^{\text{II}})$ ), for complexes **2–8**, gives the following linear equations:

$$E^\circ(\text{Co}^{\text{III/I}}) = -0.5(1)E_{\text{LUMO}}(\text{Co}^{\text{II}}) + 0.9(1)\text{EA}(\text{Co}^{\text{II}}) - 3.5(2) \quad R^2 = 0.97$$

$$E^\circ(\text{Co}^{\text{III/I}}) = -0.7(1)E_{\text{HOMO}}(\text{Co}^{\text{I}}) + 0.3(1)\text{IP}(\text{Co}^{\text{I}}) - 3.7(2) \quad R^2 = 1.00$$



**Fig. 10.** Selected relationships obtained between the redox potential for (a) the oxidation and (b–c) the reduction of  $\text{Co}(\text{II})$  complexes **1–8** of this study, with the indicated BP86/TZP calculated energies ( $E_{\text{HOMO}}(\text{Co}^{\text{II}})$ ,  $E_{\text{LUMO}}(\text{Co}^{\text{II}})$  and  $E_{\text{HOMO}}(\text{Co}^{\text{I}})$ ), as obtained both with gas phase calculations (red), as well as with calculations in DCM as solvent (black) and  $\text{CH}_3\text{CN}$  as solvent (green). (For interpretation of the references to colour in this figure legend, the reader is referred to the Web version of this article.)

Once again, a better fit ( $R^2 = 1.00$ ) is obtained when using HOMO energies, rather than LUMO energies, when considering relationships between  $E^\circ(\text{Co}^{\text{III/II}})$  and DFT calculated energies.

### 3.3.3. Influence of the solvent on DFT calculated values

All the above relationships were obtained from DFT calculations of the complexes in the gas phase ( $\epsilon = 1$ ). In order to determine the effect of increasingly polar solvents on the DFT calculations, full geometry optimizations were also obtained for complexes **1–8** in DCM ( $\epsilon = 8.9$ ) and  $\text{CH}_3\text{CN}$  ( $\epsilon = 37.5$ ) as solvent. Fig. 10 shows the relationship between redox potential and frontier MO energy. The results in Fig. 10 show that increasing solvent polarity leads to an increase in the slope of the graphs, from ca.  $-0.4$  (gas phase calculations) to  $-1$  (calculations in  $\text{CH}_3\text{CN}$ ), with sometimes a slight increase in the accuracy of the linear equations (improved  $R^2$  values), for example:

$$E^\circ(\text{Co}^{\text{III/II}}) = -0.36(4)E_{\text{HOMO}}(\text{Co}^{\text{II}}) - 3.4(4) \quad R^2 = 0.93(\text{gas phase})$$

$$E^\circ(\text{Co}^{\text{III/II}}) = -0.89(9)E_{\text{HOMO}}(\text{Co}^{\text{II}}) - 4.5(4) \quad R^2 = 0.94(\text{DCM})$$

$$E^\circ(\text{Co}^{\text{III/II}}) = -1.0(1)E_{\text{HOMO}}(\text{Co}^{\text{II}}) - 4.7(5) \quad R^2 = 0.93(\text{DCM})$$

Redox potentials obtained from voltammetry are employed in calculations of the HOMO level, since the HOMO energy ( $E_{\text{HOMO}}(\text{Co}^{\text{II}})$ ) is related directly to the absolute oxidation potential [42–44,47]. By multiplying the HOMO energy with the electron charge ( $-1$ ), the absolute oxidation potential in eV is obtained. This can be seen from the slope of  $-1$  of the graph between  $E^\circ(\text{Co}^{\text{III/II}})$  and  $E_{\text{HOMO}}(\text{Co}^{\text{II}})$ , as calculated in the experimental solvent  $\text{CH}_3\text{CN}$ . The intercept of the graph should be equal to the electron energy at the origin of the scale, in this case at the absolute potential of  $\text{Fc}^+/\text{Fc}$ . High-level *ab initio* molecular orbital theory benchmark calculated values for the absolute redox potentials of the  $\text{Fc}^+/\text{Fc}$  couple in acetonitrile, are either 4.988 V (calculated at the G3(MP2)-RAD-Full-TZ level, using gas-phase energies and COSMO-RS solvation energies) [48], or otherwise +4.97 V (calculated at the SMD-B3LYP-



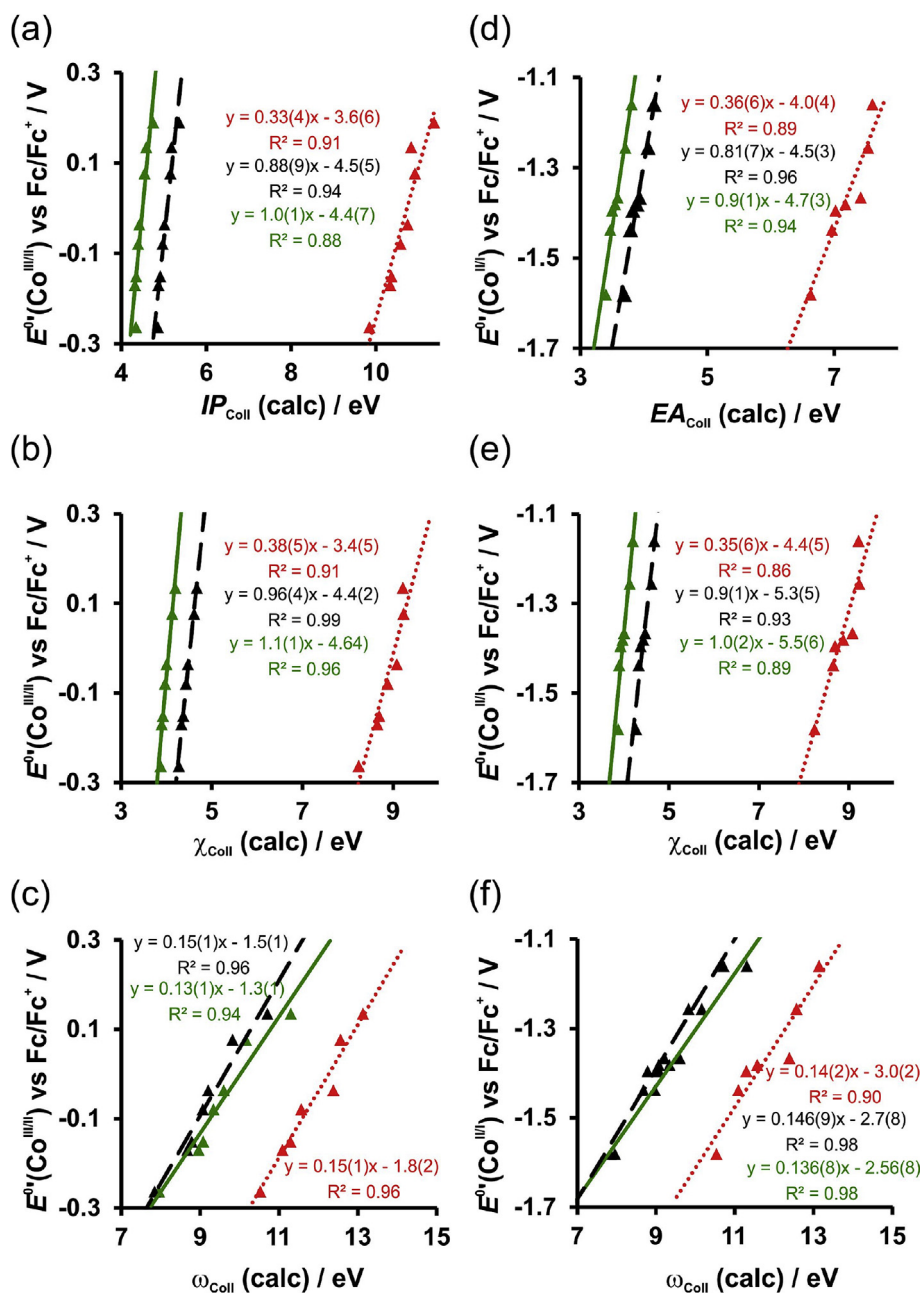
D2/def2-QZVPPD//B3LYP/LanL2TZf/6-31G(d) level) [49]. In this study we obtained a value of +4.75 V, which is very close to both reported values, see Fig. 10(a).

Similarly for the LUMO level, when evaluating either the slope of the graphs of  $E^{\circ}(\text{Co}^{\text{III/I}})$  vs  $E_{\text{LUMO}}(\text{Co}^{\text{II}})$  (Fig. 10b) or the slope of the graphs of  $E^{\circ}(\text{Co}^{\text{III/I}})$  vs  $E_{\text{HOMO}}(\text{Co}^{\text{I}})$  (Fig. 10c), we observe that DFT calculations in the experimental solvent  $\text{CH}_3\text{CN}$  do result in the expected slope of  $-1$  and an y-axis intercept close to the reported values of 4.988 V [48] or +4.97 V [49]. However, in both cases relationships between redox potentials and HOMO energies (Fig. 10a and c) gave more accurate fits (better  $R^2$  values) than between redox potentials and LUMO energies:

$$E^{\circ}(\text{Co}^{\text{III/II}}) = -0.30(8)E_{\text{LUMO}}(\text{Co}^{\text{II}}) - 4.0(7) \quad R^2 = 0.75(\text{gas})$$

$$E^{\circ}(\text{Co}^{\text{III/II}}) = -0.9(1)E_{\text{LUMO}}(\text{Co}^{\text{II}}) - 4.9(6) \quad R^2 = 0.87(\text{DCM})$$

$$E^{\circ}(\text{Co}^{\text{II/I}}) = -1.0(2)E_{\text{LUMO}}(\text{Co}^{\text{II}}) - 5.0(7) \quad R^2 = 0.83(\text{CH}_3\text{CN})$$



**Fig. 11.** Selected relationships obtained between the redox potentials for (a–c) the oxidation and (d–f) the reduction of Co(II) complexes 1–8 of this study, with the indicated BP86/TZP calculated energies ( $EA_{\text{calc}}$ ,  $IP_{\text{calc}}$ ,  $\chi_{\text{calc}}$  and  $\omega_{\text{calc}}$ ), as obtained both with gas phase calculations (red), as well as with calculations in DCM as solvent (black) and  $\text{CH}_3\text{CN}$  as solvent (green). (For interpretation of the references to colour in this figure legend, the reader is referred to the Web version of this article.)

$$E^{\text{ox}}(\text{Co}^{\text{II/I}}) = -0.42(3)E_{\text{HOMO}}(\text{Co}^{\text{I}}) - 3.9(2) \quad R^2 = 0.97(\text{gas})$$

$$E^{\text{ox}}(\text{Co}^{\text{II/I}}) = -0.84(3)E_{\text{HOMO}}(\text{Co}^{\text{I}}) - 4.6(1) \quad R^2 = 0.99(\text{DCM})$$

$$E^{\text{ox}}(\text{Co}^{\text{II/I}}) = -0.97(4)E_{\text{HOMO}}(\text{Co}^{\text{I}}) - 4.9(1) \quad R^2 = 0.99(\text{CH}_3\text{CN})$$

The effect of using increasingly polar solvents in the DFT calculations, on the calculated  $\text{IP}_{\text{calc}}$  and  $\text{EA}_{\text{calc}}$  values, as well as on the Mulliken electronegativity ( $\chi$ ) and the global electrophilicity index ( $\omega$ ), is shown in Fig. 11. The linear relationships between the  $E^{\text{ox}}(\text{Co}^{\text{II/I}})$  redox potentials and the DFT calculated energies gave high  $R^2$  values ( $>0.88$ ) with no specific trend, when comparing gas phase calculations to calculations conducted in solvents DCM or  $\text{CH}_3\text{CN}$ . The relationships obtained between redox potentials and DFT calculated energies, were obtained both from gas phase and solvent calculations with similar accuracies, therefore indicating that the computationally less expensive gas phase calculations may be used if absolute potentials are not required.

#### 4. Conclusion

Theoretical DFT calculations complemented the experimental electrochemical study, by indicating the locus of the oxidation and reduction processes of this study and also by providing an impressive variation of linear relationships between the two  $\text{Co}^{\text{II/III}}$  and  $\text{Co}^{\text{II/I}}$  redox couples and their theoretically calculated energies. The DFT calculations further shed light on the character of the irreversible reduction of the tris(5-nitro-1,10-phenanthroline) cobalt(II) complex **1**, by proving that the irreversible reduction is instead based on the  $\text{NO}_2$  group of the ligand, rather than being a  $\text{Co}^{\text{II/I}}$  process, as was observed for the other complexes **2–8** of this study. Relationships obtained between redox potentials and DFT calculated energies, as obtained from both gas phase and solvent calculations, showed similar accuracies, suggesting that the computationally less expensive gas phase calculations may be used in further studies.

#### Acknowledgements

This work has received support from the South African National Research Foundation (Grant numbers 113327 and 96111) and the Central Research Fund of the University of the Free State, Bloemfontein, South Africa. The High Performance Computing facility of the UFS is acknowledged for computer time.

#### Appendix A. Supplementary data

Supplementary data to this article can be found online at <https://doi.org/10.1016/j.electacta.2018.09.151>.

#### References

- [1] H. Ferreira, M.M. Conradie, K.G. von Eschwege, J. Conradie, Electrochemical and DFT study of the reduction of substituted phenanthrolines, *Polyhedron* 122 (2017) 147–154, <https://doi.org/10.1016/j.poly.2016.11.018>.
- [2] H. Ferreira, K.G. von Eschwege, J. Conradie, Electronic properties of Fe charge transfer complexes – a combined experimental and theoretical approach, *Electrochim. Acta* 216 (2016) 339–346, <https://doi.org/10.1016/j.electacta.2016.09.034>.
- [3] G. Nord, Some properties of 2,2' - bipyridine, 1,10-phenanthroline and their metal complexes, comments on inorganic chemistry, *J. Crit. Discuss. Current Lit.* 4 (4) (1985) 193–212, <https://doi.org/10.1080/02603598508072261>.
- [4] S. Aroua, T.K. Todorova, P. Hommes, L.-M. Chamoreau, H.-U. Reissig, V. Mougél, M. Fontecave, Synthesis, characterization, and DFT analysis of bis-terpyridyl-based molecular cobalt complexes, *Inorg. Chem.* 56 (2017) 5930–5940, <https://doi.org/10.1021/acs.inorgchem.7b00595>.
- [5] F. Gajardo, B. Loeb, Spectroscopic and electrochemical properties of a series of substituted polypyridine Co(II)/Co(III) couples and their potentiality as mediators for solar cells, *J. Chil. Chem. Soc.* 56 (2) (2011) 697–701, <https://doi.org/10.4067/S0717-97072011000200016>.
- [6] Z. Yu, N. Vlachopoulos, M. Gorlov, L. Kloo, Liquid electrolytes for dye-sensitized solar cells, *J. Chem. Soc., Dalton Trans.* 40 (2011) 10289–10303, <https://doi.org/10.1039/C1DT11023C>.
- [7] A.K.C. Mengel, W. Cho, A. Breivogel, K. Char, Y.S. Kang, K. Heinze, A bis(tridentate)cobalt polypyridine complex as mediator in dye-sensitized solar cells, *Eur. J. Inorg. Chem.* (2015) 3299–3306, <https://doi.org/10.1002/ejic.201500252>.
- [8] S. Fantacci, F. De Angelis, M.K. Nazeeruddin, M. Grätzel, Electronic and optical properties of the spiro-MeOTAD hole conductor in its neutral and oxidized forms: a DFT/TDDFT investigation, *J. Phys. Chem. C* 115 (46) (2011) 23126–23133, <https://doi.org/10.1021/jp207968b>.
- [9] G. Boschloo, A. Hagfeldt, Characteristics of the iodide/triiodide redox mediator in dye-sensitized solar cells, *Accounts Chem. Res.* 42 (11) (2009) 1819–1826, <https://doi.org/10.1021/ar900138m>.
- [10] M. Grätzel, Solar energy conversion by dye-sensitized photovoltaic cells, *Inorg. Chem.* 44 (2005) 6841–6851, <https://doi.org/10.1021/ic5008371>.
- [11] A. Kuhn, K.G. von Eschwege, J. Conradie, Electrochemical and density functional theory modeled reduction of enolized 1,3-diketones, *Electrochim. Acta* 56 (2011) 6211–6218, <https://doi.org/10.1016/j.electacta.2011.03.083>.
- [12] J. Conradie, Density functional theory calculations of Rh- $\beta$ -diketonato complexes, *J. Chem. Soc., Dalton Trans.* 44 (2015) 1503–1515, <https://doi.org/10.1039/C4DT02268H>.
- [13] M.M. Conradie, J. Conradie, Electrochemical behaviour of tris( $\beta$ -diketonato) iron(III) complexes: a DFT and experimental study, *Electrochim. Acta* 152 (2015) 512–519, <https://doi.org/10.1016/j.electacta.2014.11.128>.
- [14] S. Jie, S. Zhang, K. Wedeking, W. Zhang, H. Ma, X. Lu, Y. Deng, W.-H. Sun, Cobalt(II) complexes bearing 2-imino-1,10-phenanthroline ligands: synthesis, characterization and ethylene oligomerization, *Compt. Rendus Chem.* 9 (2006) 1500–1509, <https://doi.org/10.1016/j.crci.2006.09.007>.
- [15] J.S. Judge, W.A. Baker Jr., On the Spin Equilibrium in bis(2,2',2''-terpyridine) Cobalt(II) Salts, *Inorg. Chim. Acta.* 1 (1967) 68–72, [https://doi.org/10.1016/S0020-1693\(00\)93141-4](https://doi.org/10.1016/S0020-1693(00)93141-4).
- [16] H.A. Goodwin, Spin crossover in cobalt(II) systems, *Top. Curr. Chem.* 234 (2004) 23–47, <https://doi.org/10.1007/b95411>.
- [17] The ADF program system was obtained from Scientific Computing and Modeling, Amsterdam (<http://www.scm.com/>). For a description of the methods used in ADF, see: G. teVelde, F.M. Bickelhaupt, E.J. Baerends, C.F. Guerra, S.J.A. van Gisbergen, J.G. Snijders, T.J. Ziegler, Chemistry with ADF, *J. Comput. Chem.* 22 (2001) 931–967, <https://doi.org/10.1002/jcc.1056>.
- [18] A.D. Becke, Density-functional exchange-energy approximation with correct asymptotic behavior, *Phys. Rev. A* 38 (1988) 3098–3100, <https://doi.org/10.1103/PhysRevA.38.3098>.
- [19] J.P. Perdew, Density-functional approximation for the correlation energy of the inhomogeneous electron gas, *Phys. Rev. B* 33 (1986) 8822–8824, <https://doi.org/10.1103/PhysRevB.33.8822>. Erratum: J.P. Perdew, *Physical Reviews B* 34 (1986) 7406.
- [20] A. Klamt, G. Schüürmann, COSMO: a new approach to dielectric screening in solvents with explicit expressions for the screening energy and its gradient, *J. Chem. Soc., Perkin Trans. 2* (1993) 799–805, <https://doi.org/10.1039/P29930000799>.
- [21] A. Klamt, Conductor-like screening model for real solvents: a new approach to the quantitative calculation of solvation phenomena, *J. Phys. Chem.* 99 (1995) 2224–2235, <https://doi.org/10.1021/j100007a062>.
- [22] A. Klamt, V. Jones, Treatment of the outlying charge in continuum solvation models, *J. Chem. Phys.* 105 (1996) 9972–9981, <https://doi.org/10.1063/1.472829>.
- [23] J. England, E. Bill, T. Weyhermüller, F. Neese, M. Atanasov, K. Wieghardt, Molecular and electronic structures of homoleptic six-coordinate cobalt(II) complexes of 2,2':6',2''-terpyridine, 2,2'-bipyridine, and 1,10-phenanthroline. An experimental and computational study, *Inorg. Chem.* 54 (2015) 12002–12018, <https://doi.org/10.1021/acs.inorgchem.5b02415>.
- [24] R.S. Mulliken, A new electroaffinity scale; together with data on valence states and on valence ionization potentials and electron affinities, *J. Chem. Phys.* 2 (1934) 782–793, <https://doi.org/10.1063/1.1749394>.
- [25] M.V. Putz, N. Russo, E. Sicilia, About the Mulliken electronegativity in DFT, *Theor. Chem. Accounts* 114 (2005) 38–45, <https://doi.org/10.1007/s00214-005-0641-4>.
- [26] F. de Proft, W. Langenaeker, P. Geerlings, Ab initio determination of substituent constants in a density functional theory formalism: calculation of intrinsic group electronegativity, hardness, and softness, *J. Phys. Chem.* 97 (1993) 1826–1831, <https://doi.org/10.1021/j100111a018>.
- [27] R.G. Parr, L. von Szentpály, S. Liu, Electrophilicity index, *J. Am. Chem. Soc.* 121 (1999) 1922–1924, <https://doi.org/10.1021/ja983494x>.
- [28] D.T. Sawyer, J.L. Roberts Jr., *Experimental Electrochemistry for Chemists*, John Wiley & Sons, New York, 1974, p. 54.
- [29] D.H. Evans, K.M. O'Connell, R.A. Peterson, M.J. Kelly, Cyclic voltammetry, *J. Chem. Educ.* 60 (1983) 290–293, <https://doi.org/10.1021/ed060p290>.

- [30] G. Gritzner, J. Kuta, Recommendations on reporting electrode potentials in nonaqueous solvents, *Pure Appl. Chem.* 56 (1984) 461–466, <https://doi.org/10.1351/pac198456040461>.
- [31] L.J. Kershaw Cook, F. Tuna, M.A. Halcrow, Iron(II) and cobalt(II) complexes of tris-azanyl analogues of 2,2':6',2''-terpyridine, *J. Chem. Soc., Dalton Trans.* 42 (6) (2013) 2254–2265, <https://doi.org/10.1039/c2dt31736b>.
- [32] M. Safdari, P.W. Lohse, L. Häggman, S. Frykstrand, D. Högborg, M. Rutland, R.A. Asencio, J. Gardner, L. Kloo, A. Hagfeldt, G. Boschloo, Investigation of cobalt redox mediators and effects of TiO<sub>2</sub> film topology in dye-sensitized solar cells, *RSC Adv.* 6 (2016) 56580–56588, <https://doi.org/10.1039/c6ra07107d>.
- [33] X. Xing, Y. Zhao, Y. Li, A non-aqueous redox flow battery based on tris(1,10-phenanthroline) complexes of iron(II) and cobalt(II), *J. Power Sources* 293 (2015) 778–783, <https://doi.org/10.1016/j.jpowsour.2015.06.016>.
- [34] X. Xing, D. Zhang, Y. Li, A non-aqueous all-cobalt redox flow battery using 1,10-phenanthrolinecobalt(II) hexafluorophosphate as active species, *J. Power Sources* 279 (2015) 205–209, <https://doi.org/10.1016/j.jpowsour.2015.01.011>.
- [35] S.A. Richert, P.K.S. Tsang, D.T. Sawyer, Ligand-centered redox processes for MnL<sub>3</sub>, FeL<sub>3</sub>, and CoL<sub>3</sub> complexes (L = acetylacetonate, 8-quinolate, picolinate, 2,2'-bipyridyl, 1,10-phenanthroline) and for their tetrakis(2,6-dichlorophenyl)porphyrato complexes [M(por)], *Inorg. Chem.* 28 (1989) 2471–2475, <https://doi.org/10.1021/ic00311a044>.
- [36] A.J.L. Pombeiro, Electron-donor/acceptor properties of carbynes, carbenes, vinylidenes, allenylidenes and alkynyls as measured by electrochemical ligand parameters, *J. Organomet. Chem.* 690 (2005) 6021–6040, <https://doi.org/10.1016/j.jorganchem.2005.07.111>.
- [37] R. Freitag, J. Conradie, Electrochemical and computational chemistry study of Mn(β-diketonato)<sub>3</sub> complexes, *Electrochim. Acta* 158 (2015) 418–426, <https://doi.org/10.1016/j.electacta.2015.01.147>.
- [38] R. Liu, J. Conradie, Tris(β-diketonato)chromium(III) complexes: effect of the β-diketonate ligand on the redox properties, *Electrochim. Acta* 185 (2015) 288–296, <https://doi.org/10.1016/j.electacta.2015.10.116>.
- [39] G. Boschloo, A. Hagfeldt, Characteristics of the iodide/triiodide redox mediator in dye-sensitized solar cells, *Accounts Chem. Res.* 42 (2009) 1819–1826, <https://doi.org/10.1021/ar900138m>.
- [40] X. Wang, D.M. Stanbury, The oxidation of iodide by a series of Fe(III) complexes in acetonitrile, *Inorg. Chem.* 45 (2006) 3415–3423, <https://doi.org/10.1021/ic052022y>.
- [41] T.A. Koopmans, Über die Zuordnung von Wellenfunktionen und Eigenwerten zu den Einzelnen Elektronen Eines Atoms, *Physica* 1 (1934) 104–113, [https://doi.org/10.1016/S0031-8914\(34\)90011-2](https://doi.org/10.1016/S0031-8914(34)90011-2).
- [42] J.P. Perdew, M. Levy, Significance of the highest occupied Kohn-Sham eigenvalue, *Phys. Rev. B* 56 (1997) 16021–16028, <https://doi.org/10.1103/PhysRevB.56.16021>.
- [43] M.E. Casida, Correlated optimized effective-potential treatment of the derivative discontinuity and of the highest occupied Kohn-Sham eigenvalue: a Janak-type theorem for the optimized effective-potential model, *Phys. Rev. B* 59 (1999) 4694–4698, <https://doi.org/10.1103/PhysRevB.59.4694>.
- [44] S. Hamel, P. Duffy, M.E. Casida, D.R. Salahub, Kohn–Sham orbitals and orbital energies: fictitious constructs but good approximations all the same, *J. Electron. Spectrosc. Relat. Phenom.* 123 (2002) 345–363, [https://doi.org/10.1016/S0368-2048\(02\)00032-4](https://doi.org/10.1016/S0368-2048(02)00032-4).
- [45] U. Bozkaya, Accurate electron affinities from the extended koopmans' theorem based on orbital-optimized methods, *J. Chem. Theor. Comput.* 10 (2014) 2041–2048, <https://doi.org/10.1021/ct500186j>.
- [46] N. Heinrich, W. Koch, G. Frenking, On the use of koopmans' theorem to estimate negative electron affinities, *Chem. Phys. Lett.* 124 (1986) 20–25, [https://doi.org/10.1016/0009-2614\(86\)85005-9](https://doi.org/10.1016/0009-2614(86)85005-9).
- [47] C.M. Cardona, W. Li, A.E. Kaifer, D. Stockdale, G.C. Bazan, Electrochemical considerations for determining absolute frontier orbital energy levels of conjugated polymers for solar cell applications, *Adv. Mater.* 23 (2011) 2367–2371, <https://doi.org/10.1002/adma.201004554>.
- [48] M. Namazian, C.Y. Lin, M.L. Coote, Benchmark calculations of absolute reduction potential of ferricinium/ferrocene couple in nonaqueous solutions, *J. Chem. Theor. Comput.* 6 (2010) 2721–2725, <https://doi.org/10.1021/ct1003252>.
- [49] P.P. Romańczyk, G. Rotko, S.S. Kurek, The redox potential of the phenyl radical/anion couple and the effect there on of the lithium cation: a computational study, *Electrochem. Commun.* 48 (2014) 21–23, <https://doi.org/10.1016/j.elecom.2014.08.003>.
- [50] M.T. Ramírez-Silva, M. Gómez-Hernández, M.deL. Pacheco-Hernández, A. Rojas-Hernández, L. Galicia, Spectroscopy study of 5-amino-1,10-phenanthroline, *Spectrochim. Acta, Part A* 60 (4) (2004) 781–789, [https://doi.org/10.1016/S1386-1425\(03\)00301-9](https://doi.org/10.1016/S1386-1425(03)00301-9).
- [51] L. Gasque, G. Medina, L. Ruiz-Ramírez, R. Moreno-Esparza, Cu–O stretching frequency correlation with phenanthroline pK<sub>a</sub> values in mixed copper complexes, *Inorg. Chim. Acta* 288 (1999) 106–111, [https://doi.org/10.1016/S0020-1693\(99\)00034-1](https://doi.org/10.1016/S0020-1693(99)00034-1).
- [52] V. Ramírez-Delgado, M. Cruz-Ramírez, L.F. Hernández-Ayala, Y. Reyes-Vidal, R. Patakfalvi, J.C. García-Ramos, F.J. Tenorio, L. Ruiz-Azuara, L. Ortiz-Frade, The role of the π acceptor character of polypyridine ligands on the electrochemical response of Co(II) complexes and its effect on the homogenous electron transfer rate constant with the enzyme glucose oxidase, *J. Mexican Chem. Soc.* 59 (2015) 282–293, <http://www.redalyc.org/articulo.oa?id=47545630006>.
- [53] A.A. Schilt, G.F. Smith, Acid dissociation constants of substituted 1,10-phenanthrolines, *J. Phys. Chem.* 60 (1956) 1546–1548, <https://doi.org/10.1021/j150545a017>.
- [54] R.C. Conrad, J.V. Rund, Effect of basicity of nonreacting ligands on the rate of reaction of dithioamide with dichloro(phenanthroline)platinum(II) derivatives, *Inorg. Chem.* 11 (1972) 129–134, <https://doi.org/10.1021/ic50107a029>.



CrossMark

# Electrochemical data of Co(II) complexes containing phenanthroline functionalized ligands

Hendrik Ferreira, Marrigje M. Conradie, Jeanet Conradie\*

Department of Chemistry, University of the Free State, PO Box 339, Bloemfontein 9300, South Africa

## ARTICLE INFO

### Article history:

Received 26 September 2018

Received in revised form

8 October 2018

Accepted 15 October 2018

Available online 19 October 2018

## ABSTRACT

The data presented in this paper are related to the research article entitled “*Electrochemical properties of a series of Co(II) complexes, containing substituted phenanthrolines*” (Ferreira et al., 2018) [1]. This paper presents detailed electrochemical data of eight octahedral Co(II) complexes containing functionalized phenanthrolines-ligands. The data illustrate the shift in the Co<sup>III/II</sup> and Co<sup>II/I</sup> redox couples due to different substituents on the phenanthrolines. Polypyridine Co(II) and Co(III) complexes exhibit properties as potential mediators in dye-sensitized solar cells (DSSCs) (Gajardo and Loeb, 2011; Yu et al., 2011) [2,3]. The ability of a compound to act as a redox mediator to be used in DSSC, depends on the redox potential of the compound (Grätzel, 2005) [4]. Accurate data of the Co<sup>III/II</sup> redox couple is presented here.

© 2018 The Authors. Published by Elsevier Inc. This is an open access article under the CC BY license (<http://creativecommons.org/licenses/by/4.0/>).

## Specifications table

Subject area	Chemistry
More specific subject area	Electrochemistry
Type of data	Table, text file, graph, figure
How data was acquired	BAS 100B/W electrochemical analyzer (Electrochemical studies).
Data format	Raw and Analyzed.

DOI of original article: <https://doi.org/10.1016/j.electacta.2018.09.151>

\* Corresponding author.

E-mail address: [conradj@ufs.ac.za](mailto:conradj@ufs.ac.za) (J. Conradie).

<https://doi.org/10.1016/j.dib.2018.10.046>

2352-3409/© 2018 The Authors. Published by Elsevier Inc. This is an open access article under the CC BY license (<http://creativecommons.org/licenses/by/4.0/>).

Experimental factors	Samples was used as synthesized. The solvent-electrolyte solution in the electrochemical cell was degassed with Ar for 10 min, the sample was added, the sample-solvent-electrolyte solution was then degassed for another 2 min and the cell was kept under a blanket of purified argon during the electrochemical experiments.
Experimental features	All electrochemical experiments were done in a 2 ml electrochemical cell containing three-electrodes (a glassy carbon working electrode, a Pt auxiliary electrode and a Ag/Ag <sup>+</sup> reference electrode), connected to a BAS 100B/W electrochemical analyzer. Data obtained were exported to excel for analysis and diagram preparation.
Data source location	Department of Chemistry, University of the Free State, Nelson Mandela street, Bloemfontein, South Africa.
Data accessibility	Data is with article.
Related research article	Hendrik Ferreira, Marrigje M. Conradie and Jeanet Conradie, <i>Electrochemical properties of a series of Co(II) complexes, containing substituted phenanthrolines</i> , <i>Electrochimica Acta</i> 292 (2018) 489–501. DOI:10.1016/j.electacta.2018.09.151.

### Value of the data

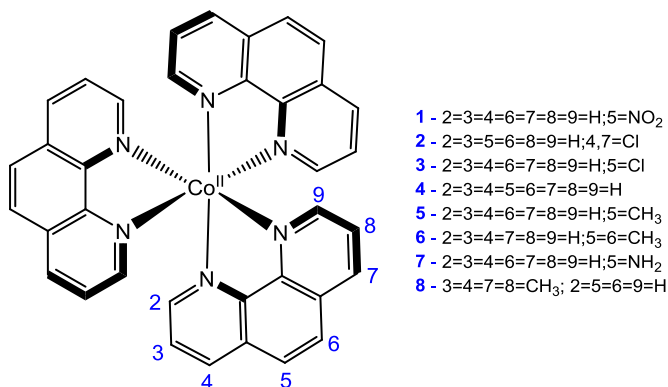
- This data provide cyclic voltammograms and detailed electrochemical data for a comprehensive series of eight functionalized phenanthroline-Co(II) complexes, for scan rates over two orders of magnitude (0.05–5.0 V s<sup>−1</sup>).
- This data illustrate the influence of differently functionalized phenanthroline ligands on the redox potential of the metal they are coordinated to.
- This data illustrate that up to three reversible redox couples can be obtained in acetonitrile as solvent for tris(1,10-phenanthroline)Cobalt(II) and differently functionalized phenanthroline-Co(II) complexes.

## 1. Data

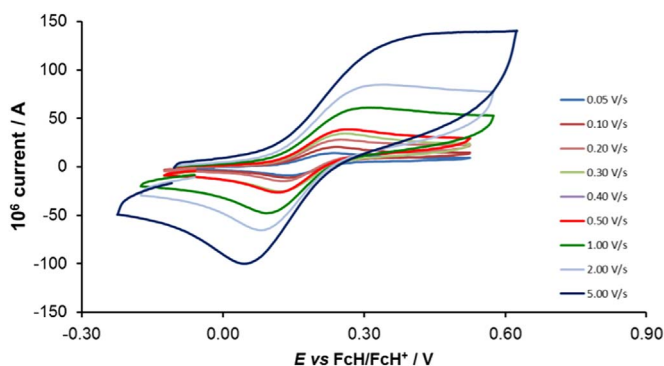
The data presented in this paper are related to the research article entitled “*Electrochemical properties of a series of Co(II) complexes, containing substituted phenanthrolines*” [1]. This paper presents detailed electrochemical data of eight octahedral Co(II) complexes containing functionalized phenanthrolines-ligands. Polypyridine Co(II) and Co(III) complexes exhibit properties as potential mediators in dye-sensitized solar cells (DSSCs) [2,3]. The ability of a compound to act as a redox mediator to be used in DSSC, depends on the redox potential of the compound [4]. The data of the eight functionalized phenanthroline-Co(II) complexes, namely tris(5-nitro-1,10-phenanthroline)Cobalt(II) nitrate, [Co(5-NO<sub>2</sub>-phen)<sub>3</sub>](NO<sub>3</sub>)<sub>2</sub> (**1**), tris(4,7-dichloro-1,10-phenanthroline)Cobalt(II) nitrate, [Co(4,7-di-Cl-phen)<sub>3</sub>](NO<sub>3</sub>)<sub>2</sub> (**2**), tris(5-chloro-1,10-phenanthroline)Cobalt(II) nitrate, [Co(5-Cl-phen)<sub>3</sub>](NO<sub>3</sub>)<sub>2</sub> (**3**), tris(1,10-phenanthroline)Cobalt(II) nitrate, [Co(phen)<sub>3</sub>](NO<sub>3</sub>)<sub>2</sub> (**4**), tris(5-methyl-1,10-phenanthroline)Cobalt(II) nitrate, [Co(5-Me-phen)<sub>3</sub>](NO<sub>3</sub>)<sub>2</sub> (**5**), tris(5,6-dimethyl-1,10-phenanthroline)Cobalt(II) nitrate, [Co(5,6-di-Me-phen)<sub>3</sub>](NO<sub>3</sub>)<sub>2</sub> (**6**), tris(1,10-phenanthroline-5-amine)Cobalt(II) nitrate, [Co(5-NH<sub>2</sub>-phen)<sub>3</sub>](NO<sub>3</sub>)<sub>2</sub> (**7**) and tris(3,4,7,8-tetramethyl-1,10-phenanthroline)Cobalt(II) nitrate, [Co(3,4,7,8-Me-phen)<sub>3</sub>](NO<sub>3</sub>)<sub>2</sub> (**8**), is presented in this contribution, see Fig. 1 for the structures of **1–8**.

Cyclic voltammograms of the complexes **1–8**, are presented in Figs. 2–9 and tabulated in Tables 1–8. The electrochemical data is obtained in CH<sub>3</sub>CN for ca 0.002 mol dm<sup>−3</sup> (or saturated) analyte solution. Complexes **3–8**, all have three reversible peaks, namely the Co<sup>III/II</sup> redox couple (peak 1), the Co<sup>III/I</sup> redox couple (peak 2) and the ligand reduction peak (peak 3). For complex **2** the ligand reduction peak (peak 3) is irreversible and for complex **1** the irreversible peak 2 is NO<sub>2</sub>-ligand based. Data at scan rates 0.05–5.00 V s<sup>−1</sup> are provided. Data for the irreversible anionic nitrate oxidation peak at ca 1.63 V vs FcH/FcH<sup>+</sup>, is not included in the tables. The data obtained in this study,

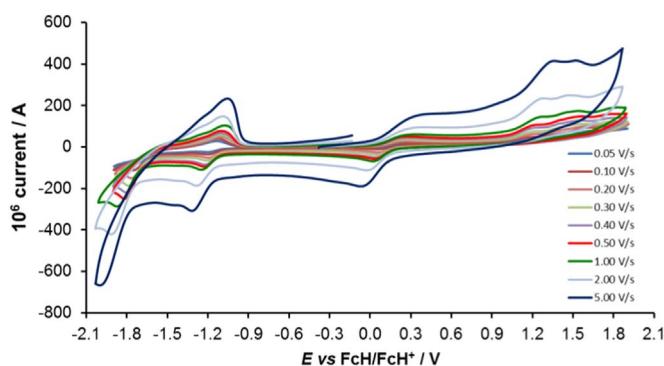




**Fig. 1.** Structure and complex numbering of the functionalized phenanthroline-Co(II) complexes.

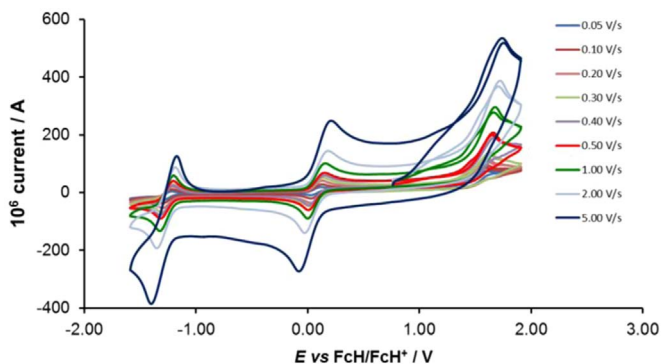


**Fig. 2.** Cyclic voltammograms of complex 1 at scan rates of 0.05 V s<sup>-1</sup> (lowest peak current) – 5.00 V s<sup>-1</sup> (highest peak current). All scans initiated in the positive direction.

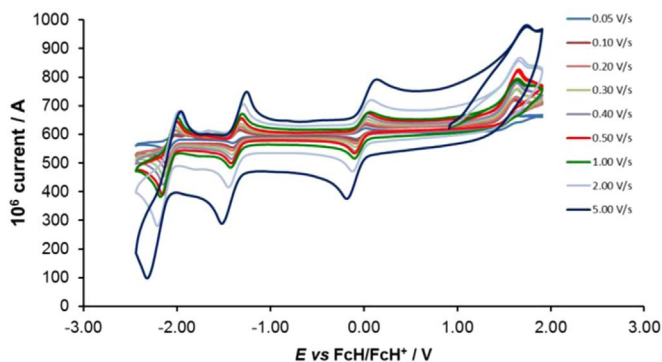


**Fig. 3.** Cyclic voltammograms of complex 2 at scan rates of 0.05 V s<sup>-1</sup> (lowest peak current) – 5.00 V s<sup>-1</sup> (highest peak current). All scans initiated in the positive direction.

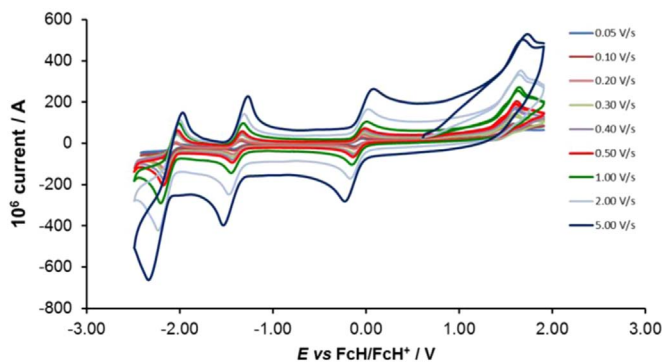
compare good with available published data on some of the complexes, namely complex **2** [5], complex **4** [6–9], complex **7** [9] and complex **8** [9], obtained under different experimental conditions (different solvents, scan rates and supporting electrolytes).



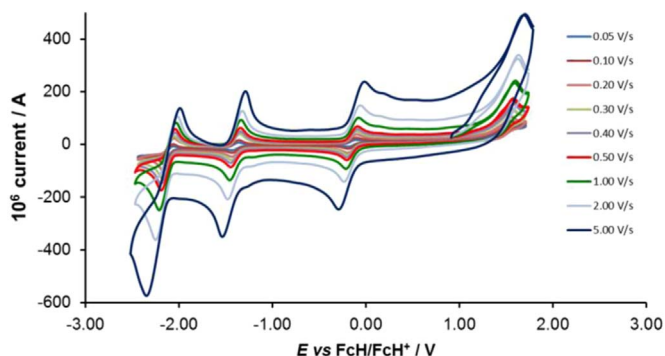
**Fig. 4.** Cyclic voltammograms of complex 3 at scan rates of  $0.05 \text{ V s}^{-1}$  (lowest peak current) –  $5.00 \text{ V s}^{-1}$  (highest peak current). All scans initiated in the positive direction.



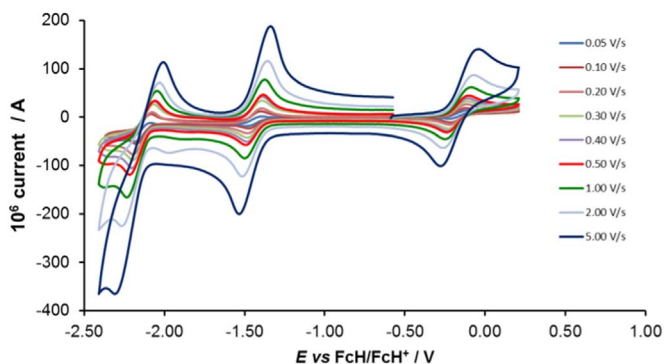
**Fig. 5.** Cyclic voltammograms of complex 4 at scan rates of  $0.05 \text{ V s}^{-1}$  (lowest peak current) –  $5.00 \text{ V s}^{-1}$  (highest peak current). All scans initiated in the positive direction.



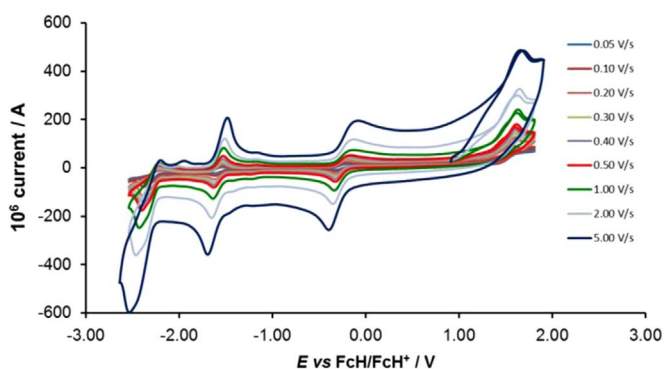
**Fig. 6.** Cyclic voltammograms of complex 5 at scan rates of  $0.05 \text{ V s}^{-1}$  (lowest peak current) –  $5.00 \text{ V s}^{-1}$  (highest peak current). All scans initiated in the positive direction.



**Fig. 7.** Cyclic voltammograms of complex 6 at scan rates of  $0.05 \text{ V s}^{-1}$  (lowest peak current) –  $5.00 \text{ V s}^{-1}$  (highest peak current). All scans initiated in the positive direction.



**Fig. 8.** Cyclic voltammograms of complex 7 at scan rates of  $0.05 \text{ V s}^{-1}$  (lowest peak current) –  $5.00 \text{ V s}^{-1}$  (highest peak current). All scans initiated in the positive direction.



**Fig. 9.** Cyclic voltammograms of complex 8 at scan rates of  $0.05 \text{ V s}^{-1}$  (lowest peak current) –  $5.00 \text{ V s}^{-1}$  (highest peak current). All scans initiated in the positive direction.



**Table 1**

Electrochemical data (potential in V vs FcH/FcH<sup>+</sup>) in CH<sub>3</sub>CN for ca 0.002 mol dm<sup>−3</sup> of complex 1 at indicated scan rates in V s<sup>−1</sup>. Peak 1 is the Co<sup>III/II</sup> redox couple.

	Scan rate/Vs <sup>−1</sup>	<i>E</i> <sub>pa</sub> /V vs FcH/FcH <sup>+</sup>	<i>E</i> <sub>pc</sub> /V vs FcH/FcH <sup>+</sup>	<i>E</i> <sup>o</sup> /V vs FcH/FcH <sup>+</sup>	Δ <i>E</i> /V
Peak 1	0.05	0.275	0.110	0.165	0.193
	0.10	0.290	0.115	0.175	0.203
	0.20	0.320	0.120	0.200	0.220
	0.30	0.290	0.110	0.180	0.200
	0.40	0.300	0.110	0.190	0.205
	0.50	0.300	0.105	0.195	0.203
	1.00	0.330	0.095	0.235	0.213
	2.00	0.415	0.050	0.365	0.233
	5.00	0.560	0.005	0.555	0.283

**Table 2**

Electrochemical data (potential in V vs FcH/FcH<sup>+</sup>) in CH<sub>3</sub>CN for ca 0.002 mol dm<sup>−3</sup> of complex 2 at indicated scan rates in V s<sup>−1</sup>. Peak 1 is the Co<sup>III/II</sup> redox couple, peak 2 the Co<sup>II/I</sup> redox couple.

	Scan rate/V s <sup>−1</sup>	<i>E</i> <sub>pa</sub> /V vs FcH/FcH <sup>+</sup>	<i>E</i> <sub>pc</sub> /V vs FcH/FcH <sup>+</sup>	<i>E</i> <sup>o</sup> /V vs FcH/FcH <sup>+</sup>	Δ <i>E</i> /V
Peak 1	0.10	0.200	0.070	0.130	0.135
	0.20	0.260	0.070	0.190	0.165
	0.30	0.250	0.050	0.200	0.150
	0.40	0.270	0.050	0.220	0.160
	0.50	0.260	0.030	0.230	0.145
	1.00	0.300	0.020	0.280	0.160
	2.00	0.380	0.000	0.380	0.190
	5.00	0.400	−0.070	0.470	0.165
Peak 2	0.10	−1.120	−1.200	0.080	−1.160
	0.20	−1.105	−1.195	0.090	−1.150
	0.30	−1.105	−1.200	0.095	−1.153
	0.40	−1.100	−1.210	0.110	−1.155
	0.50	−1.100	−1.225	0.125	−1.163
	1.00	−1.080	−1.250	0.170	−1.165
	2.00	−1.075	−1.260	0.185	−1.168
	5.00	−1.060	−1.310	0.250	−1.185

For Co(5-NO<sub>2</sub>-phen)<sub>3</sub><sup>2+</sup> complex 1, see Fig. 2 and Table 1.

For Co(4,7-di-Cl-phen)<sub>3</sub><sup>2+</sup> complex 2, see Fig. 3 and Table 2.

For Co(5-Cl-phen)<sub>3</sub><sup>2+</sup> complex 3, see Fig. 4 and Table 3.

For Co(phen)<sub>3</sub><sup>2+</sup> complex 4, see Fig. 5 and Table 4.

For Co(5-Me-phen)<sub>3</sub><sup>2+</sup> complex 5, see Fig. 6 and Table 5.

For Co(5,6-Me-phen)<sub>3</sub><sup>2+</sup> complex 6, see Fig. 7 and Table 6.

For Co(5-NH<sub>2</sub>-phen)<sub>3</sub><sup>2+</sup> complex 7, see Fig. 8 and Table 7.

For Co(3,4,7,8-Me-phen)<sub>3</sub><sup>2+</sup> complex 8, see Fig. 9 and Table 8.

## 2. Experimental design, materials, and methods

Electrochemical studies by means of cyclic voltammetry (CV) were performed either on 0.002 mol dm<sup>−3</sup> or on saturated compound solutions of the complexes in dry acetonitrile, containing 0.1 mol dm<sup>−3</sup> tetra-*n*-butylammoniumhexafluorophosphate ([<sup>n</sup>(Bu<sub>4</sub>)N][PF<sub>6</sub>]) as supporting electrolyte, under a blanket of purified argon, at 25 °C, utilizing a BAS 100B/W electrochemical analyzer. A three-electrode cell was used, with a glassy carbon (surface area 7.07 × 10<sup>−6</sup> m<sup>2</sup>) working electrode, Pt auxiliary electrode and a Ag/Ag<sup>+</sup> (0.010 mol dm<sup>−3</sup> AgNO<sub>3</sub> in CH<sub>3</sub>CN) reference electrode [10],

**Table 3**

Electrochemical data (potential in V vs FcH/FcH<sup>+</sup> and current in A) in CH<sub>3</sub>CN for ca 0.002 mol dm<sup>−3</sup> of complex 3 at indicated scan rates in V s<sup>−1</sup>. Peak 1 is the Co<sup>III/II</sup> redox couple, peak 2 the Co<sup>II/I</sup> redox couple.

	Scan rate/V s <sup>−1</sup>	<i>E</i> <sub>pa</sub> /V vs FcH/FcH <sup>+</sup>	<i>E</i> <sub>pc</sub> /V vs FcH/FcH <sup>+</sup>	<i>E</i> <sup>o</sup> /V vs FcH/FcH <sup>+</sup>	Δ <i>E</i> /V	10 <sup>6</sup> <i>I</i> <sub>pa</sub> /A	<i>I</i> <sub>pc</sub> / <i>I</i> <sub>pa</sub>
Peak 1	0.05	0.108	0.034	0.071	0.074	17.5	1.0
	0.10	0.122	0.032	0.077	0.090	26.0	1.0
	0.20	0.122	0.034	0.078	0.088	39.5	1.0
	0.30	0.136	0.022	0.079	0.114	44.2	1.0
	0.40	0.142	0.016	0.079	0.126	51.4	1.1
	0.50	0.144	0.010	0.077	0.134	63.0	1.1
	1.00	0.152	0.004	0.078	0.148	87.5	1.1
	2.00	0.176	−0.024	0.076	0.200	117.0	1.1
	5.00	0.202	−0.070	0.066	0.272	200.0	1.0
Peak 2	0.05	−1.220	−1.292	−1.256	0.072	17.0	0.9
	0.10	−1.216	−1.296	−1.256	0.080	25.0	1.0
	0.20	−1.218	−1.292	−1.255	0.074	37.0	1.0
	0.30	−1.210	−1.300	−1.255	0.090	42.3	1.1
	0.40	−1.210	−1.314	−1.262	0.104	53.0	1.0
	0.50	−1.208	−1.314	−1.261	0.106	64.8	1.0
	1.00	−1.206	−1.318	−1.262	0.112	98.0	1.0
	2.00	−1.192	−1.346	−1.269	0.154	135.0	1.0
	5.00	−1.180	−1.398	−1.289	0.218	192.0	1.2

**Table 4**

Electrochemical data (potential in V vs FcH/FcH<sup>+</sup> and current in A) in CH<sub>3</sub>CN for ca 0.002 mol dm<sup>−3</sup> of complex 4 at indicated scan rates in V s<sup>−1</sup>. Peak 1 is the Co<sup>III/II</sup> redox couple, peak 2 the Co<sup>II/I</sup> redox couple and peak 3 the ligand reduction peak.

	Scan rate/Vs <sup>−1</sup>	<i>E</i> <sub>pa</sub> /V vs FcH/FcH <sup>+</sup>	<i>E</i> <sub>pc</sub> /V vs FcH/FcH <sup>+</sup>	<i>E</i> <sup>o</sup> /V vs FcH/FcH <sup>+</sup>	Δ <i>E</i> /V	10 <sup>6</sup> <i>I</i> <sub>pa</sub> /A	<i>I</i> <sub>pc</sub> / <i>I</i> <sub>pa</sub>
Peak 1	0.05	0.012	−0.076	−0.032	0.088	17.8	1.12
	0.10	0.010	−0.082	−0.036	0.092	29.5	1.08
	0.20	0.026	−0.082	−0.028	0.108	34.5	1.10
	0.30	0.032	−0.086	−0.027	0.118	44.0	1.07
	0.40	0.038	−0.092	−0.027	0.130	51.0	1.14
	0.50	0.040	−0.094	−0.027	0.134	62.0	1.13
	1.00	0.060	−0.096	−0.018	0.156	59.0	1.20
	2.00	0.074	−0.116	−0.021	0.190	82.0	1.20
	5.00	0.130	−0.180	−0.025	0.310	136.0	1.07
Peak 2	0.05	−1.326	−1.398	−1.362	0.072	22.8	0.99
	0.10	−1.328	−1.404	−1.366	0.076	32.3	1.04
	0.20	−1.322	−1.404	−1.363	0.082	41.3	0.99
	0.30	−1.318	−1.410	−1.364	0.092	54.0	0.98
	0.40	−1.316	−1.414	−1.365	0.098	60.0	1.08
	0.50	−1.314	−1.416	−1.365	0.102	76.0	1.01
	1.00	−1.304	−1.424	−1.364	0.120	81.0	0.98
	2.00	−1.292	−1.446	−1.369	0.154	99.0	1.19
	5.00	−1.256	−1.516	−1.386	0.260	150.0	1.20
Peak 3	0.05	−2.026	−2.104	−2.065	0.078	21.0	1.93
	0.10	−2.026	−2.114	−2.070	0.088	45.0	1.51
	0.20	−2.018	−2.130	−2.074	0.112	56.0	1.47
	0.30	−2.016	−2.140	−2.078	0.124	75.0	1.41
	0.40	−2.010	−2.144	−2.077	0.134	91.0	1.43
	0.50	−2.008	−2.152	−2.080	0.144	114.0	1.37
	1.00	−1.998	−2.172	−2.085	0.174	108.0	1.41
	2.00	−1.984	−2.206	−2.095	0.222	148.0	1.44
	5.00	−1.964	−2.316	−2.140	0.352	200.7	1.5

**Table 5**

Electrochemical data (potential in V vs FcH/FcH<sup>+</sup> and current in A) in CH<sub>3</sub>CN for *ca* 0.002 mol dm<sup>−3</sup> of complex 5 at indicated scan rates in V s<sup>−1</sup>. Peak 1 is the Co<sup>III/II</sup> redox couple, peak 2 the Co<sup>III</sup> redox couple and peak 3 the ligand reduction peak.

	Scan rate/V s <sup>−1</sup>	<i>E</i> <sub>pa</sub> /V vs FcH/FcH <sup>+</sup>	<i>E</i> <sub>pc</sub> /V vs FcH/FcH <sup>+</sup>	<i>E</i> <sup>o</sup> /V vs FcH/FcH <sup>+</sup>	Δ <i>E</i> /V	10 <sup>6</sup> <i>I</i> <sub>pa</sub> /A	<i>I</i> <sub>pc</sub> / <i>I</i> <sub>pa</sub>
Peak 1	0.05	−0.046	−0.118	−0.082	0.072	22.0	1.0
	0.10	−0.042	−0.116	−0.079	0.074	25.0	1.1
	0.20	−0.036	−0.122	−0.079	0.086	37.5	1.0
	0.30	−0.028	−0.126	−0.077	0.098	45.0	1.1
	0.40	−0.026	−0.130	−0.078	0.104	54.5	1.1
	0.50	−0.018	−0.134	−0.076	0.116	62.0	1.3
	1.00	0.002	−0.144	−0.071	0.146	84.0	1.1
	2.00	0.014	−0.166	−0.076	0.180	120.0	1.1
	5.00	0.070	−0.222	−0.076	0.292	188.0	1.1
Peak 2	0.05	−1.350	−1.418	−1.384	0.068	22.5	0.9
	0.10	−1.348	−1.414	−1.381	0.066	25.0	1.0
	0.20	−1.342	−1.422	−1.382	0.080	39.5	1.0
	0.30	−1.338	−1.428	−1.383	0.090	48.0	1.0
	0.40	−1.332	−1.430	−1.381	0.098	56.0	1.1
	0.50	−1.332	−1.436	−1.384	0.104	69.0	1.0
	1.00	−1.322	−1.448	−1.385	0.126	104.0	1.0
	2.00	−1.312	−1.470	−1.391	0.158	144.0	1.0
	5.00	−1.274	−1.528	−1.401	0.254	230.0	1.0
Peak 3	0.05	−2.046	−2.128	−2.087	0.082	37.1	1.3
	0.10	−2.050	−2.138	−2.094	0.088	45.8	1.3
	0.20	−2.046	−2.156	−2.101	0.110	61.0	1.4
	0.30	−2.034	−2.160	−2.097	0.126	84.0	1.3
	0.40	−2.030	−2.168	−2.099	0.138	105.0	1.3
	0.50	−2.026	−2.174	−2.100	0.148	124.0	1.2
	1.00	−2.012	−2.204	−2.108	0.192	172.0	1.3
	2.00	−2.002	−2.228	−2.115	0.226	214.0	1.3
	5.00	−1.974	−2.332	−2.153	0.358	250.0	1.6

**Table 6**

Electrochemical data (potential in V vs FcH/FcH<sup>+</sup> and current in A) in CH<sub>3</sub>CN for *ca* 0.002 mol dm<sup>−3</sup> of complex 6 at indicated scan rates in V s<sup>−1</sup>. Peak 1 is the Co<sup>III/II</sup> redox couple, peak 2 the Co<sup>III</sup> redox couple and peak 3 the ligand reduction peak.

	Scan rate/V s <sup>−1</sup>	<i>E</i> <sub>pa</sub> /V vs FcH/FcH <sup>+</sup>	<i>E</i> <sub>pc</sub> /V vs FcH/FcH <sup>+</sup>	<i>E</i> <sup>o</sup> /V vs FcH/FcH <sup>+</sup>	Δ <i>E</i> /V	10 <sup>6</sup> <i>I</i> <sub>pa</sub> /A	<i>I</i> <sub>pc</sub> / <i>I</i> <sub>pa</sub>
Peak 1	0.05	−0.118	−0.180	−0.149	0.062	11.0	0.9
	0.10	−0.114	−0.188	−0.151	0.074	23.0	1.0
	0.20	−0.108	−0.188	−0.148	0.080	33.0	1.0
	0.30	−0.104	−0.192	−0.148	0.088	42.0	1.0
	0.40	−0.096	−0.198	−0.147	0.102	49.0	1.0
	0.50	−0.094	−0.198	−0.146	0.104	57.0	1.0
	1.00	−0.086	−0.210	−0.148	0.124	80.0	1.0
	2.00	−0.068	−0.228	−0.148	0.160	112.0	1.0
	5.00	−0.026	−0.288	−0.157	0.262	173.0	1.0
Peak 2	0.05	−1.366	−1.428	−1.397	0.062	13.4	0.9
	0.10	−1.360	−1.430	−1.395	0.070	25.7	0.9
	0.20	−1.352	−1.432	−1.392	0.080	43.5	0.8
	0.30	−1.352	−1.436	−1.394	0.084	48.0	0.9
	0.40	−1.344	−1.444	−1.394	0.100	56.0	0.9
	0.50	−1.346	−1.444	−1.395	0.098	63.0	1.0
	1.00	−1.340	−1.454	−1.397	0.114	93.0	1.0
	2.00	−1.326	−1.476	−1.401	0.150	127.0	0.9
	5.00	−1.292	−1.532	−1.412	0.240	204.0	1.0
Peak 3	0.05	−2.064	−2.146	−2.105	0.082	29.5	1.3
	0.10	−2.068	−2.152	−2.110	0.084	41.2	1.3
	0.20	−2.058	−2.162	−2.110	0.104	60.5	1.3
	0.30	−2.054	−2.172	−2.113	0.118	72.5	1.3
	0.40	−2.046	−2.190	−2.118	0.144	87.0	1.3
	0.50	−2.046	−2.184	−2.115	0.138	103.0	1.3
	1.00	−2.034	−2.206	−2.120	0.172	144.0	1.3
	2.00	−2.022	−2.246	−2.134	0.224	188.0	1.3
	5.00	−1.994	−2.342	−2.168	0.348	238.0	1.5

**Table 7**

Electrochemical data (potential in V vs FcH/FcH<sup>+</sup> and current in A) in CH<sub>3</sub>CN for *ca* 0.002 mol dm<sup>−3</sup> of complex 7 at indicated scan rates in V s<sup>−1</sup>. Peak 1 is the Co<sup>III/II</sup> redox couple, peak 2 the Co<sup>III</sup> redox couple and peak 3 the ligand reduction peak.

	Scan rate/V s <sup>−1</sup>	<i>E</i> <sub>pa</sub> /V vs FcH/FcH <sup>+</sup>	<i>E</i> <sub>pc</sub> /V vs FcH/FcH <sup>+</sup>	<i>E</i> <sup>o</sup> /V vs FcH/FcH <sup>+</sup>	Δ <i>E</i> /V	10 <sup>6</sup> <i>I</i> <sub>pa</sub> /A	<i>I</i> <sub>pc</sub> / <i>I</i> <sub>pa</sub>
Peak 1	0.05	−0.128	−0.216	−0.172	0.088	12.5	1.0
	0.10	−0.127	−0.213	−0.170	0.086	16.2	1.0
	0.20	−0.121	−0.218	−0.170	0.097	23.3	1.0
	0.30	−0.116	−0.227	−0.172	0.111	29.0	1.0
	0.40	−0.116	−0.230	−0.173	0.114	35.0	0.9
	0.50	−0.109	−0.234	−0.172	0.125	41.0	0.9
	1.00	−0.091	−0.244	−0.168	0.153	55.5	0.9
	2.00	−0.080	−0.256	−0.168	0.176	78.0	0.8
	5.00	−0.053	−0.272	−0.163	0.219	130.5	0.8
Peak 2	0.05	−1.401	−1.486	−1.444	0.085	15.4	1.0
	0.10	−1.402	−1.473	−1.438	0.071	20.5	0.9
	0.20	−1.398	−1.480	−1.439	0.082	29.0	0.9
	0.30	−1.393	−1.482	−1.438	0.089	32.5	1.1
	0.40	−1.391	−1.485	−1.438	0.094	42.8	1.0
	0.50	−1.388	−1.491	−1.440	0.103	51.0	0.9
	1.00	−1.376	−1.497	−1.437	0.121	75.0	0.9
	2.00	−1.360	−1.515	−1.438	0.155	109.0	0.9
	5.00	−1.340	−1.533	−1.437	0.193	179.0	0.9
Peak 3	0.05	−2.088	−2.186	−2.137	0.098	28.2	1.1
	0.10	−2.086	−2.174	−2.130	0.088	29.4	1.4
	0.20	−2.079	−2.194	−2.137	0.115	38.2	1.5
	0.30	−2.071	−2.195	−2.133	0.124	47.8	1.4
	0.40	−2.066	−2.199	−2.133	0.133	52.0	1.6
	0.50	−2.063	−2.215	−2.139	0.152	54.4	1.7
	1.00	−2.049	−2.232	−2.141	0.183	69.4	1.8
	2.00	−2.037	−2.263	−2.150	0.226	85.8	1.9
	5.00	−2.010	−2.303	−2.157	0.293	133.4	2.0

**Table 8**

Electrochemical data (potential in V vs FcH/FcH<sup>+</sup> and current in A) in CH<sub>3</sub>CN for *ca* 0.002 mol dm<sup>−3</sup> of complex 8 at indicated scan rates in V s<sup>−1</sup>. Peak 1 is the Co<sup>III/II</sup> redox couple, peak 2 the Co<sup>III</sup> redox couple and peak 3 the ligand reduction peak.

	Scan rate/Vs <sup>−1</sup>	<i>E</i> <sub>pa</sub> /V vs FcH/FcH <sup>+</sup>	<i>E</i> <sub>pc</sub> /V vs FcH/FcH <sup>+</sup>	<i>E</i> <sup>o</sup> /V vs FcH/FcH <sup>+</sup>	Δ <i>E</i> /V	10 <sup>6</sup> <i>I</i> <sub>pa</sub> /A	<i>I</i> <sub>pc</sub> / <i>I</i> <sub>pa</sub>
Peak 1	0.05	−0.216	−0.314	−0.265	0.098	13.2	1.0
	0.10	−0.210	−0.320	−0.263	0.110	19.5	1.1
	0.20	−0.210	−0.314	−0.262	0.104	28.5	1.1
	0.30	−0.200	−0.316	−0.258	0.116	34.5	1.2
	0.40	−0.192	−0.318	−0.255	0.126	39.0	1.3
	0.50	−0.182	−0.324	−0.253	0.142	43.0	1.4
	1.00	−0.166	−0.326	−0.246	0.160	56.0	1.4
	2.00	−0.142	−0.336	−0.239	0.194	86.0	1.3
	5.00	−0.136	−0.348	−0.242	0.212	137.0	1.3
Peak 2	0.05	−1.546	−1.610	−1.578	0.064	14.0	1.0
	0.10	−1.560	−1.615	−1.581	0.055	20.8	1.0
	0.20	−1.542	−1.616	−1.579	0.074	31.5	1.0
	0.30	−1.540	−1.616	−1.578	0.076	39.5	1.0
	0.40	−1.534	−1.622	−1.578	0.088	45.0	1.0
	0.50	−1.532	−1.628	−1.580	0.096	53.5	1.1
	1.00	−1.530	−1.626	−1.578	0.096	81.0	1.0
	2.00	−1.526	−1.634	−1.580	0.108	117.5	1.0
	5.00	−1.514	−1.646	−1.580	0.132	190.0	1.1
Peak 3	0.05	−2.196	−2.382	−2.289	0.186	10.0	4.0
	0.10	−2.202	−2.298	−2.250	0.096	8.0	6.1
	0.20	−2.204	−2.392	−2.298	0.188	12.0	6.3
	0.30	−2.218	−2.396	−2.307	0.178	19.0	4.4
	0.40	−2.218	−2.402	−2.310	0.184	22.0	4.6
	0.50	−2.222	−2.400	−2.311	0.178	20.0	5.6
	1.00	−2.222	−2.428	−2.325	0.206	22.0	7.1
	2.00	−2.218	−2.462	−2.340	0.244	22.0	10.3
	5.00	−2.204	−2.532	−2.368	0.328	27.0	13.0

mounted on a Luggin capillary [11]. Scan rates for the CVs were 0.050–5.000 V s<sup>-1</sup>. Successive experiments under the same experimental conditions showed that all oxidation and reduction potentials were reproducible within 0.010 V under our experimental conditions. Electrochemical data in Tables 1–8 is obtained from the cyclic voltammograms presented in Figs. 2–9. Potentials tabulated are referenced against the FcH/FcH<sup>+</sup> couple, as suggested by IUPAC [12].

## Acknowledgments

This work has received support from the South African National Research Foundation (Grant nos. 113327 and 96111), Pretoria, South Africa, and the Central Research Fund of the University of the Free State, Bloemfontein, South Africa.

## Transparency document. Supplementary material

Transparency document associated with this article can be found in the online version at <https://doi.org/10.1016/j.dib.2018.10.046>.

## References

- [1] H. Ferreira, M.M. Conradie, J. Conradie, Electrochemical properties of a series of Co(II) complexes, containing substituted phenanthrolines, *Electrochim. Acta* 292 (2018) 489–501. <https://doi.org/10.1016/j.electacta.2018.09.151>.
- [2] F. Gajardo, B. Loeb, Spectroscopic and electrochemical properties of a series of substituted polypyridine Co(II)/Co(III) couples and their potentiality as mediators for solar cells, *J. Chil. Chem. Soc.* 56 (2) (2011) 697–701. <https://doi.org/10.4067/S0717-97072011000200016>.
- [3] Z. Yu, N. Vlachopoulos, M. Gorlov, L. Kloo, Liquid electrolytes for dye-sensitized solar cells, *J. Chem. Soc. Dalton Trans.* 40 (2011) 10289–10303. <https://doi.org/10.1039/C1DT11023C>.
- [4] M. Grätzel, Solar energy conversion by dye-sensitized photovoltaic cells, *Inorg. Chem.* 44 (2005) 6841–6851. <https://doi.org/10.1021/ic0508371>.
- [5] M. Safdari, P.W. Lohse, L. Häggman, S. Frykstrand, D. Högberg, M. Rutland, R.A. Asencio, J. Gardner, L. Kloo, A. Hagfeldt, G. Boschloo, Investigation of cobalt redox mediators and effects of TiO<sub>2</sub> film topology in dye-sensitized solar cells, *RSC Adv.* 6 (2016) 56580–56588. <https://doi.org/10.1039/c6ra07107d>.
- [6] S.A. Richert, P.K.S. Tsang, D.T. Sawyer, Ligand-centered redox processes for MnL<sub>3</sub>, FeL<sub>3</sub>, and CoL<sub>3</sub> complexes (L = acetylacetonate, 8-Quinoline, Picolinate, 2,2'-Bipyridyl, 1,10-Phenanthroline) and for their Tetrakis( 2,6-dichlorophenyl) porphinato complexes [M(Por)], *Inorg. Chem.* 28 (1989) 2471–2475. <https://doi.org/10.1021/ic00311a044>.
- [7] X. Xing, Y. Zhao, Y. Li, A non-aqueous redox flow battery based on tris(1,10-phenanthroline) complexes of iron(II) and cobalt(II), *J. Power Sources* 293 (2015) 778–783. <https://doi.org/10.1016/j.jpowsour.2015.06.016>.
- [8] X. Xing, D. Zhang, Y. Li, A non-aqueous all-cobalt redox flow battery using 1,10-phenanthrolinecobalt(II) hexafluorophosphate as active species, *J. Power Sources* 279 (2015) 205–209. <https://doi.org/10.1016/j.jpowsour.2015.01.011>.
- [9] F. Gajardo, B. Loeb, Spectroscopic and electrochemical properties of a series of substituted polypyridine Co(II)/Co(III) couples and their potentiality as mediators for solar cells, *J. Chil. Chem. Soc.* 56 (2) (2011) 697–701. <https://doi.org/10.4067/S0717-97072011000200016>.
- [10] D.T. Sawyer, J.L. Roberts Jr., *Experimental Electrochemistry for Chemists*, John Wiley & Sons, New York (1974) 54.
- [11] D.H. Evans, K.M. O'Connell, R.A. Peterson, M.J. Kelly, Cyclic voltammetry, *J. Chem. Educ.* 60 (1983) 290–293. <https://doi.org/10.1021/ed060p290>.
- [12] G. Gritzner, J. Kuta, Recommendations on reporting electrode potentials in nonaqueous solvents, *Pure Appl. Chem.* 56 (1984) 461–466. <https://doi.org/10.1351/pac198456040461>.

# Chapter 4

---

## **Electrochemical and electronic properties of a series of substituted polypyridine ligands and their Co(II) complexes**

Hendrik Ferreira, Murrigje M. Conradie, Jeanet Conradie

Published by Inorganica Chimica Acta

DOI: 10.1016/j.ica.2018.10.020

## **Cyclic voltammetry data of polypyridine ligands and Co(II)-polypyridine complexes**

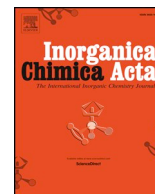
Hendrik Ferreira, Murrigje M. Conradie, Jeanet Conradie

Data in Brief

DOI: 10.1016/j.dib.2018.12.043







## Research paper

## Electrochemical and electronic properties of a series of substituted polypyridine ligands and their Co(II) complexes

Hendrik Ferreira, Murrigje M. Conradie, Jeanet Conradie\*

Department of Chemistry, PO Box 339, University of the Free State, Bloemfontein 9300, South Africa

## ARTICLE INFO

## Keywords:

Cobalt  
Reduction potential  
DFT  
Polypyridine ligands

## ABSTRACT

DFT calculations show that, due to Jahn-Teller distortion, the  $d^7$   $[\text{Co}(\text{N},\text{N})_3]^{2+}$  complexes, with  $S = \frac{1}{2}$  ( $\text{N},\text{N}$  = bipyridine or substituted bipyridine ligand) have two longer axial and four shorter equatorial Co-N bonds (elongation Jahn-Teller), while  $[\text{Co}(\text{terpyridine})_2]^{2+}$  with  $S = \frac{1}{2}$ , instead has two shorter central (axial) Co-N bonds and four longer distal Co-N bonds (compression Jahn-Teller), since in the latter, the distal Co-N bonds are more flexible than the Co-N axial bonds in the rigid structure of the tridentate terpyridine ligand. The same trend is observed for the related high spin  $S = 3/2$  Co(II) complexes, though less pronounced. The cyclic voltammograms of  $[\text{Co}(\text{terpyridine})_2]^{2+}$  and a series of the  $[\text{Co}(\text{N},\text{N})_3]^{2+}$  complexes show at least three chemically as well as electrochemically reversible redox couples, namely  $\text{Co}^{\text{III/II}}$ ,  $\text{Co}^{\text{II/I}}$  and a ligand based reduction of the polypyridine-Co(I) complex. The reduction of the uncoordinated free polypyridine ligand is more than 0.5 V more negative than the reduction of the coordinated ligand in the polypyridine-Co(I) complex.

## 1. Introduction

The aromatic *N*-donor ligands, phenanthroline and bipyridine, both coordinate bidentately to most metals (e.g. Cr [1], Mn, Fe [2], Co, Ni, Cu, Zn [3]), while terpyridine is a tridentate ligand which coordinates to metals at three meridional sites [4,5]. This complexation leads to various octahedral  $\text{M}(\text{N},\text{N})_3^n$  and  $\text{M}(\text{N},\text{N},\text{N})_2^n$  complexes (where  $\text{N},\text{N}$  = bidentate phen, or bpy ligands with two N donor atoms; and  $\text{N},\text{N},\text{N}$  = tridentate tpy ligand with three N donor atoms;  $n$  = charge of complex). The electrochemical behaviour of tris-bipyridine-cobalt and bis-terpyridine-cobalt in organic solvents has been reported under various conditions, see Table 5. It has been shown that substitution of the H at the 4,4' position of bipyridine with methoxy or Cl, leads to an decrease or increase in the Co(III)/Co(II) redox couple of 0.23 V and 0.19 V respectively, compared to that of tris-bipyridine-cobalt(II) (0.56 V vs NHE in  $\text{CH}_3\text{CN}$ ) [6]. We have previously reported on the reduction potential of differently substituted phenanthroline ligands [7] and the influence which different substituents on the ligands exert on the reduction potential of the free ligand, and the metal which it is co-ordinated to [8,9]. Here we present electrochemical results obtained for a selected series of polypyridine ligands, as well as their corresponding polypyridine-Co(II) complexes, all obtained under the same experimental conditions. Fig. 1 shows the ligands and polypyridine-Co(II) complexes of this study, with polypyridine ligands 2,2':6',2''-

terpyridine (tpy, ligand 1a, complex 1), 2,2'-bipyridyl (bpy, ligand 2a, complex 2), 4,4'-dimethyl-2,2'-bipyridine (4,4'-di-Me-bpy, ligand 3a, complex 3), 4,4'-Di-*tert*-butyl-2,2'-bipyridyl (4,4'-di-*t*-Bu-bpy, ligand 4a, complex 4) and 4,4'-dimethoxy-2,2'-bipyridine (4,4'-di-Me-bpy, ligand 5a, complex 5).

## 2. Experimental

## 2.1. General

The polypyridine ligands were obtained from Sigma Aldrich and used as is. UV-visible spectra and infrared spectra were measured on a Shimadzu UV-2550 spectrometer and a Bruker Tensor 27 FTIR spectrophotometer respectively.

## 2.2. Synthesis

The paramagnetic [10,11] polypyridine-Co(II) complexes (containing the anion  $(\text{NO}_3)_2$ ) were synthesized according to literature methods, with slight modifications [12]:  $\text{Co}(\text{NO}_3)_2 \cdot 6\text{H}_2\text{O}$  was dissolved in a minimum of absolute ethanol. A slight excess of the desired ligand (3.3 eq bipyridine for  $\text{Co}(\text{N},\text{N})_3^{2+}$  or 2.2 eq for  $\text{Co}(\text{N},\text{N},\text{N})_2^{2+}$  terpyridine) was also dissolved in a minimum of absolute ethanol. The  $\text{Co}(\text{NO}_3)_2 \cdot 6\text{H}_2\text{O}$  solution was added dropwise to the respective ligand

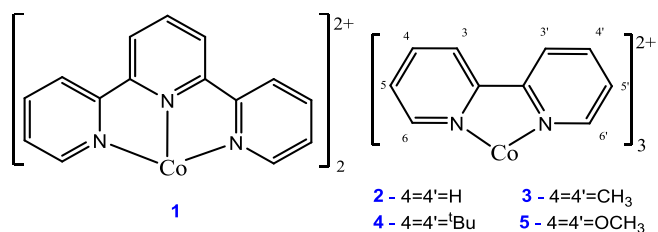
\* Corresponding author.

E-mail address: [conradj@ufs.ac.za](mailto:conradj@ufs.ac.za) (J. Conradie).<https://doi.org/10.1016/j.ica.2018.10.020>

Received 10 July 2018; Received in revised form 14 October 2018; Accepted 14 October 2018

Available online 16 October 2018

0020-1693/© 2018 Elsevier B.V. All rights reserved.



**Fig. 1.** The series of  $\text{Co}(\text{N},\text{N},\text{N})_2^{2+}$  and  $\text{Co}(\text{N},\text{N})_3^{2+}$  complexes employed in this study. N,N,N = the tridentate tpy ligand with three N donor atoms (complex 1) and N,N = the bpy or substituted bpy ligands, with two N donor atoms (complexes 2–5).

solution whilst stirring. The mixture was left to stir for 6–8 h. A precipitate formed in each case. The mixture was filtered and the precipitate left to dry overnight in air. The electrochemical behaviour of complexes 1, 2 and 5 has been reported previously (see Table 5), while that of complexes 3 and 4 is reported here for the first time.

#### 2.2.1. Characterization data for bis(2,2':6',2''-terpyridine)Cobalt(II) nitrate, $[\text{Co}(\text{tpy})_2](\text{NO}_3)_2$ (1)

Yield 49.8%. Colour: light yellow. Melting point greater than 310 °C.  $\lambda_{\text{max}}(\text{methanol}) = 317 \text{ nm}$ ;  $\epsilon = 70652 \text{ mol}^{-1} \text{ dm}^3 \text{ cm}^{-1}$ .  $\nu_{\text{C-N}} = 1333 \text{ cm}^{-1}$ . Elemental Anal. Calc. for  $\text{CoC}_{30}\text{N}_6\text{H}_{22}\text{N}_2\text{O}_6$ : C, 55.5; H, 3.4. Found: C, 55.5; H, 3.3%.

#### 2.2.2. Characterization data tris(2,2'-bipyridyl)Cobalt(II) nitrate, $[\text{Co}(\text{bpy})_3](\text{NO}_3)_2$ (2)

Yield 82.2%. Colour: light yellow. Melting point 184 °C.  $\lambda_{\text{max}}(\text{methanol}) = 294 \text{ nm}$ ;  $\epsilon = 23579 \text{ mol}^{-1} \text{ dm}^3 \text{ cm}^{-1}$ .  $\nu_{\text{C-N}} = 1337 \text{ cm}^{-1}$ . Elemental Anal. Calc. for  $\text{CoC}_{30}\text{N}_6\text{H}_{24}\text{N}_2\text{O}_6$ : C, 55.3; H, 3.7. Found: C, 55.3; H, 3.6%.

#### 2.2.3. Characterization data tris(4,4'-dimethyl-2,2'-bipyridine)Cobalt(II) nitrate, $[\text{Co}(\text{4,4'-di-Me-bpy})_3](\text{NO}_3)_2$ (3)

Yield 84.8%. Colour: light yellow. Melting point greater than 310 °C.  $\lambda_{\text{max}}(\text{methanol}) = 292 \text{ nm}$ ;  $\epsilon = 23579 \text{ mol}^{-1} \text{ dm}^3 \text{ cm}^{-1}$ .  $\nu_{\text{C-N}} = 1332 \text{ cm}^{-1}$ . Elemental Anal. Calc. for  $\text{CoC}_{36}\text{N}_6\text{H}_{36}\text{N}_2\text{O}_6$ : C, 58.8; H, 4.9. Found: C, 58.9; H, 4.8%.

#### 2.2.4. Characterization data tris(4,4'-Di-tert-butyl-2,2'-bipyridyl)Cobalt(II) nitrate, $[\text{Co}(\text{4,4'-di-}^t\text{Bu-bpy})_3](\text{NO}_3)_2$ (4)

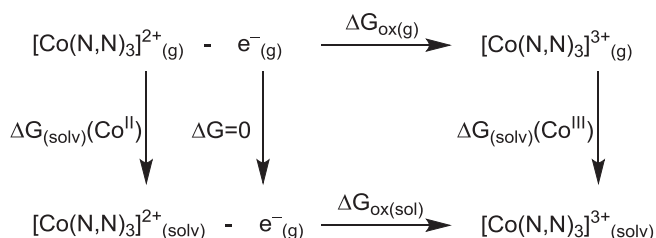
Yield 81.8%. Colour: light yellow. Melting point greater than 245 °C.  $\lambda_{\text{max}}(\text{methanol}) = 292 \text{ nm}$ ;  $\epsilon = 31533 \text{ mol}^{-1} \text{ dm}^3 \text{ cm}^{-1}$ .  $\nu_{\text{C-N}} = 1333 \text{ cm}^{-1}$ . Elemental Anal. Calc. for  $\text{CoC}_{54}\text{N}_6\text{H}_{72}\text{N}_2\text{O}_6$ : C, 65.6; H, 7.3. Found: C, 65.4; H, 7.2%.

#### 2.2.5. Characterization data tris(4,4'-dimethoxy-2,2'-bipyridine)Cobalt(II) nitrate, $[\text{Co}(\text{4,4'-di-OMe-bpy})_3](\text{NO}_3)_2$ (5)

Yield 83.2%. Colour: light yellow. Melting point 223 °C.  $\lambda_{\text{max}}(\text{methanol}) = 224 \text{ nm}$ ;  $\epsilon = 87302 \text{ mol}^{-1} \text{ dm}^3 \text{ cm}^{-1}$ .  $\nu_{\text{C-N}} = 1329 \text{ cm}^{-1}$ . Elemental Anal. Calc. for  $\text{CoC}_{36}\text{N}_6\text{H}_{36}\text{N}_2\text{O}_{12}$ : C, 52.0; H, 4.4. Found: C, 51.8; H, 4.3%.

### 2.3. Theoretical calculations

Density functional theory (DFT) calculations were performed, using the Amsterdam Density Functional program (ADF2014 and updates) [13]. The GGA functionals BP86 [14,15] and OLYP [16,17], as well as the hybrid functional B3LYP [14,17,18], with the TZP (Triple  $\zeta$  polarized) basis set, were used. All complexes were fully optimized in the gas phase, spin unrestricted with spin  $S = 1/2$ ,  $3/2$  and  $5/2$  for Co(II) [10,11],  $S = 0$ , 1 and 2 for Co(I) (reduced), and spin  $S = 0$ , 1 and 2 for Co(III) (oxidized). The absolute redox potential were calculated from  $E_{\text{calculated, absolute}} = \frac{-\Delta G_{\text{ox(sol)}}}{nF}$  where  $-\Delta G_{\text{ox(sol)}}$  was obtained from the



**Scheme 1.** Thermodynamic cycle for the absolute potential of  $\text{Co}(\text{N},\text{N})_3^{2+}$  (where N,N = the bpy or substituted bpy ligands), for complexes 2 – 5. The cycle for  $\text{Co}(\text{N},\text{N},\text{N})_2^{2+}$  (with N,N,N = tpy) for complex 1, is similar.  $\Delta G_{\text{ox(g)}}$  = free energy change in gas phase;  $\Delta G_{\text{(solv)}}$  = solvation energy of gas phase species;  $\Delta G_{\text{ox(sol)}}$  = change of free energy in solution.

thermodynamic cycle shown in Scheme 1 [19], where  $n$  is the number of transferred electrons and  $F$  is the Faraday constant. Redox calculations utilized the gas phase optimized geometries obtained with the B3LYP/6-311G(d,p) functional and basis set, as implemented in the Gaussian 09 package [20]. Frequency calculations were performed on all optimized structures at the same level of theory as geometry optimizations. Minima exhibited only positive frequencies. Single point calculations in  $\text{CH}_3\text{CN}$  solvent (dielectric constant = 36.64) were performed with the default solvent model IEFPCM. The absolute redox potential was converted to a relative redox potential versus the Ferrocene/Ferrocenium ( $\text{Fc}/\text{Fc}^+$ ) couple, by subtracting an experimentally obtained absolute reduction potential of  $\text{Fc}/\text{Fc}^+$  in acetonitrile solution (4.980 V [21]), from the calculated absolute redox potential:  $E_{\text{calculated vs Fc/Fc}^+} = \frac{-\Delta G_{\text{ox(sol)}}}{nF} - E_{\text{Fc/Fc}^+}$

### 2.4. Electrochemistry

Electrochemical studies by means of cyclic voltammetry (CV) and linear sweep voltammograms (LSVs) were performed, either on  $0.002 \text{ mol dm}^{-3}$  or on saturated compound solutions of the free ligands 1a – 5a and their corresponding complexes 1 – 5, in dry acetonitrile containing  $0.1 \text{ mol dm}^{-3}$  tetra-*n*-butylammoniumhexafluorophosphate ( $[\text{tBu}_4\text{N}][\text{PF}_6]$ ) as supporting electrolyte, under a blanket of purified argon, at 25 °C, utilizing a BAS 100B/W electrochemical analyser. A three-electrode cell was used, with a glassy carbon (surface area  $7.07 \times 10^{-6} \text{ m}^2$ ) working electrode, Pt auxiliary electrode and a  $\text{Ag}/\text{Ag}^+$  ( $0.010 \text{ mol dm}^{-3}$   $\text{AgNO}_3$  in  $\text{CH}_3\text{CN}$ ) reference electrode [22], mounted on a Luggin capillary [23]. Scan rates for the CVs were  $0.050$ – $5.000 \text{ V s}^{-1}$ , and the scan rate for LSVs was  $0.002 \text{ V s}^{-1}$ . Successive experiments under the same experimental conditions showed that all oxidation and reduction potentials were reproducible within  $0.010 \text{ V}$ . All cited potentials were referenced against the Ferrocene/Ferrocenium ( $\text{Fc}/\text{Fc}^+$ ) couple, as suggested by IUPAC [24]. For different solvents under our experimental conditions, Ferrocene (Fc) exhibited a peak separation of  $\Delta E_p = E_{\text{pa}} - E_{\text{pc}} = 0.070 \text{ V}$  and ratio  $i_{\text{pc}}/i_{\text{pa}} = 1.00$  in solvents  $\text{CH}_3\text{CN}$  and  $\text{CH}_2\text{Cl}_2$ , but  $\Delta E_p = 0.090 \text{ V}$  and ratio  $i_{\text{pc}}/i_{\text{pa}} = 0.97$  in solvent THF [25], where  $E_{\text{pa}}$  ( $E_{\text{pc}}$ ) = anodic (cathodic) peak potential and  $i_{\text{pa}}$  ( $i_{\text{pc}}$ ) = anodic (cathodic) peak current.  $\Delta E_p$  for an electrochemically reversible process is  $0.059 \text{ V}$  [23], but based on the  $\Delta E_p$  values of ferrocene obtained in different solvents under our experimental conditions, values up to  $0.090 \text{ V}$ , will be considered to be electrochemically reversible [25,26].

## 3. Results and discussion

### 3.1. Synthesis of complexes

The cobalt complexes  $\text{Co}(\text{N},\text{N},\text{N})_2^{2+}$  complex 1 and  $\text{Co}(\text{N},\text{N})_3^{2+}$  complexes 2 – 5, were synthesized by adapting a typical published procedure [12], see Scheme 2.  $\text{Co}(\text{NO}_3)_2 \cdot 6\text{H}_2\text{O}$  was used instead of  $\text{Co}(\text{ClO}_4)_2$ , due to the explosion hazard posed by dry perchlorate salts.



near degenerate HOMO-1 and HOMO-2 (Fig. 2, also see Table S2 for further detail). The Co-N distances are given in Table 2 for complexes 1 – 5. The Co-N distances decrease slightly in going from complex 2 to 5 with increasingly electron donating substituents, as quantified by the *para* Hammett constants and the ease of reduction, see Table 6 in the Electrochemistry section below. The Co–N distances in the Co(III) complexes 1 – 5 are shorter than in the related Co(II) and Co(I) complexes, see bond lengths in Table 2.

### 3.2.2. Co(II) complexes

It is well known that the spin state of spin cross over (SCO) polypyridine-Co(II) complexes depends on various factors determined by the environment of the complex, such as the nature of the counter anions [11,29], the temperature [10,30], pressure [31], solvent [11] or solvent in crystal lattice [29]. DFT can be used for discriminating among spin states of transition metal complexes, but it is a delicate matter, with a delicate energy balance [28,29,32,33]. Generally, the “classic” pure functionals such as BLYP, PW91 and BP86 favour low spin states, while the hybrid functionals such as B3LYP favour the opposite. DFT calculations on the spin-crossover complex Fe(salen)(NO), showed that the newer pure functionals OLYP and OPBE, as well as the hybrid functional B3LYP\*, predict nearly isoenergetic  $S = 1/2$  and  $3/2$  states, as required for a spin-crossover complex [34]. The polypyridine-Co(II) complexes 1 – 5 of this study contain the anion  $(\text{NO}_3)_2$ , and are reported to be low spin  $S = 1/2$  complexes at room temperature [10,11]. Therefore the BP86 functional that predicts low spin  $S = 1/2$  for polypyridine-Co(II) complexes 1 – 5, will mainly be used here to evaluate the properties of the low and high spin Co(II) complexes 1 – 5.

Results for both the low-spin  $S = 1/2$  ( $t_{2g}^6 e_g^1$ ) and high spin  $S = 3/2$  ( $t_{2g}^5 e_g^2$ )  $d^7$  polypyridine-Co(II) complexes are given in Tables 2 and 3. The  $S = 3/2$  geometries of the bipyridyl-Co(II) complexes 2 – 5 converged to near  $D_3$  symmetry, while the  $S = 1/2$  optimized geometries exhibit near  $C_2$  symmetry, with elongation of the axial bonds due to Jahn-Teller distortion (Table 2). The Co-N bond lengths of the Co(II)  $S = 3/2$  geometries (ca. 1.97 Å) are ca. 0.18 Å longer than the Co-N bond lengths of the corresponding Co(III)  $S = 0$  complexes. The Co(II)  $S = 1/2$  complexes have two even longer axial (ca. 2.21 Å) and four shorter equatorial (ca. 1.97 Å) Co-N bonds, due to Jahn-Teller distortion. The Mulliken spin population on the Co metal, for complexes 2 – 5 is 0.98 ( $S = 1/2$ ) and 2.6 ( $S = 3/2$ ), consistent with low and high spin Co(II).

The relative energies for both the low-spin  $S = 1/2$  ( $t_{2g}^6 e_g^1$ ) and high spin  $S = 3/2$  ( $t_{2g}^5 e_g^2$ )  $d^7$   $[\text{Co}(\text{tpy})_2]^{2+}$  complex 1, are given in Table 1 for a selection of functionals. Both the high and low spin geometries exhibit

near  $D_{2d}$  symmetry. The pseudo-Jahn-Teller instability of the  $S = 1/2$  state, may lead to a lower  $C_{2v}$  symmetry [35], though the  $C_{2v}$  symmetry geometry was only 0.03 eV lower in energy than the  $D_{2d}$  symmetry. Both OLYP and BP86 favour the low spin geometry, while the B3LYP functional favours the high spin geometry by 0.12 eV, in agreement with published DFT calculations [28]. Due to Jahn-Teller distortion (compression), the two central (axial) Co-N bond lengths of low spin  $[\text{Co}(\text{tpy})_2]^{2+}$  are 0.21–0.23 Å shorter, with four longer distal Co-N bonds, see Table 2. The Mulliken spin population on Co is near 1 for the  $S = 1/2$  geometries (Table 3), consistent with a low spin Co(II) centre.

For the high spin  $S = 3/2$  geometry, the  $D_2$  and  $D_{2d}$  geometries respectively were 0.05–0.06 eV and 0.11–0.18 eV higher in energy than the geometries without any symmetry constraint. Results for the high spin  $[\text{Co}(\text{tpy})_2]^{2+}$  structure are given in Table 2. The two central (axial) Co-N bonds of the high spin  $[\text{Co}(\text{tpy})_2]^{2+}$  complex, are only 0.10 Å shorter, with four longer distal Co-N bonds, i.e. the difference is much less pronounced for the high spin  $S = 3/2$  geometry, than the ca. 0.22 Å that was obtained for low spin  $[\text{Co}(\text{tpy})_2]^{2+}$ . The Mulliken spin population on Co is 2.60–2.69 for the  $S = 3/2$  geometries (Table 3), consistent with a high spin Co(II) centre.

### 3.2.3. Co(I) complexes

The  $S = 1$  spin state is more than 0.6 eV stable (depending on the functional used) than the  $S = 0$  state for the  $d^8$  ( $t_{2g}^6 e_g^2$ ) polypyridine-Co(I) complexes. The terpyridine-Co(I) complex 1 exhibits  $D_{2d}$  symmetry and the bipyridyl-Co(I) complexes 2 – 5 exhibit near  $D_3$  symmetry. The four distal Co-N bonds are ca. 0.13 Å longer than the two central (axial) Co-N bonds in terpyridine-Co(I) complex 1, since the Co-N axial bond is less flexible than the distal Co-N bonds in the rigid structure of the tridentate terpyridine ligand, while all six the Co-N bonds in the bipyridyl-Co(I) complexes 2 – 5 are of equal length, see Table 2. The spin population of ca. 2.1 on Co (Table 3) confirms that polypyridine-Co(I) complexes 1 – 5 are true Co(I) complexes with  $S = 1$ . The Co(I)-N bonds are slightly longer than the Co(II)-N bonds, and significantly longer than the Co(III) bonds.

### 3.2.4. Redox potentials

The theoretical B3LYP/6-311G(d,p) calculated redox potentials,  $E_{\text{calc}}$ , for the  $\text{Co}^{\text{III/II}}$  redox couple of the complexes of this study (according to Scheme 1) are given in Table 4. Experimentally measured redox potentials,  $E_{\text{exp}}^{\text{ox}}$ , (see Section 3.4 below) were added for comparative purposes. The results obtained show that the DFT level used can reproduce the experimental redox potentials with a lowest and highest absolute error of 0.18 and 0.06 V respectively, with a mean absolute error (MAD) of 0.033 V. This MAD value is comparable to published MAD values between 1.62 and 0.059 V (depending on the

**Table 3**

Summary of average Mulliken spin values of the BP86/TZP calculated geometries of the Co(II) complexes 1 – 5, as well as their reduced Co(I) complexes.

	Co(II) $S = 1/2$		Co(II) $S = 3/2$		Co(I) $S = 1$	
	Co	N	Co	N	Co	N
<b>Complex 1</b>	0.899	-0.015; 0.048 <sup>a</sup>	2.601	0.060; 0.064 <sup>a</sup>	2.188	0.029; 0.037 <sup>a</sup>
<b>Complex 2</b>	0.892	0.066; 0.002 <sup>b</sup>	2.612	0.062	2.073	0.034
<b>Complex 3</b>	0.890	0.064; 0.002 <sup>b</sup>	2.610	0.061	2.091	0.034
<b>Complex 4</b>	0.890	0.064; 0.002 <sup>b</sup>	2.606	0.061	2.053	0.034
<b>Complex 5</b>	0.886	0.062; 0.002 <sup>b</sup>	2.610	0.060	2.106	0.033

<sup>a</sup> Complex 1: the first value is the average of the two shorter central (axial) Co-N bonds; the second value is the average of the four longer distal Co-N bonds (z-in compression).

<sup>b</sup> Complex 2–5, Co(II)  $S = 1/2$ : the first value is the average of the 2 longer tetragonal/axial elongated Co-N bonds, the second value is the average of the 4 shorter equatorial bonds.

**Table 4**

Experimental and calculated redox potentials (in V) of the  $\text{Co}^{\text{III/II}}$  couple of the indicated  $\text{Co}(\text{N}_3\text{N}_2)_2^{2+}$  and  $\text{Co}(\text{N}_3\text{N}_3)_3^{2+}$  complexes (including an additional complex 6 from literature).

No	N <sub>3</sub> N <sub>2</sub> or N <sub>3</sub> N <sub>3</sub>	Absolute $E_{\text{calc}}$	$E_{\text{calc}}$ vs $\text{Fc}/\text{Fc}^+$	$E_{\text{exp}}^{\text{ox}}$ vs $\text{Fc}/\text{Fc}^+$	Absolute error = $ E_{\text{calc}} - E_{\text{exp}}^{\text{ox}} $
1	Tpy	4.900	−0.080	−0.136	0.056
2	Bpy	4.843	−0.137	−0.081	0.056
3	4,4'-di-Me-bpy	4.651	−0.329	−0.213	0.116
4	4,4'-di-tBu-bpy	4.644	−0.336	−0.238	0.098
5	4,4'-di-OMe-bpy	4.542	−0.438	−0.266	0.172
6	4,4'-di-Cl-bpy	5.189	0.209	0.130 <sup>a</sup>	0.079
Mean absolute error (MAD)					<b>0.033</b>

<sup>a</sup> From reference [6].



**Table 5**

Experimental and selected published electrochemical data for the reduction potentials (in V) of Co(II) complexes **1** – **6**, obtained in the indicated solvents vs the indicated reference electrodes.

Complex number	Ligand N,N	Reference electrode <sup>a</sup>	Solvent	$[\text{Co}^{\text{III}}(\text{N},\text{N})_2]^{3+}/[\text{Co}^{\text{II}}(\text{N},\text{N})_2]^{2+}$		$[\text{Co}^{\text{II}}(\text{N},\text{N})_2]^{2+}/[\text{Co}^{\text{I}}(\text{N},\text{N})_2]^{1+}$		$[\text{Co}^{\text{I}}(\text{N},\text{N})_2]^+ / [\text{Co}^{\text{I}}(\text{N},\text{N})(\text{N},\text{N}^-)]^0$		Reference
				Reported	vs Fc/Fc <sup>+</sup>	Reported	vs Fc/Fc <sup>+</sup>	Reported	vs Fc/Fc <sup>+</sup>	
<b>1</b>	tpy	Fc/Fc <sup>+</sup>	CH <sub>3</sub> CN		−0.136		−1.189		−2.075	This study
<b>1</b>	tpy	SSCE	DMF	0.27	−0.15	−0.77	−1.19	−1.66	−2.08	[42]
<b>1</b>	tpy	SSCE	acetone	0.32	−0.10					[43]
<b>1</b>	tpy	SSCE	CH <sub>3</sub> CN	0.30	−0.12					[44]
<b>1</b>	tpy	Fc/Fc <sup>+</sup>	CH <sub>3</sub> CN		−0.13		−1.17		−2.04	[39]
<b>1</b>	tpy	Fc/Fc <sup>+</sup>	DMF/H <sub>2</sub> O		−0.17		−1.17		−2.03	[45]
<b>1</b>	tpy	Fc/Fc <sup>+</sup>	CH <sub>3</sub> CN		−0.139		−1.183		−2.056	[46]
<b>2</b>	bpy	Fc/Fc <sup>+</sup>	CH <sub>3</sub> CN		−0.081		−1.369		−2.032	this study
<b>2</b>	bpy	NHE	CH <sub>3</sub> CN	0.56	−0.10					[6]
<b>2</b>	bpy	SCE	CH <sub>3</sub> CN	0.34	−0.08	−0.95	−1.37	−1.57	−1.99	[47]
<b>2</b>	bpy	Fc/Fc <sup>+</sup>	CH <sub>3</sub> CN		0.07		−1.21			[48]
<b>3</b>	4,4'-di-Me-bpy	Fc/Fc <sup>+</sup>	CH <sub>3</sub> CN		−0.213		−1.517		−2.107	this study
<b>4</b>	4,4'-di-tBu-bpy	Fc/Fc <sup>+</sup>	CH <sub>3</sub> CN		−0.238		−1.484		−2.093	this study
<b>5</b>	4,4'-di-OMe-bpy	Fc/Fc <sup>+</sup>	CH <sub>3</sub> CN		−0.266		−1.673		−2.141	this study
<b>5</b>	4,4'-di-OMe-bpy	NHE	CH <sub>3</sub> CN	0.370	−0.290					[6]
<b>6</b>	4,4'-di-Cl-bpy	NHE	CH <sub>3</sub> CN	0.790	0.130					[6]

<sup>a</sup> To convert published potential values vs Fc/Fc<sup>+</sup>, the following values have been used:  $E^\circ(\text{Fc/Fc}^+) = 0.66(5) \text{ V}$  vs SHE in [<sup>n</sup>Bu<sub>4</sub>N][PF<sub>6</sub>]/CH<sub>3</sub>CN [49]; Saturated calomel (SCE) = 0.2444 V vs SHE; Calomel electrode, saturated NaCl (SSCE) = 0.2360 vs SHE.

method and level of theory used), obtained for redox calculations of Fischer-Type chromium aminocarbene complexes [36]. The linear fit of the  $E_{\text{calc}}^{\circ}$  versus  $E_{\text{exp}}^{\circ}$  values for the substituted Co(bipy)<sub>3</sub><sup>2+</sup> complexes **2** – **6**, afforded a R<sup>2</sup> value of 0.99, which is similar to the published R<sup>2</sup> value of 0.97, obtained for the linear fit between the calculated Fe<sup>III/II</sup> reduction potentials vs experimentally determined reduction potentials of a series of substituted Fe(bipy)<sub>3</sub><sup>2+</sup> complexes [37].

### 3.3. Molecular orbital interpretation of oxidation and reduction

The frontier molecular orbitals (FMO) of a complex play an important role in the reduction and oxidation of the complex, since reduction and oxidation involve the addition or removal of an electron to or from a FMO of the complex respectively.

The locus of the reduction centre of the polypyridyl ligands **1a** – **5a**, and the S = 0 Co(III) complexes **1** – **5** can therefore be identified by evaluating the nature of their respective LUMOs, see Fig. 3. Since in rare cases a reorganisation of the molecular orbitals (MOs) occurs after reduction, consequently leading to the reduction of a higher unoccupied MO [38], it is good to also evaluate the HOMO or the spin density profile of the reduced compound. The polypyridine-Co(II) complexes **1** – **5** of this study contain the anion (NO<sub>3</sub>)<sub>2</sub>, which are reported to be low spin S = 1/2 complexes at room temperature [10,11]. Therefore, the reduced polypyridine-Co(II) complexes **1** – **5** are modelled here as low spin S = 1/2. Since the polypyridyl ligands **1a** – **5a** and the Co(III) complexes **1** – **5** are diamagnetic (no unpaired electrons), the spin density profile of

the reduced ligands and complexes shows the distribution of the added unpaired electron, see Fig. 3. The spin plots in Fig. 3 show that the first reduction of polypyridyl ligands **1a** – **5a** will thus lead to the formation of an anion radical, with the added electron distributed over the heterocyclic rings, while the Co(III) reduction of complexes **1** – **5** is metal based, i.e. Co<sup>III/II</sup> reduction. This assignment of the locus of reduction to Co is in agreement with the experimental electrochemical Co(III) reduction process, as measured by cyclic voltammetry, which will be discussed in the next section. The Co-d character of the Co(II) HOMO was also used to assign the Co(III/II) redox couple of a series of bis-terpyridine based Co(II) complexes [4]. The character of the spin plots of the reduced complexes **1** – **5** are all very similar (Fig. 3), indicating that the substituents on the polypyridyl ligands do not change the locus of the reduction centre for complexes **1** – **5**.

The locus of the reduction of the Co(II) S = 1/2 complex is its LUMO, where the electron is added upon reduction. The spin plot of the reduced Co(I) complex will show the distribution of the added electron. The spin plot of Co(I) and the Co(II) LUMO for complexes **1** – **5**, as visualized in Fig. 4, clearly show that the Co(II) reduction is metal based, therefore it is a Co<sup>II/I</sup> reduction.

The locus of the reduction of the Co(I) S = 1 complex also is its LUMO, where the electron is added upon reduction. However this LUMO of Co(I), also shown in Fig. 4, is mainly on one of the coordinated polypyridyl ligands, implying that reduction of the Co(I) complex in this case will involve the polypyridyl N,N-ligands instead. These assignments are in agreement with the experimentally observed

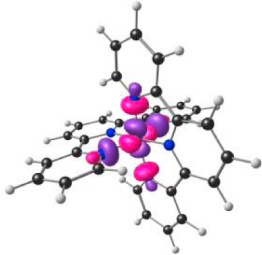
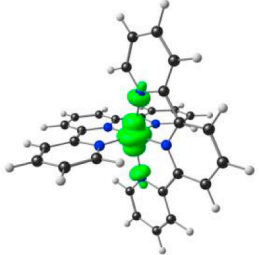
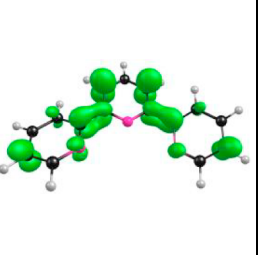
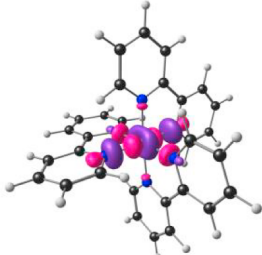
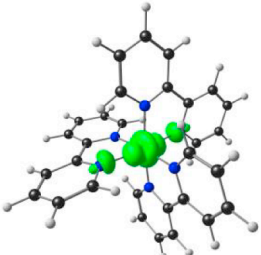
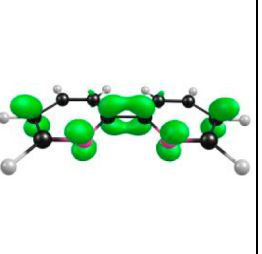
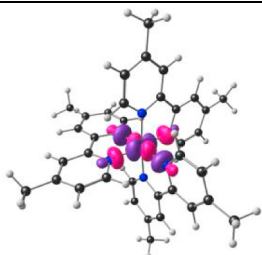
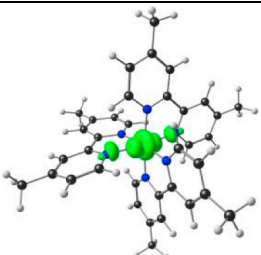
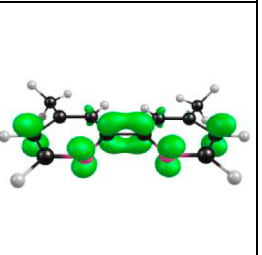
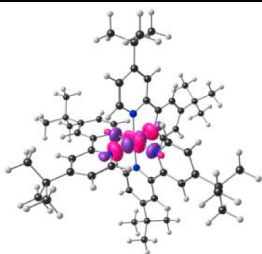
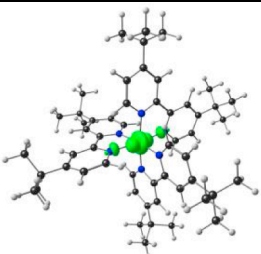
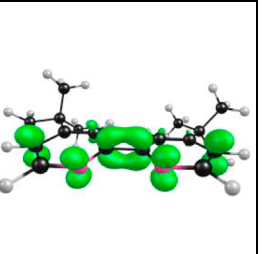
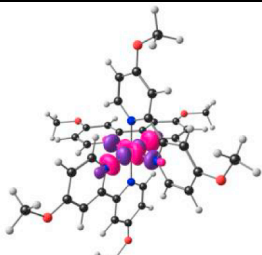
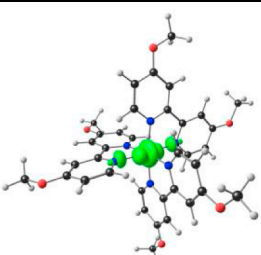
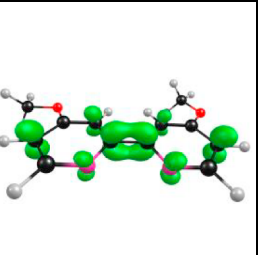
**Table 6**

Electrochemical data (V vs Fc/Fc<sup>+</sup>) of Co(II) complexes **1** – **5**, related Fe(II) complexes from literature, as well as their corresponding polypyridyl free ligands **1a** – **5a**.

No	Ligand	$E^\circ(\text{Co}^{\text{III/II}})/\text{V}$	$E^\circ(\text{Co}^{\text{II/I}})/\text{V}$	$E^\circ(\text{Co}^{\text{I}} \text{ reduction})/\text{V}$	$E^\circ(\text{Fe}^{\text{III/II}})/\text{V}^a$	$E_{\text{pc}}(\text{ligand})/\text{V}$	$\sigma_{\text{para}}^b$
<b>1</b>	tpy	−0.136	−1.189	−2.075	0.720	−2.584	–
<b>2</b>	bpy	−0.081	−1.369	−2.032	0.682	−2.641	0
<b>3</b>	4,4'-di-Me-bpy	−0.213	−1.517	−2.107	0.523	−2.679	−0.17
<b>4</b>	4,4'-di-tBu-bpy	−0.238	−1.484	−2.093		−2.720	−0.10
<b>5</b>	4,4'-di-OMe-bpy	−0.266	−1.673	−2.141	0.363	−2.656	−0.27

<sup>a</sup>  $E^\circ(\text{Fe}^{\text{III/II}})$  from reference [8].

<sup>b</sup> Hammett constants  $\sigma_{\text{para}}$  obtained from reference [41].

	LUMO of Co(III) involved in the Co <sup>III/II</sup> redox process	Spin plot of Co(II) S = 1/2, showing the distribution of the added electron during the Co <sup>III/II</sup> redox process	Spin plot of the reduced ligand
<b>1</b> Co(tpy) <sub>2</sub> <sup>n+</sup>			
<b>2</b> Co(bpy) <sub>3</sub> <sup>n+</sup>			
<b>3</b> Co(4,4'-di-CH <sub>3</sub> -py) <sub>3</sub> <sup>n+</sup>			
<b>4</b> Co(4,4'-di- <sup>t</sup> Bu <sub>3</sub> -py) <sub>3</sub> <sup>n+</sup>			
<b>5</b> Co(4,4'-di-OCH <sub>3</sub> -py) <sub>3</sub> <sup>n+</sup>			

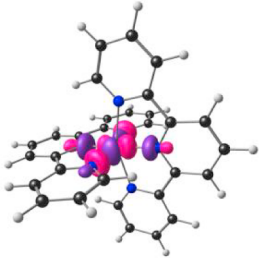
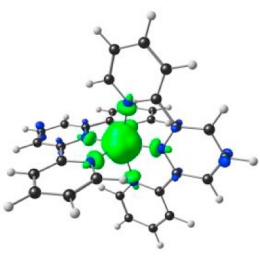
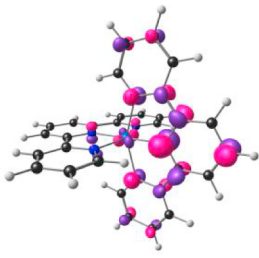
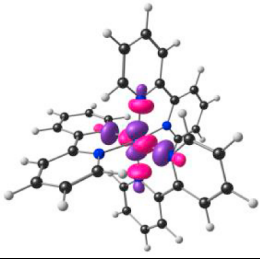
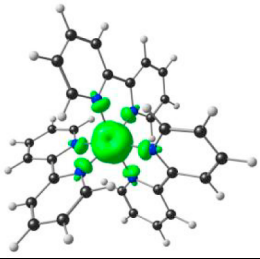
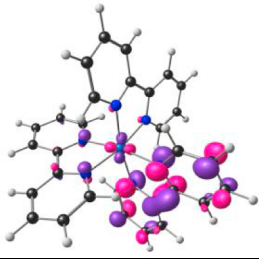
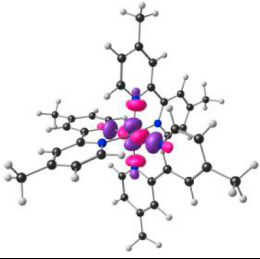
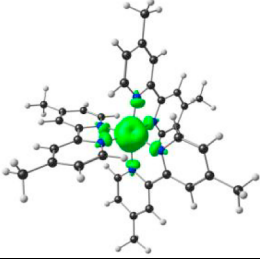
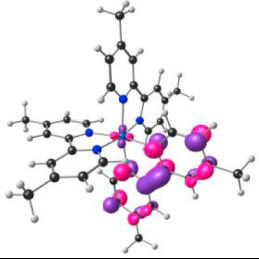
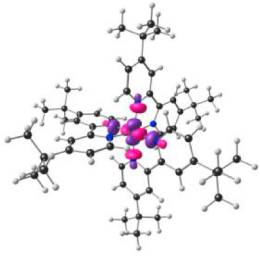
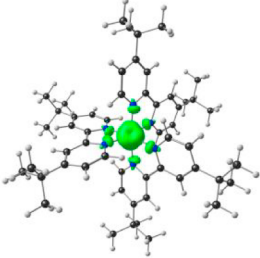
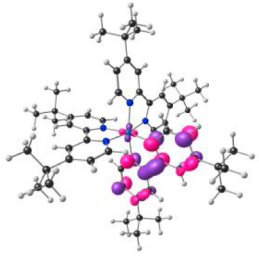

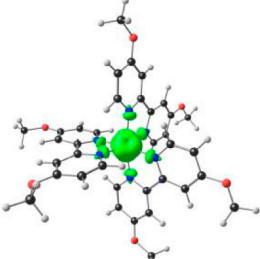
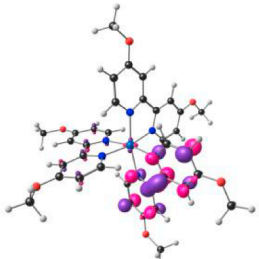
**Fig. 3.** DFT calculated BP86/TZP spin density plot and LUMO of the indicated complexes 1–5, showing the locus of the Co<sup>III/II</sup> redox process. The contour used for the MO and spin figures are 0.06 and 0.006 e/Å<sup>3</sup> respectively.

electrochemical reduction processes of the Co(II) and Co(I) complexes, as measured by cyclic voltammetry, which are presented in the next section.

### 3.4. Electrochemistry

Fig. 5 (top) shows the 0.100 and 0.300 V s<sup>-1</sup> cyclic voltammetry scan and linear sweep voltammograms for [Co(tpy)<sub>2</sub>](NO<sub>3</sub>)<sub>2</sub>, complex

1, of this study, over a broad potential window. Four chemically and electrochemically reversible redox couples were observed in the solvent window for CH<sub>3</sub>CN, as well as a few irreversible oxidation or reduction peaks. The chemically and electrochemically reversible redox couple at −0.136 V vs Fc/Fc<sup>+</sup> (ΔE = 0.084 V at 0.100 V s<sup>-1</sup>), is ascribed to the Co<sup>III/II</sup> redox couple, while the other chemically and electrochemically reversible redox couple at −1.189 V vs Fc/Fc<sup>+</sup> (ΔE = 0.086 V at 0.100 V s<sup>-1</sup>), is attributed to the Co<sup>II/I</sup> redox couple. Further, the

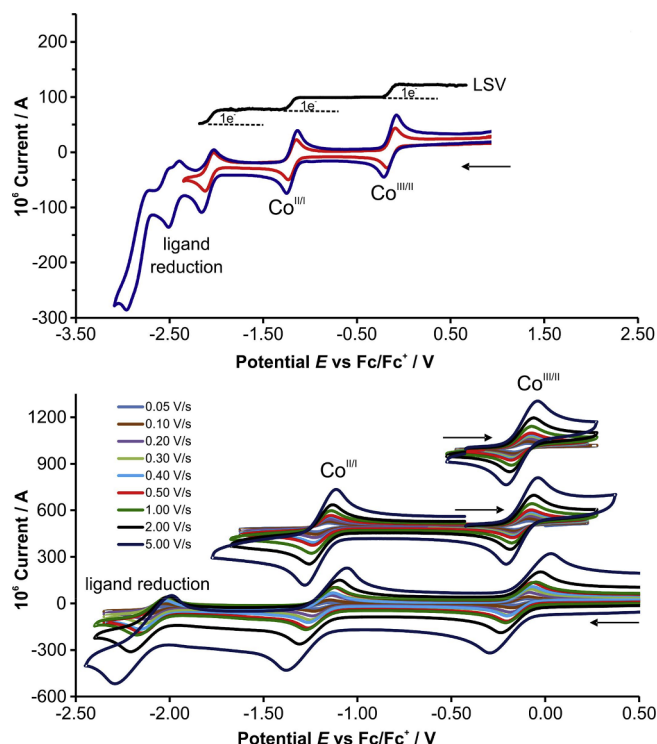
	LUMO of Co(II) involved in the Co <sup>III</sup> redox process	Spin plot of Co(I), showing the distribution of the added electron during Co <sup>III</sup> redox process	LUMO of Co(I) involved in the Co <sup>I</sup> ligand based reduction process
1 Co(tpy) <sub>2</sub> <sup>n+</sup>			
2 Co(bpy) <sub>3</sub> <sup>n+</sup>			
3 Co(4,4'-di-CH <sub>3</sub> -py) <sub>3</sub> <sup>n+</sup>			
4 Co(4,4'-di- <sup>t</sup> Bu <sub>3</sub> -py) <sub>3</sub> <sup>n+</sup>			
5 Co(4,4'-di-OCH <sub>3</sub> -py) <sub>3</sub> <sup>n+</sup>			

**Fig. 4.** The DFT calculated BP86/TZP spin density plot and LUMO of Co(tpy)<sub>2</sub><sup>1+</sup> and Co(bpy)<sub>3</sub><sup>1+</sup> (middle and right) as well as the LUMO of Co(tpy)<sub>2</sub><sup>2+</sup> and Co(bpy)<sub>3</sub><sup>2+</sup> (left), showing the locus of the Co<sup>II/I</sup> and Co(I)-polypyridyl complex reduction processes. The contours used for the MO and spin figures, are 0.06 and 0.006 e/Å<sup>3</sup> respectively.

chemically and electrochemically reversible peak at  $-2.075$  V vs Fc/Fc<sup>+</sup> ( $\Delta E = 0.090$  V at  $0.100$  V s<sup>-1</sup>) is ascribed to ligand reduction, therefore [Co<sup>I</sup>(tpy)<sub>2</sub>]<sup>2+</sup>/[Co<sup>I</sup>(tpy)(tpy<sup>-</sup>)]<sup>0</sup> reduction. The next reduction peak at  $-2.44$  V vs Fc/Fc<sup>+</sup> ( $\Delta E = 0.130$  V at  $0.300$  V s<sup>-1</sup>), is ascribed to a second ligand based reduction, namely [Co<sup>I</sup>(tpy)(tpy<sup>-</sup>)]<sup>0</sup>/[Co<sup>I</sup>(tpy<sup>-</sup>)<sub>2</sub>]<sup>-</sup> [39]. This assignment is in agreement with reported electrochemical data on [Co(tpy)<sub>2</sub>]<sup>2+</sup> and [Co(tpy)<sub>2</sub>]<sup>3+</sup> (see Table 5), as well as with the DFT computational chemistry study presented

above. Linear responses were obtained for the plots of the peak currents versus the square root of the scan rate, for the oxidation of [Co<sup>II</sup>(tpy)<sub>2</sub>]<sup>2+</sup> to [Co<sup>III</sup>(tpy)<sub>2</sub>]<sup>3+</sup>, also for the reduction of [Co<sup>II</sup>(tpy)<sub>2</sub>]<sup>2+</sup> to [Co<sup>I</sup>(tpy)<sub>2</sub>]<sup>1+</sup>, as well as for the reduction of [Co<sup>I</sup>(tpy)<sub>2</sub>]<sup>1+</sup> to [Co<sup>I</sup>(tpy)(tpy<sup>-</sup>)]<sup>0</sup> (see Supporting Information associated with this manuscript). The linear response of peak currents versus the square root of the scan rate, indicates diffusion-controlled electrochemical processes for the three main redox events of [Co(tpy)<sub>2</sub>]





**Fig. 5.** Top: Cyclic voltammogram (CV) at only two scan rates  $0.100 \text{ V s}^{-1}$  (red) and  $0.300 \text{ V s}^{-1}$  (navy), as well as the linear sweep voltammogram (LSV, black, scan rate  $0.002 \text{ V s}^{-1}$ ) obtained for either ca.  $0.002 \text{ mol dm}^{-3}$  or a saturated solution of  $[\text{Co}(\text{tpy})_2](\text{NO}_3)_2$  (complex 1), in solvent  $\text{CH}_3\text{CN}/0.1 \text{ mol dm}^{-3}$   $[\text{Bu}_4\text{N}][\text{PF}_6]$ , on a glassy carbon-working electrode. Bottom: Cyclic voltammograms of a  $0.002 \text{ mol dm}^{-3}$  solution of  $[\text{Co}(\text{tpy})_2](\text{NO}_3)_2$  (complex 1), at nine different scan rates ( $0.05$ – $5.00 \text{ V s}^{-1}$ ), over different potential ranges. (For interpretation of the references to colour in this figure legend, the reader is referred to the web version of this article.)

$(\text{NO}_3)_2$ , complex 1. The sigmoidal curves in Fig. 5 are the linear sweep voltammograms (LSVs) for electrolysis, obtained for the oxidation and the reduction of  $[\text{Co}(\text{tpy})_2](\text{NO}_3)_2$ , complex 1. The value of the limiting current of a LSV, is directly proportional to the concentration of the complex  $[\text{Co}(\text{tpy})_2](\text{NO}_3)_2$ , and can therefore be used for quantitative analysis [40]. The limiting current values obtained for the different oxidation and reduction processes of complex 1, can therefore be compared. The LSV for complex 1 shows a 1:1:1 ratio for the  $\text{Co}^{\text{III/II}}$ ,  $\text{Co}^{\text{II/I}}$  and  $[\text{Co}(\text{tpy})_2]^+ / [\text{Co}(\text{tpy})(\text{tpy}^-)]^0$  redox processes, consistent with an observed  $1e^-$  transfer process for each redox process. The first three cell reactions observed can be written as:

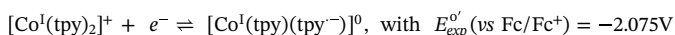
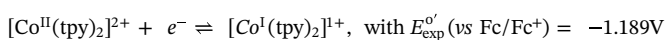
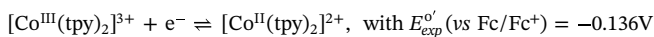
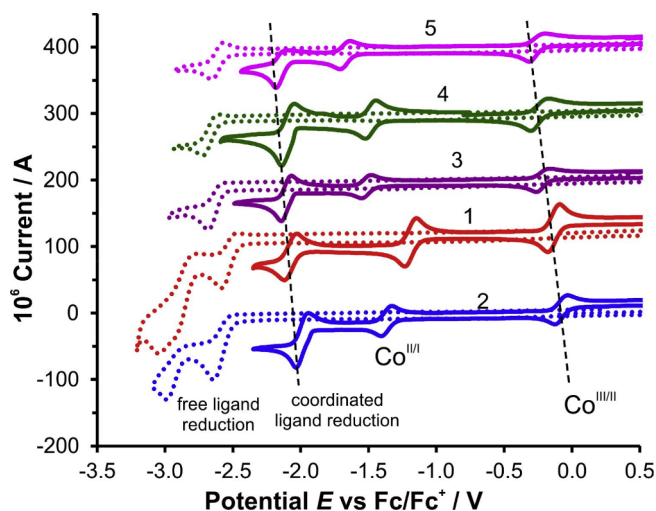


Fig. 5 (bottom) shows the CVs for  $[\text{Co}(\text{tpy})_2](\text{NO}_3)_2$ , complex 1, obtained over different potential ranges. The same redox character is obtained when the  $\text{Co}^{\text{III/II}}$  redox couple is scanned alone, or when the  $\text{Co}^{\text{III/II}}$  and  $\text{Co}^{\text{II/I}}$  redox couples are scanned together, or when all three redox couples are scanned together.

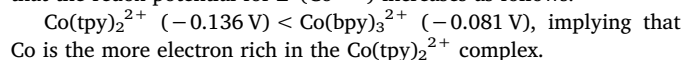
The  $0.100 \text{ V s}^{-1}$  cyclic voltammetry scans of the free polypyridine ligands **1a**–**5a**, as well as their corresponding polypyridine-Co(II) complexes **1**–**5**, are shown in Fig. 6, with data provided in Table 6. Each polypyridine-Co(II) complex **1**–**5** shows a chemically and electrochemically reversible  $\text{Co}^{\text{III/II}}$  redox couple, followed by a chemically and electrochemically reversible  $\text{Co}^{\text{II/I}}$  redox couple, followed by the reduction of the coordinated polypyridine ligand in the polypyridine-Co



**Fig. 6.** Cyclic voltammograms at only one scan rate of  $0.100 \text{ V s}^{-1}$ , obtained for either ca.  $0.002 \text{ mol dm}^{-3}$ , or saturated solutions of both the free ligands **1a**–**5a** (dotted lines), as well as their corresponding Co(II) complexes **1**–**5** (solid lines), in a  $\text{CH}_3\text{CN}$  solution with  $0.1 \text{ mol dm}^{-3}$   $[\text{Bu}_4\text{N}][\text{PF}_6]$  at supporting electrolyte, using a glassy carbon-working electrode.

(I) complexes. The reduction of the free uncoordinated polypyridine ligands **1a**–**5a** is more than  $0.5 \text{ V}$  more negative than that of the ligand based reduction redox processes of  $[\text{Co}(\text{N},\text{N},\text{N})_2]^+ / [\text{Co}(\text{N},\text{N},\text{N})(\text{N},\text{N},\text{N})]^{0+}$  (complex **1**) and  $[\text{Co}(\text{N},\text{N})_3]^+ / [\text{Co}(\text{N},\text{N})_2(\text{N},\text{N})]^{0+}$  (complexes **2**–**5**). In Table 5 the electrochemical data of polypyridine-Co(II) complexes **1**–**5** is compared with available electrochemical data from literature, and also electrochemical data of the uncoordinated ligand is provided in Table 6. From Table 5 it is clear that the current electrochemical redox data obtained in  $\text{CH}_3\text{CN}$  with the  $\text{Fc/Fc}^+$  couple as reference, agrees well with available literature values obtained under different experimental conditions (varying solvents, reference electrodes and supporting electrolytes). The electrochemical data for complexes **3** and **4** is reported here for the first time.

Comparing the CVs of the unsubstituted complexes **1** and **2**, we see that the redox potential for  $E^{\text{O}'}(\text{Co}^{\text{III/II}})$  increases as follows:



For the  $\text{Co}(4,4\text{-di-X-bpy})_3^{2+}$  complexes with  $\text{X} = \text{H}$  (**2**), Me (**3**),  $t\text{Bu}$  (**4**) or OMe (**5**), we observe that the redox potential for both  $E^{\text{O}'}(\text{Co}^{\text{III/II}})$  and  $E^{\text{O}'}(\text{Co}^{\text{II/I}})$  increases as follows:

OMe (**5**) <  $t\text{Bu}$  (**4**)  $\approx$  Me (**3**) < H (**2**), in agreement with the order of the *para* Hammett constants  $\sigma_{\text{para}}$ : OMe ( $-0.27$ ) < Me ( $-0.17$ )  $\approx$   $t\text{Bu}$  ( $-0.10$ ) < H ( $0$ ) [41]. The OMe group donates more electron density to Co than H, leading to a more negative redox potential for complex **5** (with  $\text{X} = \text{OMe}$ ) than for complex **2** (with  $\text{X} = \text{H}$ ).

Electrochemical data of complexes **1**–**5**, the free ligands **1a**–**5a**, as well as related Fe(II)-pyridyl complexes (Table 6), all show a similar trend in ease of reduction: namely that the reduction generally becomes increasingly difficult (more negative) in going from complex **1** to **5**, therefore as the substituent on the ligand becomes increasingly electron donating. This similar influence exerted by ligands **1a**–**5a** on the reduction of their corresponding Co– as well as their Fe-pyridyl complexes, indicates that good electronic communication exists between the ligand and the metal which it is coordinated to.

#### 4. Conclusion

DFT calculations show that  $d^6 \text{Co}(\text{tpy})_2^{3+}$  and  $d^6 \text{Co}(\text{N},\text{N})_3^{3+}$  complexes (where N,N = bpy or substituted bpy ligands), are low spin  $t_{2g}^6 e_g^0$  complexes of near  $D_{2d}$  and  $D_3$  symmetry respectively. Due to Jahn-Teller distortion, the  $d^7 [\text{Co}(\text{N},\text{N})_3]^{2+}$  complexes with  $S = 1/2$  have

two longer axial and four shorter equatorial Co–N bonds, while the  $d^7$   $[\text{Co}(\text{tpy})_2]^{2+}$  complex with  $S = 1/2$  has two shorter central (axial) Co–N bonds and four longer distal Co–N bonds, since in the latter complex, the distal Co–N bonds are more flexible than the Co–N axial bond in the rigid structure of the tridentate terpyridine ligand. The same trend is observed for the related high spin  $S = 3/2$  Co(II) complexes, though less pronounced. The  $d^8$   $\text{Co}(\text{tpy})_2^{1+}$  and  $\text{Co}(\text{N}_3\text{N})_3^{1+}$  complexes are paramagnetic with  $S = 1$ , exhibiting  $D_{2d}$  and near  $D_3$  symmetry respectively.

The electrochemical reduction of the polypyridine free ligands generally is irreversible at low scan rates. However, when coordinated to Co, the reduction of the coordinated ligand is reversible at all scan rates and occurs at ca. 0.5 V more positive than that of the free uncoordinated ligand. The electrochemical data obtained for a series of polypyridine–Co(II) complexes, shows that the ease of reduction of the Co metal or the coordinated ligands is directly influenced by the electronic properties of the groups substituted on the polypyridine ligand, the redox potential is increasing with increasingly electronegative substituents on the ligands. Similar trends were observed for the  $\text{Co}^{\text{III/II}}$  redox couple, the  $\text{Co}^{\text{II/I}}$  redox couple, the ligand based reduction of the Co(I) complex, as well as the reduction potential of the free ligand.

## Acknowledgements

This work has received support from the National Research Foundation (Grant numbers 113327 and 96111) and the Central Research Fund of the University of the Free State, Bloemfontein, South Africa. The High Performance Computing facility of the UFS and the Centre for High Performance Computing (CHPC), South Africa are acknowledged for computer time.

## Appendix A. Supplementary data

Supplementary data to this article can be found online at <https://doi.org/10.1016/j.ica.2018.10.020>.

## References

- [1] C.C. Scarborough, S. Sproules, T. Weyhermüller, S. de Beer, K. Wieghardt, Electronic and Molecular Structures of the Members of the Electron Transfer Series  $[\text{Cr}(\text{bpy})_3]^n$  ( $n = 3+, 2+, 1+, 0$ ): An X-ray Absorption Spectroscopic and Density Functional Theoretical Study, *Inorganic Chem.* 50 (2011) 12446–12462, <https://doi.org/10.1021/ic201123x>.
- [2] K.G. von Eschwege, J. Conradie, Iron Phenanthrolines: A Density Functional Theory Study, *Inorg. Chim. Acta* 471 (2017) 391–396, <https://doi.org/10.1016/j.ica.2017.11.047>.
- [3] G. Nord, Some Properties of 2,2'-Bipyridine, 1,10-Phenanthroline and Their Metal Complexes, *Comments Inorganic Chem. J. Critical Discuss. Curr. Literature* 4 (4) (1985) 193–212, <https://doi.org/10.1080/02603598508072261>.
- [4] S. Aroua, T.K. Todorova, P. Hommes, L.-M. Chamoreau, H.-U. Reissig, V. Mougél, M. Fontecave, Synthesis, Characterization, and DFT Analysis of Bis-Terpyridyl-Based Molecular Cobalt Complexes, *Inorg. Chem.* 56 (2017) 5930–5940, <https://doi.org/10.1021/acs.inorgchem.7b00595>.
- [5] J. England, E. Bill, T. Weyhermüller, F. Neese, M. Atanasov, K. Wieghardt, Molecular and Electronic Structures of Homoleptic Six-Coordinate Cobalt(II) Complexes of 2,2':6',2"-Terpyridine, 2,2'-Bipyridine, and 1,10-Phenanthroline. An Experimental and Computational Study, *Inorganic Chem.* 54 (2015) 12002–12018, <https://doi.org/10.1021/acs.inorgchem.5b02415>.
- [6] M. Safdari, P.W. Lohse, L. Häggman, S. Frykstrand, D. Högberg, M. Rutland, R.A. Asencio, J. Gardner, L. Kloos, A. Hagfeldt, G. Boschloo, Investigation of cobalt redox mediators and effects of  $\text{TiO}_2$  film topology in dye-sensitized solar cells, *Royal Soc. Chem. Adv.* 6 (2016) 56580–56588, <https://doi.org/10.1039/c6ra07107d>.
- [7] H. Ferreira, M.M. Conradie, K.G. von Eschwege, J. Conradie, Electrochemical and DFT study of the reduction of substituted phenanthrolines, *Polyhedron* 122 (2017) 147–154, <https://doi.org/10.1016/j.poly.2016.11.018>.
- [8] H. Ferreira, K.G. von Eschwege, J. Conradie, Electronic Properties of Fe Charge Transfer Complexes - a Combined Experimental and Theoretical Approach, *Electrochim. Acta* 216 (2016) 339–346, <https://doi.org/10.1016/j.electacta.2016.09.034>.
- [9] H. Ferreira, M.M. Conradie, J. Conradie, Electrochemical properties of a series of Co(II) complexes, containing substituted phenanthrolines, *Electrochim. Acta* 292 (2018) 489–501, <https://doi.org/10.1016/j.electacta.2018.09.151>.
- [10] J.S. Judge, W.A. Baker Jr., On the Spin Equilibrium in bis(2,2',2"-terpyridine) Cobalt(II) Salts, *Inorg. Chim. Acta* 1 (1967) 68–72, [https://doi.org/10.1016/S0020-1693\(00\)93141-4](https://doi.org/10.1016/S0020-1693(00)93141-4).
- [11] H.A. Goodwin, Spin Crossover in Cobalt(II) Systems, *Top. Curr. Chem.* 234 (2004) 23–47, <https://doi.org/10.1007/b95411>.
- [12] Joel T. Kirner, C. Michael Elliott, Are High-Potential Cobalt Tris(bipyridyl) Complexes Sufficiently Stable to Be Efficient Mediators in Dye-Sensitized Solar Cells? Synthesis, Characterization, and Stability Tests, *J. Phys. Chem. C* 119 (31) (2015) 17502–17514, <https://doi.org/10.1021/acs.jpcc.5b02513>.
- [13] G. te Velde, F.M. Bickelhaupt, E.J. Baerends, C.F. Guerra, S.J.A. van Gisbergen, J.G. Snijders, T.J. Ziegler, The ADF program system was obtained from Scientific Computing and Modeling, Amsterdam (<http://www.scm.com/>). For a description of the methods used in ADF, see *Chemistry with ADF*, *J. Comput. Chem.* 22 (2001) 931–967, <https://doi.org/10.1002/jcc.1056>.
- [14] A.D. Becke, Density-functional exchange-energy approximation with correct asymptotic behavior, *Physical Reviews A* 38 (1988) 3098–3100, <https://doi.org/10.1103/PhysRevA.38.3098>.
- [15] J.P. Perdew, Density-functional approximation for the correlation energy of the inhomogeneous electron gas, *Phys. Rev. B* 33 (1986) 8822–8824; Erratum: J.P. Perdew, *Phys. Rev. B* 34 (1986) 7406, [doi:10.1103/PhysRevB.33.8822](https://doi.org/10.1103/PhysRevB.33.8822).
- [16] N.C. Handy, A.J. Cohen, Left-Right Correlation Energy, *Mol. Phys.* 99 (2001) 403–412, <https://doi.org/10.1103/PhysRevB.33.8822>.
- [17] C.T. Lee, W.T. Yang, R.G. Parr, Development of the Colle-Salvetti correlation-energy formula into a functional of the electron-density, *Phys. Rev. B* 37 (1988) 785–789, <https://doi.org/10.1103/PhysRevB.37.785>.
- [18] P.J. Stephens, F.J. Devlin, C.F. Chabalowski, M.J. Frisch, Ab Initio Calculation of Vibrational Absorption and Circular Dichroism Spectra Using Density Functional Force Fields, *J. Phys. Chem.* 98 (1994) 11623–11627, <https://doi.org/10.1021/j100096a001>.
- [19] A.V. Marenich, J. Ho, M.L. Coote, C.J. Cramer, D.G. Truhlar, Computational electrochemistry: Prediction of liquid-phase reduction potentials, *Phys. Chem. Chem. Phys.* 16 (2014) 15068–15106, <https://doi.org/10.1039/C4CP01572J>.
- [20] M.J. Frisch, G.W. Trucks, H.B. Schlegel, G.E. Scuseria, M.A. Robb, J.R. Cheeseman, G. Scalmani, V. Barone, B. Mennucci, G.A. Petersson, H. Nakatsuji, M. Caricato, X. Li, H.P. Hratchian, A.F. Izmaylov, J. Bloino, G. Zheng, J.L. Sonnenberg, M. Hada, M. Ehara, K. Toyota, R. Fukuda, J. Hasegawa, M. Ishida, T. Nakajima, Y. Honda, O. Kitao, H. Nakai, T. Vreven, J.A. Montgomery (Jr.), J.E. Peralta, F. Ogliaro, M. Bearpark, J.J. Heyd, E. Brothers, K.N. Kudin, V.N. Staroverov, R. Kobayashi, J. Normand, K. Raghavachari, A. Rendell, J.C. Burant, S.S. Iyengar, J. Tomasi, M. Cossi, N. Rega, J.M. Millam, M. Klene, J.E. Knox, J.B. Cross, V. Bakken, C. Adamo, J. Jaramillo, R. Gomperts, R.E. Stratmann, O. Yazyev, A.J. Austin, R. Cammi, C. Pomelli, J.W. Ochterski, R.L. Martin, K. Morokuma, V.G. Zakrzewski, G.A. Voth, P. Salvador, J.J. Dannenberg, S. Dapprich, A.D. Daniels, Ö. Farkas, J.B. Foresman, J.V. Ortiz, J. Cioslowski, D.J. Fox, Gaussian 09, Revision D.01, Gaussian, Inc., Wallingford, CT, 2009.
- [21] M. Namazian, C.Y. Lin, M.L. Coote, Benchmark Calculations of Absolute Reduction Potential of Ferricinium / Ferrocene Couple in Nonaqueous Solutions, *J. Chem. Theory Comput.* 6 (2010) 2721–2725, <https://doi.org/10.1021/ct1003252>.
- [22] D.T. Sawyer, J.L. Roberts Jr., *Experimental Electrochemistry for Chemists*, John Wiley & Sons, New York, 1974, p. 54.
- [23] D.H. Evans, K.M. O'Connell, R.A. Peterson, M.J. Kelly, Cyclic Voltammetry, *J. Chem. Educ.* 60 (1983) 290–293, <https://doi.org/10.1021/ed060p290>.
- [24] G. Gritzner, J. Kuta, Recommendations on reporting electrode potentials in non-aqueous solvents, *Pure Appl. Chem.* 56 (1984) 461–466, <https://doi.org/10.1351/pac198456040461>.
- [25] M.J. Cook, I. Chambrier, G.F. White, E. Fourie, J.C. Swarts, Electrochemical and EPR studies of two substituted bis-cadmium tris-phthalocyanine complexes: Elucidation of unexpectedly different free-radical character, *Dalton Trans.* 7 (2009) 1136–1144, <https://doi.org/10.1039/b811451j>.
- [26] A. Auger, A.J. Muller, J.C. Swarts, Remarkable isolation, structural characterisation and electrochemistry of unexpected scrambling analogues of 5-ferrocenyl-10,20-diphenylporphyrin, *Dalton Trans.* 33 (2007) 3623–3633, <https://doi.org/10.1039/B811451J>.
- [27] A. Vargas, M. Zerara, E. Krausz, A. Hauser, L. Max, L. Daku, Density-Functional Theory Investigation of the Geometric, Energetic, and Optical Properties of the Cobalt(II)tris(2,2'-bipyridine) Complex in the High-Spin and the Jahn-Teller Active Low-Spin States, *J. Chem. Theory Comput.* 2 (2006) 1342–1359, <https://doi.org/10.1021/ct6001384>.
- [28] A. Vargas, I. Krivokapic, A. Hauser, L.M.L. Daku, Towards accurate estimates of the spin-state energetics of spin-crossover complexes within density functional theory: a comparative case study of cobalt(II) complexes, *Phys. Chem. Chem. Phys.* 15 (2013) 3752–3763, <https://doi.org/10.1039/c3cp44336a>.
- [29] I. Krivokapic, M. Zerara, M.L. Daku, A. Vargas, C. Enachescu, C. Ambrus, P. Tregenna-Piggott, N. Amstutz, E. Krausz, A. Hauser, Spin-crossover in cobalt(II) imine complexes, *Coord. Chem. Rev.* 251 (2007) 364–378, <https://doi.org/10.1016/j.ccr.2006.05.006>.
- [30] C.A. Kilner, M.A. Halcrow, An unusual discontinuity in the thermal spin transition in  $[\text{Co}(\text{terpy})_2][\text{BF}_4]_2$ , *Dalton Trans.* 39 (2010) 9008–9012, <https://doi.org/10.1039/c0dt00295j>.
- [31] A. Hauser, N. Amstutz, S. Delahaye, A. Sadki, S. Schenker, R. Sieber, M. Zerara, Fine Tuning the Electronic Properties of  $[\text{M}(\text{bpy})_3]^{2+}$  Complexes by Chemical Pressure ( $\text{M} = \text{Fe}^{2+}$ ,  $\text{Ru}^{2+}$ ,  $\text{Co}^{2+}$ ,  $\text{bpy} = 2,2'$ -Bipyridine, *Struct. Bond.* 106 (2004) 81–96, <https://doi.org/10.1007/b11307>.
- [32] D.N. Bowman, E. Jakubikova, Low-Spin versus High-Spin Ground State in Pseudo-Octahedral Iron Complexes, *Inorg. Chem.* 51 (2012) 6011–6019, <https://doi.org/10.1021/ic202344w>.
- [33] J. Sirirak, D. Sertphon, W. Phonsri, P. Harding, D.J. Harding, Comparison of density functionals for the study of the high spin low spin gap in Fe(III) spin crossover

- complexes, *Int. J. Quantum Chem.* 117 (9) (2017) e25362, <https://doi.org/10.1002/qua.25362>.
- [34] J. Conradie, A. Ghosh, DFT Calculations on the Spin-Crossover Complex Fe(salen)(NO): A Quest for the Best Functional, *J. Phys. Chem. B (Lett.)* 111 (2007) 12621–12624, <https://doi.org/10.1021/jp074480t>.
- [35] S. Kremer, W. Henke, D. Reinen, High-spin-low-spin equilibria of cobalt(2+) in the terpyridine complexes Co(terpy)2X2.nH2O, *Inorg. Chem.* 21 (1982) 3013–3022, <https://doi.org/10.1021/ic00138a019>.
- [36] H. Kvapilová, I. Hoskovicová, J. Ludvík, S. Zálší, J. Heyrovský, Theoretical Predictions of Redox Potentials of Fischer-Type Chromium Aminocarbene Complexes, *Organometallics* 33 (18) (2014) 4964–4972, <https://doi.org/10.1021/om500259u>.
- [37] D.C. Ashley, E. Jakubikova, Tuning the Redox Potentials and Ligand Field Strength of Fe(II) Polypyridines: The Dual  $\pi$ -Donor and  $\pi$ -Acceptor Character of Bipyridine, *Inorg. Chem.* 57 (2018) 9907–9917, <https://doi.org/10.1021/acs.inorgchem.8b01002>.
- [38] J. Ferrando-Soria, O. Fabelo, M. Castellano, J. Cano, S. Fordham, H.-C. Zhou, Multielectron oxidation in a ferromagnetically coupled dinickel(II) triple mesocate, *Chem. Commun.* 51 (2015) 13381–13384, <https://doi.org/10.1039/C5CC03544A>.
- [39] L.J. Kershaw Cook, F. Tuna, M.A. Halcrow, Iron(II) and cobalt(II) complexes of tris-azanyl analogues of 2,2':6',2''-terpyridine, *J. Chem. Soc. Dalton Trans.* 42 (6) (2013) 2254–2265, <https://doi.org/10.1039/c2dt31736b>.
- [40] D.A. Skoog, D.M. West, F.J. Holler, *Fundamentals of Analytical Chemistry*, 7th edition, Saunders College Publishing, Fort Worth, 1991, pp. 468–469.
- [41] C. Hansch, A. Leo, R.W. Taft, A Survey of Hammett Substituent Constants and Resonance and Field Parameters, *Chem. Rev.* 91 (2) (1991) 165–195, <https://doi.org/10.1021/cr00002a004>.
- [42] C. Arana, S. Yan, M. Keshavarz-K, K.T. Potts, H.D. Abruna, Electrocatalytic Reduction of Carbon Dioxide with Iron, Cobalt, and Nickel Complexes of Terdentate Ligands, *Inorg. Chem.* 31 (17) (1992) 3680–3682, <https://doi.org/10.1021/ic00043a034>.
- [43] T. Ayers, S. Scott, J. Goins, N. Caylor, D. Hathcock, S.J. Slattery, D.L. Jameson, Redox and spin state control of Co(II) and Fe(II) N-heterocyclic complexes, *Inorg. Chim. Acta* 307 (2000) 7–12, [https://doi.org/10.1016/S0020-1693\(00\)00179-1](https://doi.org/10.1016/S0020-1693(00)00179-1).
- [44] J. Chambers, B. Eaves, D. Parker, R. Claxton, P.S. Ray, S.J. Slattery, Inductive influence of 40-terpyridyl substituents on redox and spin state properties of iron(II) and cobalt(II) bis-terpyridyl complexes, *Inorg. Chim. Acta* 359 (2006) 2400–2406, <https://doi.org/10.1016/j.ica.2005.12.065>.
- [45] N. Elgrishi, M.B. Chambers, V. Artero, M. Fontecave, Terpyridine complexes of first row transition metals and electrochemical reduction of CO<sub>2</sub> to CO, *Phys. Chem. Chem. Phys.* 16 (2014) 13635–13644, <https://doi.org/10.1039/C4CP00451E>.
- [46] M.G.B. Drew, M.R.S. Foreman, A. Geist, M.J. Hudson, F. Marken, V. Norman, M. Weigl, Synthesis, structure, and redox states of homoleptic d-block metal complexes with bis-1,2,4-triazin-3-yl-pyridine and 1,2,4-triazin-3-yl-bipyridine extractants, *Polyhedron* 25 (4) (2006) 888–900, <https://doi.org/10.1016/j.poly.2005.09.030>.
- [47] S.A. Richert, P.K.S. Tsang, D.T. Sawyer, Ligand-Centered Redox Processes for MnL<sub>3</sub>, FeL<sub>3</sub>, and CoL<sub>3</sub> Complexes (L = Acetylacetonate, 8-Quinolinate, Picolinate, 2,2'-Bipyridyl, 1,10-Phenanthroline) and for Their Tetrakis(2,6-dichlorophenyl)porphyrinato Complexes [M(Por)], *Inorg. Chem.* 28 (1989) 2471–2475, <https://doi.org/10.1021/ic00311a044>.
- [48] D. Cabrala, P.C. Howlett, J.M. Pringle, X. Zhanga, D. MacFarlane, Electrochemistry of tris(2,2'-bipyridyl) cobalt(II) in ionic liquids and aprotic molecular solvents on glassy carbon and platinum electrodes, *Electrochim. Acta* 180 (2015) 419–426, <https://doi.org/10.1016/j.electacta.2015.08.135>.
- [49] A.J.L. Pombeiro, Electron-donor/acceptor properties of carbynes, carbenes, vinylidenes, allenylidenes and alkynyls as measured by electrochemical ligand parameters, *J. Organomet. Chem.* 690 (2005) 6021–6040, <https://doi.org/10.1016/j.jorganchem.2005.07.111>.



ELSEVIER

Contents lists available at ScienceDirect

## Data in Brief

journal homepage: [www.elsevier.com/locate/dib](http://www.elsevier.com/locate/dib)

CrossMark

## Data Article

## Cyclic voltammetry data of polypyridine ligands and Co(II)-polypyridine complexes

Hendrik Ferreira, Marrigje M. Conradie, Jeanet Conradie\*

Department of Chemistry, University of the Free State, PO Box 339, Bloemfontein, 9300, South Africa

## ARTICLE INFO

## Article history:

Received 20 November 2018

Received in revised form

9 December 2018

Accepted 12 December 2018

Available online 16 December 2018

## ABSTRACT

The data presented in this article is related to the research article entitled “Electrochemical and electronic properties of a series of substituted polypyridine ligands and their Co(II) complexes” (Ferreira et al., 2019). This data article presents electrochemical data of five polypyridine ligands, as well as of the three redox couples of each of their corresponding five polypyridine-containing Co(II) complexes. All complexes exhibit two Co-based redox couples ( $\text{Co}^{\text{III/II}}$  and  $\text{Co}^{\text{II/I}}$ ), as well as a ligand-based reduction of the Co(I) complex.

© 2018 The Authors. Published by Elsevier Inc. This is an open access article under the CC BY license (<http://creativecommons.org/licenses/by/4.0/>).

## Specifications table

Subject area	Chemistry
More specific subject area	Electrochemistry
Type of data	Table, text file, graph, figure
How data were acquired	BAS 100B/W electrochemical analyzer (Electrochemical studies).
Data format	Raw and analyzed.

DOI of original article: <https://doi.org/10.1016/j.ica.2018.10.020>

\* Corresponding author.

E-mail address: [conradj@ufs.ac.za](mailto:conradj@ufs.ac.za) (J. Conradie).<https://doi.org/10.1016/j.dib.2018.12.043>

2352-3409/© 2018 The Authors. Published by Elsevier Inc. This is an open access article under the CC BY license (<http://creativecommons.org/licenses/by/4.0/>).

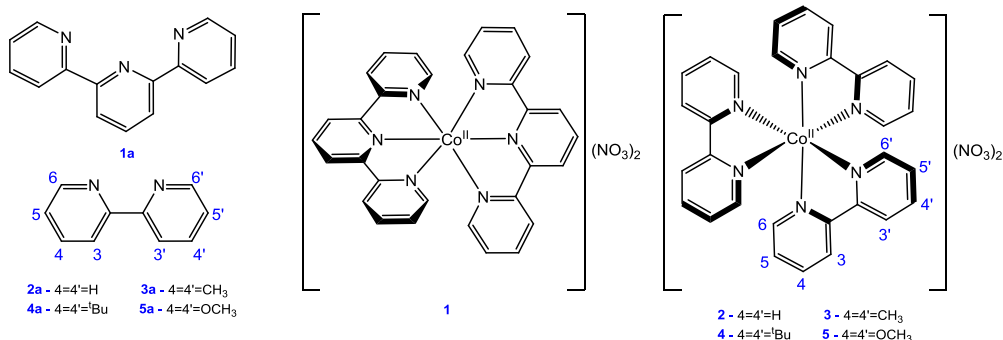
Experimental factors	Samples were used as synthesized. The solvent-electrolyte solution in the electrochemical cell was degassed with Ar for 10 min, the sample was added, the sample-solvent-electrolyte solution was then degassed for another 2 min and the cell was kept under a blanket of purified argon during the electrochemical experiments.
Experimental features	All electrochemical experiments were done in a 2 ml electrochemical cell containing three-electrodes (a glassy carbon working electrode, a Pt auxiliary electrode and a Ag/Ag <sup>+</sup> reference electrode), connected to a BAS 100B/W electrochemical analyzer. Data obtained was exported to excel for analysis and diagram preparation.
Data source location	Department of Chemistry, University of the Free State, Nelson Mandela Street, Bloemfontein, South Africa.
Data accessibility	Data is with article.
Related research article	Hendrik Ferreira, Marringje M. Conradie and Jeanet Conradie, Electrochemical and electronic properties of a series of substituted polypyridine ligands and their Co(II) complexes, <i>Inorganica Chimica Acta</i> , 2019, 486, 26–35. DOI 10.1016/j.ica.2018.10.020 [1].

### Value of the data

- This data provides cyclic voltammograms for five polypyridine ligands, 2,2':6',2''-terpyridine (tpy, ligand **1a**), 2,2'-dipyridyl (bpy, ligand **2a**), 4,4'-dimethyl-2,2'-bipyridine (4,4'-di-Me-bpy, ligand **3a**), 4,4'-di-tert-butyl-2,2'-dipyridyl (4,4'-di-<sup>t</sup>Bu-bpy, ligand **4a**) and 4,4'-dimethoxy-2,2'-bipyridine (4,4'-di-OMe-bpy, ligand **5a**).
- This data provides cyclic voltammograms and detailed electrochemical data for Co(tpy)<sub>2</sub>(NO<sub>3</sub>)<sub>2</sub>, complex **1**, Co(bpy)<sub>3</sub>(NO<sub>3</sub>)<sub>2</sub>, complex **2**, Co(4,4'-di-Me-bpy)<sub>3</sub>(NO<sub>3</sub>)<sub>2</sub>, complex **3**, Co(4,4'-di-<sup>t</sup>Bu-bpy)<sub>3</sub>(NO<sub>3</sub>)<sub>2</sub>, complex **4** and Co(4,4'-di-OMe-bpy)<sub>3</sub>(NO<sub>3</sub>)<sub>2</sub>, complex **5**.
- The current contribution is the first to present complete electrochemical data for all three reversible redox peaks at different scan rates, over two orders of magnitudes, for terpyridine-Co(II), bipyridine-Co(II), as well as substituted bipyridine-Co(II) complexes.
- Accurate redox data is important to determine the potential of a compound, in order to determine its suitability to act as a redox mediator, to be used in dye-sensitized solar cells (DSSC) [2–4].

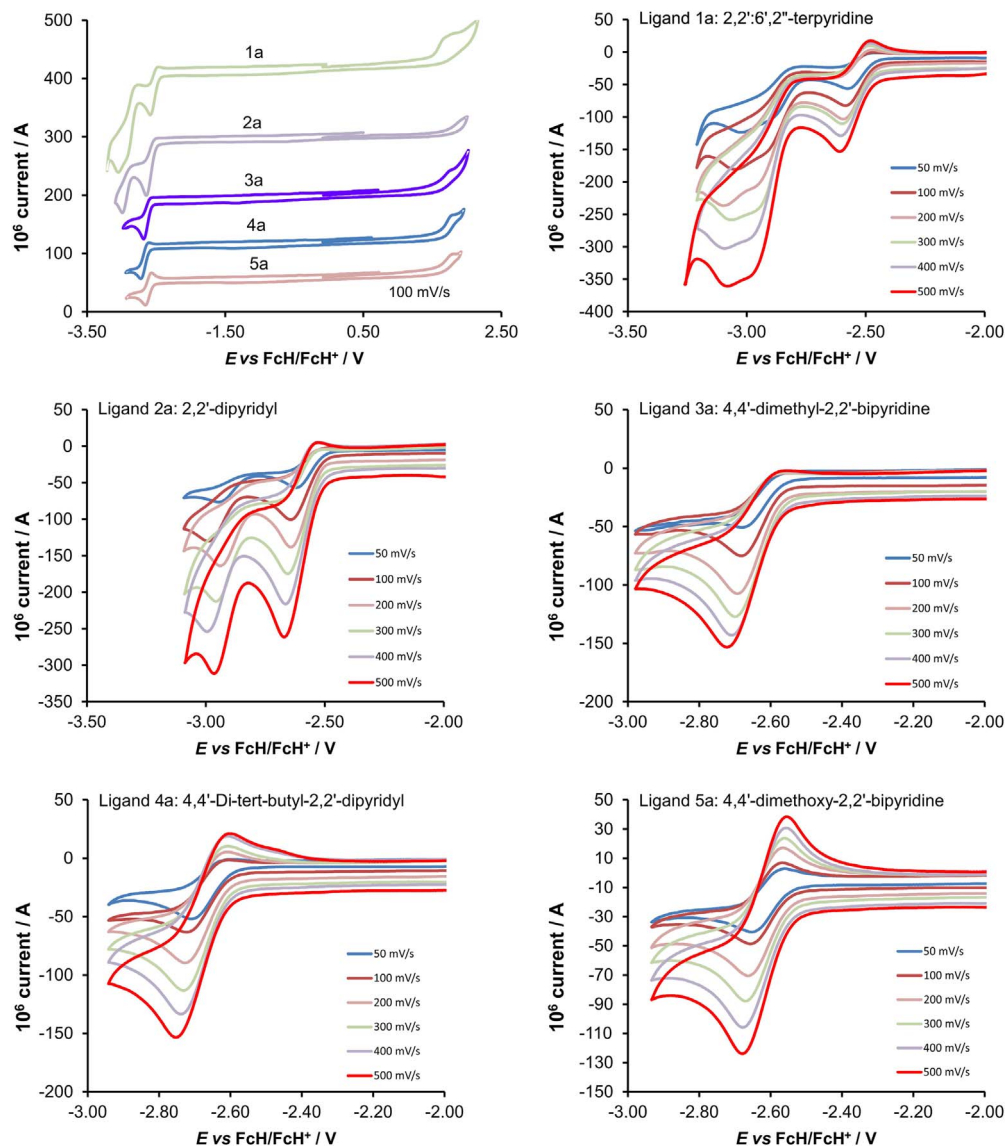
### 1. Data

Fig. 1 gives the structures of ligands **1a–5a** and complexes **1–5**. Fig. 2 shows the cyclic voltammetry (CV) scans for the polypyridyl free ligands **1a–5a** at different scan rates (0.10 V s<sup>−1</sup> scans from [1]). Cyclic voltammograms of the complexes **1–5**, showing four redox events each, are presented in



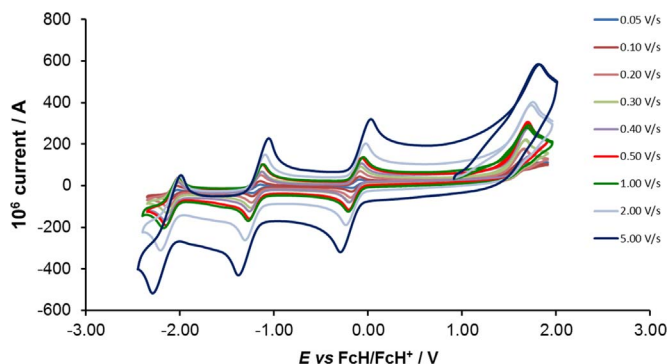
**Fig. 1.** Structure and numbering of the terpyridine (**1a**) and substituted bipyridine (**2a–5a**) ligands, as well as the terpyridine-Co(II) complex **1** and substituted bipyridine-Co(II) complexes, **2–5**.



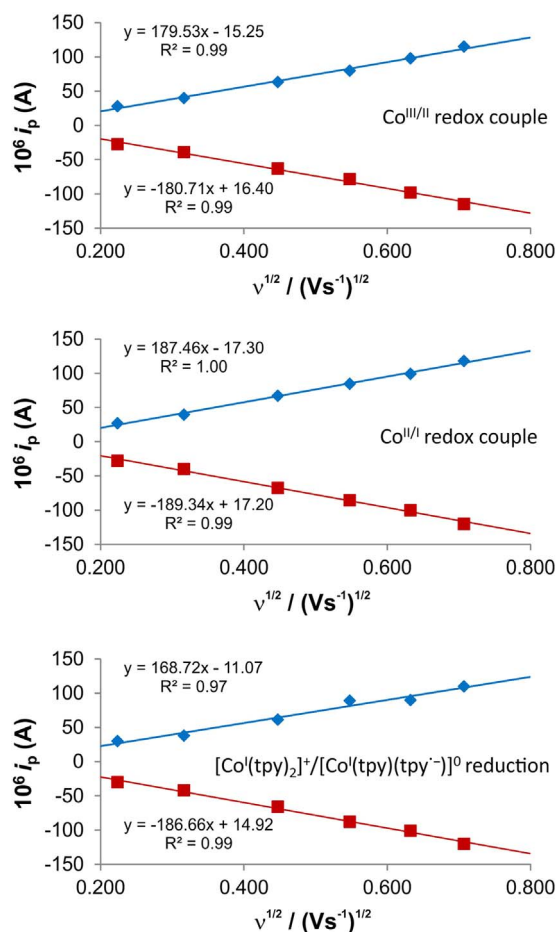


**Fig. 2.** Cyclic voltammograms of ca.  $0.002 \text{ mol dm}^{-3}$  or saturated solutions of the free ligands **1a–5a**, at the indicated scan rates ( $0.10 \text{ V s}^{-1}$  top left for the comparative graph and  $0.05\text{--}0.50 \text{ V s}^{-1}$  for all other graphs). The reduction peak of ligand **5a** is chemically ( $i_{pa}/i_{pc} = 0.9$ ) and electrochemically ( $\Delta E_p = E_{pa} - E_{pc} = 0.088 \text{ V}$ ) reversible at all scan rates above  $0.05 \text{ V s}^{-1}$ , while the reduction of free ligands **2a–5a** **1a – 4a** is irreversible at low scan rates.

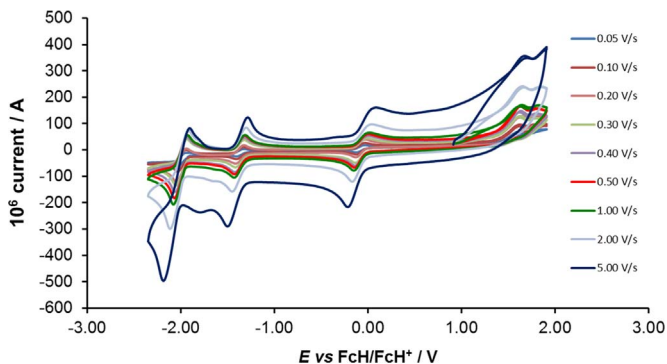
**Figs. 3–8** ( $0.10 \text{ V s}^{-1}$  scans from [1]), with the data summarized in **Tables 1–5**. The redox events are the  $\text{Co}^{\text{III/II}}$  redox couple (peak 1), the  $\text{Co}^{\text{II/I}}$  redox couple (peak 2) and the ligand reduction peak (peak 3), as well as an irreversible peak at ca.  $1.63 \text{ V}$  vs  $\text{FcH/FcH}^+$  (preliminary assigned to anionic nitrate oxidation). The data obtained in this data article, compares well with available published data on some of the redox events for some of the complexes, namely complex **1** [5–10], complex **2** [11–13] and complex **5** [11]; obtained under different experimental conditions (different solvents, scan rates



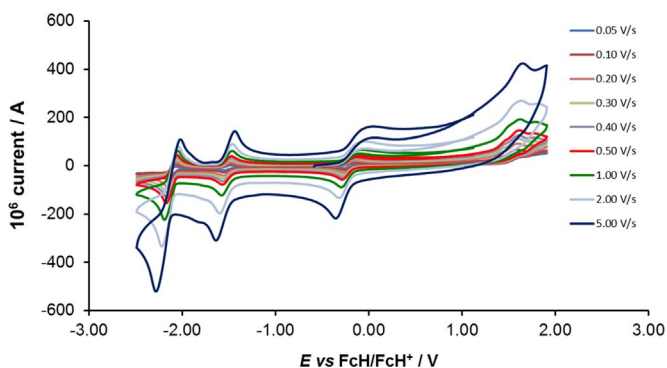
**Fig. 3.** Cyclic voltammograms of complex 1,  $[\text{Co}(\text{tpy})_2](\text{NO}_3)_2$ , at scan rates of  $0.05 \text{ V s}^{-1}$  (lowest peak current) –  $5.00 \text{ V s}^{-1}$  (highest peak current). All scans were initiated in the positive direction from 1 V. Data is summarized in Table 1.



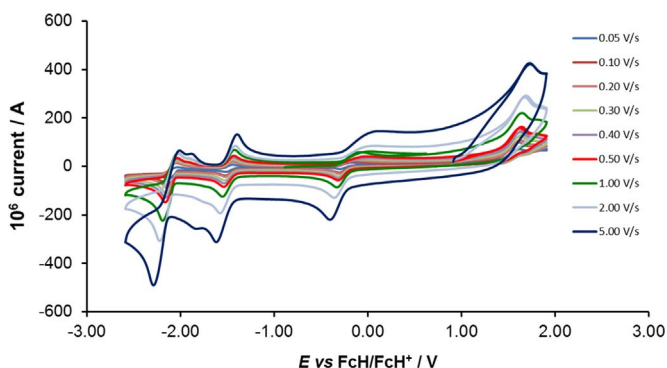
**Fig. 4.** The linear relationship between the peak currents ( $i_p$ ) vs the square root of the scan rate ( $v^{1/2}$ ) for the three main redox events, in the CV of  $[\text{Co}(\text{tpy})_2](\text{NO}_3)_2$  (complex 1) in Fig. 3. This relationship can be described by the linear Randles–Sevcik equation  $i_p = (2.69 \times 10^5) n^{1.5} A D^{0.5} C v^{0.5}$  ( $n$  = the number of exchanged electrons,  $A$  = electrode area ( $\text{cm}^2$ ),  $D$  = diffusion coefficient ( $\text{cm}^2 \text{ s}^{-1}$ ),  $C$  = bulk concentration ( $\text{mol cm}^{-3}$ ) of the electroactive species).



**Fig. 5.** Cyclic voltammograms of  $[\text{Co}(\text{bpy})_2](\text{NO}_3)_2$  (complex **2**), at scan rates of  $0.05 \text{ V s}^{-1}$  (lowest peak current) –  $5.00 \text{ V s}^{-1}$  to  $5.00 \text{ V s}^{-1}$  (highest peak current). All scans were initiated in the positive direction from 1 V. Data is summarized in Table 2.

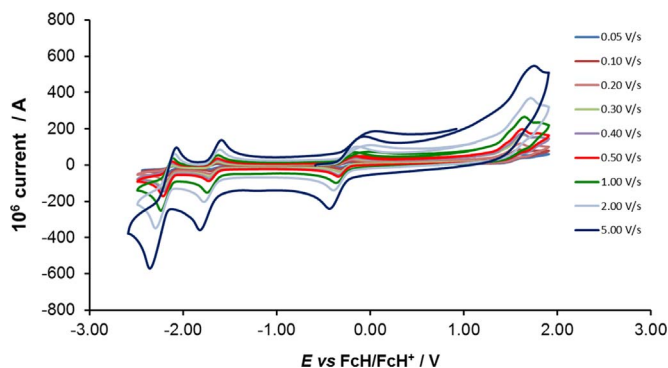


**Fig. 6.** Cyclic voltammograms of  $[\text{Co}(4,4'\text{-Me-bpy})_2](\text{NO}_3)_2$  (complex **3**), at scan rates of  $0.05 \text{ V s}^{-1}$  (lowest peak current) –  $5.00 \text{ V s}^{-1}$  to  $5.00 \text{ V s}^{-1}$  (highest peak current). All scans were initiated in the positive direction from 1 V. Data is summarized in Table 3.



**Fig. 7.** Cyclic voltammograms of  $[\text{Co}(4,4'\text{-tBu-bpy})_2](\text{NO}_3)_2$  (complex **4**), at scan rates of  $0.05 \text{ V s}^{-1}$  (lowest peak current) –  $5.00 \text{ V s}^{-1}$  to  $5.00 \text{ V s}^{-1}$  (highest peak current). All scans were initiated in the positive direction from 1 V. Data is summarized in Table 4.





**Fig. 8.** Cyclic voltammograms of  $[\text{Co}(4,4'\text{-OMe-bpy})_2](\text{NO}_3)_2$  (complex **5**), at scan rates of  $0.05 \text{ V s}^{-1}$  (lowest peak current) –  $5.00 \text{ V s}^{-1}$  to  $5.00 \text{ V s}^{-1}$  (highest peak current). All scans were initiated in the positive direction from 1 V. Data is summarized in Table 5.

**Table 1**

Electrochemical data (potential in V vs  $\text{FcH}/\text{FcH}^+$  and current in A) obtained in  $\text{CH}_3\text{CN}$  for *ca.*  $0.002 \text{ mol dm}^{-3}$  of  $[\text{Co}(\text{tpy})_2](\text{NO}_3)_2$  (complex **1**), at indicated scan rates in  $\text{V s}^{-1}$ . Peak 1 is the  $\text{Co}^{\text{III/II}}$  redox couple, peak 2 the  $\text{Co}^{\text{II/I}}$  redox couple and peak 3 the ligand reduction peak.PI

	Scan rate	$E_{\text{pa}}$	$E_{\text{pc}}$	$E^{\circ'}$	$\Delta E$	$10^6 I_{\text{pa}}$	$I_{\text{pc}}/I_{\text{pa}}$
Peak 1	0.05	−0.090	−0.174	−0.132	0.084	28.0	1.0
	0.10	−0.094	−0.178	−0.136	0.084	40.0	1.0
	0.20	−0.088	−0.184	−0.136	0.096	63.5	1.0
	0.30	−0.080	−0.192	−0.136	0.112	80.0	1.0
	0.40	−0.072	−0.208	−0.140	0.136	98.0	1.0
	0.50	−0.072	−0.202	−0.137	0.130	115.0	1.0
	1.00	−0.054	−0.208	−0.131	0.154	113.0	1.0
	2.00	−0.030	−0.234	−0.132	0.204	165.0	1.0
	5.00	0.026	−0.294	−0.134	0.320	248.0	1.0
Peak 2	0.05	−1.148	−1.230	−1.189	0.082	27.0	1.0
	0.10	−1.146	−1.232	−1.189	0.086	39.5	1.0
	0.20	−1.140	−1.240	−1.190	0.100	67.0	1.0
	0.30	−1.134	−1.248	−1.191	0.114	84.5	1.0
	0.40	−1.130	−1.262	−1.196	0.132	99.0	1.0
	0.50	−1.126	−1.262	−1.194	0.136	118.0	1.0
	1.00	−1.116	−1.274	−1.195	0.158	115.0	1.0
	2.00	−1.098	−1.308	−1.203	0.210	168.0	1.0
	5.00	−1.058	−1.378	−1.218	0.320	263.0	1.0
Peak 3	0.05	−2.028	−2.120	−2.074	0.092	30.0	1.0
	0.10	−2.030	−2.120	−2.075	0.090	38.0	1.1
	0.20	−2.022	−2.128	−2.075	0.106	61.5	1.1
	0.30	−2.020	−2.138	−2.079	0.118	89.0	1.0
	0.40	−2.020	−2.154	−2.087	0.134	90.0	1.1
	0.50	−2.014	−2.148	−2.081	0.134	110.0	1.1
	1.00	−2.012	−2.174	−2.093	0.162	110.0	1.1
	2.00	−2.006	−2.208	−2.107	0.202	155.0	1.1
	5.00	−1.990	−2.290	−2.140	0.300	205.0	1.2

**Table 2**

Electrochemical data (potential in V vs FcH/FcH<sup>+</sup> and current in A) obtained in CH<sub>3</sub>CN for ca. 0.002 mol dm<sup>−3</sup> of [Co(bpy)<sub>2</sub>](NO<sub>3</sub>)<sub>2</sub> (complex **2**), at indicated scan rates in V s<sup>−1</sup>. Peak 1 is the Co<sup>III/II</sup> redox couple, peak 2 the Co<sup>III/I</sup> redox couple and peak 3 the ligand reduction peak.

	Scan rate	<i>E</i> <sub>pa</sub>	<i>E</i> <sub>pc</sub>	<i>E</i> <sup>o'</sup>	Δ <i>E</i>	10 <sup>6</sup> <i>I</i> <sub>pa</sub>	<i>I</i> <sub>pc</sub> / <i>I</i> <sub>pa</sub>
Peak 1	0.05	−0.038	−0.120	−0.079	0.082	16.5	1.0
	0.10	−0.038	−0.124	−0.081	0.086	23.0	1.1
	0.20	−0.032	−0.128	−0.080	0.096	34.0	1.1
	0.30	−0.016	−0.134	−0.075	0.118	36.5	1.2
	0.40	−0.002	−0.140	−0.071	0.138	43.0	1.2
	0.50	0.000	−0.144	−0.072	0.144	46.0	1.2
	1.00	0.008	−0.150	−0.071	0.158	49.0	1.2
	2.00	0.034	−0.168	−0.067	0.202	66.0	1.4
Peak 2	5.00	0.086	−0.216	−0.065	0.302	100.0	1.4
	0.05	−1.332	−1.402	−1.367	0.070	16.5	1.1
	0.10	−1.334	−1.404	−1.369	0.070	23.5	0.9
	0.20	−1.330	−1.412	−1.371	0.082	35.0	1.1
	0.30	−1.324	−1.416	−1.370	0.092	40.0	1.2
	0.40	−1.320	−1.420	−1.370	0.100	45.0	1.3
	0.50	−1.318	−1.426	−1.372	0.108	55.0	1.2
	1.00	−1.316	−1.428	−1.372	0.112	56.0	1.2
Peak 3	2.00	−1.304	−1.448	−1.376	0.144	83.0	1.2
	5.00	−1.288	−1.500	−1.394	0.212	120.0	1.3
	0.05	−1.950	−2.028	−1.989	0.078	33.5	1.1
	0.10	−1.946	−2.032	−1.989	0.086	46.5	1.2
	0.20	−1.944	−2.048	−1.996	0.104	57.0	1.5
	0.30	−1.934	−2.052	−1.993	0.118	83.0	1.2
	0.40	−1.932	−2.062	−1.997	0.130	96.0	1.2
	0.50	−1.930	−2.066	−1.998	0.136	110.0	1.2
	1.00	−1.928	−2.078	−2.003	0.150	118.0	1.2
	2.00	−1.920	−2.116	−2.018	0.196	156.0	1.3
	5.00	−1.906	−2.186	−2.046	0.280	230.0	1.3

**Table 3**

Electrochemical data (potential in V vs FcH/FcH<sup>+</sup> and current in A) obtained in CH<sub>3</sub>CN for ca. 0.002 mol dm<sup>−3</sup> of [Co(4,4'-Me-bpy)<sub>2</sub>](NO<sub>3</sub>)<sub>2</sub> (complex **3**), at indicated scan rates in V s<sup>−1</sup>. Peak 1 is the Co<sup>III/II</sup> redox couple, peak 2 the Co<sup>III/I</sup> redox couple and peak 3 the ligand reduction peak.

	Scan rate	<i>E</i> <sub>pa</sub>	<i>E</i> <sub>pc</sub>	<i>E</i> <sup>o'</sup>	Δ <i>E</i>	10 <sup>6</sup> <i>I</i> <sub>pa</sub>	<i>I</i> <sub>pc</sub> / <i>I</i> <sub>pa</sub>
Peak 1	0.05	−0.166	−0.262	−0.214	0.096	10.0	1.2
	0.10	−0.162	−0.264	−0.213	0.102	15.0	1.2
	0.20	−0.152	−0.268	−0.210	0.116	20.0	1.4
	0.30	−0.146	−0.274	−0.210	0.128	25.5	1.4
	0.40	−0.132	−0.276	−0.204	0.144	28.5	1.5
	0.50	−0.132	−0.284	−0.208	0.152	33.0	1.4
	1.00	−0.104	−0.296	−0.200	0.192	44.0	1.6
	2.00	−0.058	−0.318	−0.188	0.260	58.0	1.7
Peak 2	5.00	0.040	−0.352	−0.156	0.392	95.0	1.5
	0.05	−1.482	−1.546	−1.514	0.064	11.5	1.0
	0.10	−1.486	−1.548	−1.517	0.062	16.0	1.1
	0.20	−1.482	−1.554	−1.518	0.072	22.5	1.2
	0.30	−1.480	−1.562	−1.521	0.082	28.0	1.2
	0.40	−1.476	−1.564	−1.520	0.088	34.0	1.2
	0.50	−1.478	−1.568	−1.523	0.090	40.0	1.2
	1.00	−1.468	−1.578	−1.523	0.110	57.0	1.3
	2.00	−1.464	−1.598	−1.531	0.134	88.0	1.4
	5.00	−1.440	−1.636	−1.538	0.196	155.0	1.0

**Table 3** (continued)

	Scan rate	$E_{pa}$	$E_{pc}$	$E^{\circ'}$	$\Delta E$	$10^6 I_{pa}$	$I_{pc}/I_{pa}$
Peak 3	0.05	−2.068	−2.138	−2.103	0.070	23.0	1.2
	0.10	−2.070	−2.144	−2.107	0.074	340.0	1.2
	0.20	−2.066	−2.154	−2.110	0.088	50.5	1.2
	0.30	−2.062	−2.164	−2.113	0.102	65.0	1.2
	0.40	−2.056	−2.166	−2.111	0.110	75.0	1.2
	0.50	−2.058	−2.172	−2.115	0.114	90.0	1.2
	1.00	−2.048	−2.190	−2.119	0.142	123.0	1.2
	2.00	−2.042	−2.220	−2.131	0.178	174.0	1.2
	5.00	−2.022	−2.280	−2.151	0.258	240.0	1.4

**Table 4**

Electrochemical data (potential in V vs FcH/FcH<sup>+</sup> and current in A) obtained in CH<sub>3</sub>CN for ca. 0.002 mol dm<sup>−3</sup> of [Co(4,4'-tBu-bpy)<sub>2</sub>](NO<sub>3</sub>)<sub>2</sub> (complex **4**), at indicated scan rates in V s<sup>−1</sup>. Peak 1 is the Co<sup>III/II</sup> redox couple, peak 2 the Co<sup>III</sup> redox couple and peak 3 the ligand reduction peak.

	Scan rate	$E_{pa}$	$E_{pc}$	$E^{\circ'}$	$\Delta E$	$10^6 I_{pa}$	$I_{pc}/I_{pa}$
Peak 1	0.05	−0.184	−0.294	−0.239	0.110	13.0	1.2
	0.10	−0.174	−0.302	−0.238	0.128	20.5	1.2
	0.20	−0.144	−0.298	−0.221	0.154	21.0	1.4
	0.30	−0.044	−0.310	−0.177	0.266	21.5	1.6
	0.40	0.020	−0.312	−0.146	0.332	25.0	1.6
	0.50	0.002	−0.316	−0.157	0.318	28.0	1.6
	1.00	−0.088	−0.328	−0.208	0.240	55.0	1.3
	2.00	0.050	−0.358	−0.154	0.408	48.0	1.8
	5.00	0.114	−0.402	−0.144	0.516	53.0	2.4
Peak 2	0.05	−1.448	−1.516	−1.482	0.068	14.0	0.9
	0.10	−1.448	−1.520	−1.484	0.072	24.0	1.1
	0.20	−1.444	−1.520	−1.482	0.076	25.0	1.2
	0.30	−1.440	−1.530	−1.485	0.090	32.0	1.2
	0.40	−1.434	−1.532	−1.483	0.098	36.0	1.3
	0.50	−1.434	−1.536	−1.485	0.102	43.0	1.3
	1.00	−1.426	−1.548	−1.487	0.122	65.0	1.3
	2.00	−1.418	−1.574	−1.496	0.156	82.0	1.4
	5.00	−1.400	−1.616	−1.508	0.216	126.0	1.3
Peak 3	0.05	−2.034	−2.130	−2.082	0.096	28.0	1.3
	0.10	−2.046	−2.140	−2.093	0.094	42.5	1.3
	0.20	−2.046	−2.146	−2.096	0.100	45.0	1.4
	0.30	−2.040	−2.156	−2.098	0.116	56.0	1.4
	0.40	−2.038	−2.162	−2.100	0.124	67.0	1.3
	0.50	−2.038	−2.164	−2.101	0.126	75.0	1.4
	1.00	−2.028	−2.190	−2.109	0.162	115.0	1.3
	2.00	−2.028	−2.222	−2.125	0.194	136.0	1.4
	5.00	−2.012	−2.288	−2.150	0.276	195.0	1.5

and supporting electrolytes). The linear responses obtained for the graphs of the peak currents vs the square root of the scan rate, for three main redox events in the CV of complex **1** (see Fig. 4), are in agreement with the Randles–Sevcik equation [14].

## 2. Experimental design, materials, and methods

Electrochemical studies, by means of cyclic voltammetry (CV), were performed at 25 °C on a BAS 100B/W electrochemical analyser under inert conditions as described previously [1]. The concentration of the analyte was 0.002 mol dm<sup>−3</sup> or saturated. The solvent was dry acetonitrile and the

**Table 5**  
Electrochemical data (potential in V vs FcH/FcH<sup>+</sup> and current in A) obtained in CH<sub>3</sub>CN for ca. 0.002 mol dm<sup>−3</sup> of [Co(4,4′-OMe-bpy)<sub>2</sub>](NO<sub>3</sub>)<sub>2</sub> (complex **5**), at indicated scan rates in V s<sup>−1</sup>. Peak 1 is the Co<sup>III/II</sup> redox couple, peak 2 the Co<sup>III/I</sup> redox couple and peak 3 the ligand reduction peak.

	Scan rate	<i>E</i> <sub>pa</sub>	<i>E</i> <sub>pc</sub>	<i>E</i> <sup>o</sup>	Δ <i>E</i>	10 <sup>6</sup> <i>I</i> <sub>pa</sub>	<i>I</i> <sub>pc</sub> / <i>I</i> <sub>pa</sub>
Peak 1	0.05	−0.218	−0.314	−0.266	0.096	13.0	1.2
	0.10	−0.216	−0.316	−0.266	0.100	19.0	1.2
	0.20	−0.210	−0.324	−0.267	0.114	29.5	1.2
	0.30	−0.192	−0.330	−0.261	0.138	33.0	1.3
	0.40	−0.196	−0.338	−0.267	0.142	40.0	1.3
	0.50	−0.192	−0.340	−0.266	0.148	47.0	1.2
	1.00	−0.170	−0.366	−0.268	0.196	64.0	1.3
	2.00	−0.146	−0.390	−0.268	0.244	93.0	1.2
Peak 2	5.00	−0.072	−0.434	−0.253	0.362	135.0	1.2
	0.05	−1.640	−1.706	−1.673	0.066	13.0	1.1
	0.10	−1.638	−1.708	−1.673	0.070	18.0	1.2
	0.20	−1.638	−1.714	−1.676	0.076	22.5	1.5
	0.30	−1.634	−1.728	−1.681	0.094	37.5	1.1
	0.40	−1.636	−1.724	−1.680	0.088	34.0	1.6
	0.50	−1.632	−1.728	−1.680	0.096	40.0	1.5
	1.00	−1.628	−1.744	−1.686	0.116	53.0	2.0
Peak 3	2.00	−1.608	−1.778	−1.693	0.170	87.0	1.5
	5.00	−1.588	−1.818	−1.703	0.230	120.0	1.8
	0.05	−2.084	−2.178	−2.131	0.094	14.0	1.7
	0.10	−2.102	−2.180	−2.141	0.078	17.0	2.3
	0.20	−2.122	−2.196	−2.159	0.074	27.5	2.3
	0.30	−2.118	−2.216	−2.167	0.098	48.0	1.7
	0.40	−2.120	−2.210	−2.165	0.090	51.0	2.0
	0.50	−2.116	−2.214	−2.165	0.098	65.0	1.8
	1.00	−2.110	−2.238	−2.174	0.128	99.0	1.6
	2.00	−2.090	−2.296	−2.193	0.206	156.0	1.4
	5.00	−2.072	−2.356	−2.214	0.284	250.0	1.4

supporting electrolyte 0.1 mol dm<sup>−3</sup> tetra-*n*-butylammoniumhexafluorophosphate ([<sup>n</sup>(Bu)<sub>4</sub>N][PF<sub>6</sub>]). A three-electrode cell comprising of a glassy carbon (surface area 7.07 × 10<sup>−6</sup> m<sup>2</sup>) working electrode, Pt auxiliary electrode and a Ag/Ag<sup>+</sup> (0.010 mol dm<sup>−3</sup> AgNO<sub>3</sub> in CH<sub>3</sub>CN) reference electrode [15], mounted on a Luggin capillary [16] was used.

### Acknowledgments

This work has received support from the South African National Research Foundation (Grant numbers 113327 and 96111) and the Central Research Fund of the University of the Free State, Bloemfontein, South Africa.

### Transparency document. Supporting information

Transparency document associated with this article can be found in the online version at <https://doi.org/10.1016/j.dib.2018.12.043>.

## References

- [1] H. Ferreira, M.M. Conradie, J. Conradie, Electrochemical and electronic properties of a series of substituted polypyridine ligands and their Co(II) complexes, *Inorg. Chim. Acta* 486 (2019) 26–35. <https://doi.org/10.1016/j.ica.2018.10.020>.
- [2] F. Gajardo, B. Loeb, Spectroscopic and electrochemical properties of a series of substituted polypyridine Co(II)/Co(III) couples and their potentiality as mediators for solar cells, *J. Chil. Chem. Soc.* 56 (2) (2011) 697–701. <https://doi.org/10.4067/S0717-97072011000200016>.
- [3] Z. Yu, N. Vlachopoulos, M. Gorlov, L. Kloo, Liquid electrolytes for dye-sensitized solar cells, *J. Chem. Soc. Dalton Trans.* 40 (2011) 10289–10303. <https://doi.org/10.1039/C1DT11023C>.
- [4] M. Grätzel, Solar energy conversion by dye-sensitized photovoltaic cells, *Inorg. Chem.* 44 (2005) 6841–6851. <https://doi.org/10.1021/ic0508371>.
- [5] C. Arana, S. Yan, M. Keshavarz-K, K.T. Potts, H.D. Abruna, Electrocatalytic reduction of carbon dioxide with iron, cobalt, and nickel complexes of terdentate ligands, *Inorg. Chem.* 31 (17) (1992) 3680–3682. <https://doi.org/10.1021/ic00043a034>.
- [6] T. Ayers, S. Scott, J. Goins, N. Caylor, D. Hathcock, S.J. Slattery, D.L. Jameson, Redox and spin state control of Co(II) and Fe(II) N-heterocyclic complexes, *Inorg. Chim. Acta* 307 (2000) 7–12. [https://doi.org/10.1016/S0020-1693\(00\)00179-1](https://doi.org/10.1016/S0020-1693(00)00179-1).
- [7] J. Chambers, B. Eaves, D. Parker, R. Claxton, P.S. Ray, S.J. Slattery, Inductive influence of 40-terpyridyl substituents on redox and spin state properties of iron(II) and cobalt(II) bis-terpyridyl complexes, *Inorg. Chim. Acta* 359 (2006) 2400–2406. <https://doi.org/10.1016/j.ica.2005.12.065>.
- [8] N. Elgrishi, M.B. Chambers, V. Artero, M. Fontecave, Terpyridine complexes of first row transition metals and electrochemical reduction of CO<sub>2</sub> to CO, *Phys. Chem. Chem. Phys.* 16 (2014) 13635–13644. <https://doi.org/10.1039/C4CP00451E>.
- [9] M.G.B. Drew, M.R.S. Foreman, A. Geist, M.J. Hudson, F. Marken, V. Norman, M. Weigl, Synthesis, structure, and redox states of homoleptic d-block metal complexes with bis-1,2,4-triazin-3-yl-pyridine and 1,2,4-triazin-3-yl-bipyridine extractants, *Polyhedron* 25 (4) (2006) 888–900. <https://doi.org/10.1016/j.poly.2005.09.030>.
- [10] L.J. Kershaw Cook, F. Tuna, M.A. Halcrow, Iron(II) and cobalt(II) complexes of tris-azinyl analogues of 2,2':6',2''-terpyridine, *J. Chem. Soc. Dalton Trans.* 42 (6) (2013) 2254–2265. <https://doi.org/10.1039/c2dt31736b>.
- [11] M. Safdari, P.W. Lohse, L. Häggman, S. Frykstrand, D. Högberg, M. Rutland, R.A. Asencio, J. Gardner, L. Kloo, A. Hagfeldt, G. Boschloo, Investigation of cobalt redox mediators and effects of TiO<sub>2</sub> film topology in dye-sensitized solar cells, *R. Soc. Chem. Adv.* 6 (2016) 56580–56588. <https://doi.org/10.1039/c6ra07107d>.
- [12] S.A. Richert, P.K.S. Tsang, D.T. Sawyer, Ligand-Centered Redox Processes for MnL<sub>3</sub>, FeL<sub>3</sub>, and CoL<sub>3</sub> Complexes (L = Acetylacetonate, 8-Quinolate, Picolinate, 2,2'-Bipyridyl, 1,10-Phenanthroline) and for Their Tetraakis(2,6-dichlorophenyl)porphinato Complexes [M(Por)], *Inorg. Chem.* 28 (1989) 2471–2475. <https://doi.org/10.1021/ic00311a044>.
- [13] D. Cabrala, P.C. Howlett, J.M. Pringle, X. Zhanga, D. MacFarlane, Electrochemistry of tris(2,2'-bipyridyl) cobalt(II) in ionic liquids and aprotic molecular solvents on glassy carbon and platinum electrodes, *Electrochim. Acta* 180 (2015) 419–426. <https://doi.org/10.1016/j.electacta.2015.08.135>.
- [14] P.T. Kissinger, W.R. Heineman, *Cyclic voltammetry*, *J. Chem. Educ.* 60 (1983) 702–706.
- [15] D.T. Sawyer, J.L. Roberts Jr., *Experimental Electrochemistry for Chemists*, John Wiley & Sons, New York (1974) 54.
- [16] D.H. Evans, K.M. O'Connell, R.A. Peterson, M.J. Kelly, *Cyclic voltammetry*, *J. Chem. Educ.* 60 (1983) 290–293. <https://doi.org/10.1021/ed060p290>.

# Chapter 5

---

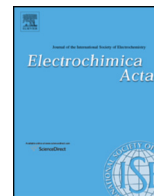
## **Electronic properties of Fe charge transfer complexes - A combined experimental and theoretical approach**

Hendrik Ferreira, Karel G. von Eschwege, Jeanet Conradie

Published by Electrochimica Acta

DOI: 10.1016/j.electacta.2016.09.034





# Electronic properties of Fe charge transfer complexes – A combined experimental and theoretical approach



Hendrik Ferreira, Karel G. von Eschwege\*, Jeanet Conradie\*

Department of Chemistry, University of the Free State, P.O. Box 339, Bloemfontein, 9300, South Africa

## ARTICLE INFO

### Article history:

Received 4 July 2016

Received in revised form 5 September 2016

Accepted 6 September 2016

Available online 8 September 2016

### Keywords:

DFT  
electrochemistry  
iron phenanthroline  
bipyridyl  
dye-sensitized  
solar cell

## ABSTRACT

Dye-sensitized solar cell technology holds huge potential in renewable electricity generation of the future. Due to demand urgency, ways need to be explored to reduce research time and cost. Against this background, quantum computational chemistry is illustrated to be a reliable tool at the onset of studies in this field, simulating charge transfer, spectral (solar energy absorbed) and electrochemical (ease by which electrons may be liberated) tuning of related photo-responsive dyes. Comparative experimental and theoretical DFT studies were done under similar conditions, involving an extended series of electrochemically altered phenanthrolines, bipyridyl and terpyridyl complexes of  $\text{Fe}^{\text{II}}$ .  $\text{Fe}^{\text{II/III}}$  oxidation waves vary from 0.363 V for *tris*(3,6-dimethoxybipyridyl) $\text{Fe}^{\text{II}}$  to 0.894 V (*versus*  $\text{Fc}/\text{Fc}^+$ ) for the 5-nitrophenanthroline complex. Theoretical DFT computed ionization potentials in the bipyridyl sub-series achieved an almost 100% linear correlation with experimental electrochemical oxidation potentials, while the phenanthroline sub-series gave  $R^2 = 0.95$ . Apart from the terpyridyl complex which accorded an almost perfect match, in general, TDDFT oscillators were computed at slightly lower energies than what was observed experimentally, while molecular HOMO and LUMO renderings reveal desired complexes with directional charge transfer propensities.

© 2016 Elsevier Ltd. All rights reserved.

## 1. Introduction

More than 70 years ago (1942) Fe-phenanthrolines, also known as ferroins, gained renown as titration redox indicators, with  $\text{Fe}^{\text{II}}$  complexes changing color from red to blue during oxidation to  $\text{Fe}^{\text{III}}$  [1]. Shortly thereafter (1954) its metal-to-ligand charge transfer properties became a topic of investigation [2], which eventually led to its inclusion in modern-day dye-sensitized solar cell (DSSC) research. Mostly, bipyridyl complexes of  $\text{Ru}^{\text{II}}$ , but also  $\text{Re}^{\text{I}}$ ,  $\text{Os}^{\text{II}}$ ,  $\text{Fe}^{\text{II}}$  and  $\text{Cu}^{\text{I}}$  are involved as dyes in solar cell research and applications [3]. Due to scarcity of the platinum group metals and consequent high cost, a search for earth abundant alternatives ensued, especially so amongst the first row transition metals. The short-lived excited states of these metals hamper charge injection into the  $\text{TiO}_2$  conduction band of DSSC's. Charge injection in the case of  $\text{Fe}^{\text{II}}$  polypyridyl  $[\text{Fe}^{\text{II}}(\text{bpy})_x]^{2+}$  complexes nevertheless do take place – in the ultrafast time domain [4]. Fe-phenanthroline and pyridyl derivatives have the advantage of absorbing strongly in the UV-visible section of the solar emission spectrum [5]. Weber,

Constable and Housecroft concluded in their review article on earth-abundant element DSC research that: “The final impression is one of optimism that in the mid-term it may be possible to partially or completely replace materials based on platinum group metals by those involving Earth abundant metals. Our primary aim in writing this review was to . . . encourage further research in this area.” [6].

In view of the above we set about to systematically and comprehensively investigate series of metal-to-ligand charge transfer complexes, building up a database from which dyes for further research may be selected. To illustrate the prediction capability of theoretical DFT techniques, with the purpose to prevent time consuming and expensive experimental routines, spectral and redox properties were experimentally measured and correlated with quantum computational data. Towards this goal a complex series consisting of electronically altered derivatives of  $\text{Fe}^{\text{II}}$  phenanthroline, bipyridyl and terpyridyl complexes was synthesized. The study follows as part of a larger group, starting with the simple and progressing towards more involved molecular systems. Initial findings, based on the neat electrochemical behavior of a series of simple *para*-substituted nitrobenzenes, showed how experimental reduction potentials may theoretically be predicted to more than 99% accuracy by linear correlation with

\* Corresponding authors.

E-mail addresses: [veschwkg@ufs.ac.za](mailto:veschwkg@ufs.ac.za) (K.G. von Eschwege), [conradj@ufs.ac.za](mailto:conradj@ufs.ac.za) (J. Conradie).



readily obtained computed LUMO (lowest unoccupied molecular orbital) energies [7]. Similar studies then followed, progressing to bidentate ligands [8,9], its metal [10–16] and bimetallic complexes [17]. Recently Demissie et al. involved relativistic DFT methods to calculate Gibbs free energies, by this alternative method also obtaining results in close agreement with experimental redox data [18].

Up to date, computational studies involving the large hexa-coordinated Fe complexes under discussion here, are largely absent in published literature. One reason may be the expense in computational time required by these large structures. As for its electrochemistry, to our knowledge only two wide-ranging comparative investigations were published. These involved cyclic voltammetry studies of altogether seventeen 4,7-substitution-altered Fe-phenanthrolines [19,20].

## 2. Experimental

### 2.1. General

Solvents were used, as supplied by Merck (AR grade). Syntheses chemicals were reagent grade and used as purchased from Sigma-Aldrich.  $^1\text{H}$  NMR spectra were obtained on a Bruker AVANCE II 600 MHz spectrometer. UV-visible spectra of dilute solutions in quartz cuvettes were recorded on a Shimadzu UV-2550 spectrometer and Infrared stretching frequencies were measured on a Bruker Tensor 27 FTIR spectrophotometer.

### 2.2. Synthesis Procedure

Adapted from a published method [21,22], the following general procedure was followed to synthesize the series of thirteen  $\text{Fe}^{\text{II}}$ -phenanthroline and pyridyl complexes, using commercially available ligands:

Ferrous ammonium sulfate (1.002 g, 0.00255 mol) was dissolved in water (0.005 L) that contains  $\text{H}_2\text{SO}_4$  (0.001 L, 0.005 M). 1,10-Phenanthroline (1.613 g, 0.00895 mol) was dissolved in hot water (0.030 L) that contains  $\text{HClO}_4$  (0.002 L, 1 M). While stirring, the ferrous solution was added dropwise to the hot ligand solution. A saturated  $\text{NaClO}_4$  solution was then added dropwise until precipitation of the ferrous complex perchlorate salt occurred. The mixture was left on a hot water bath for 30 minutes, after which it was cooled to room temperature and filtered. The product precipitate was left to dry in air, yielding pure  $[\text{Fe}^{\text{II}}(1,10\text{-phen})_3](\text{ClO}_4)_2$  (Product yields varied from 60 to 90%. Due to explosion hazard posed by dry perchlorate salts, melting points were not determined.).

### 2.3. $\text{Fe}^{\text{II}}$ complex derivatives

#### 2.3.1. *Tris(5-nitro-1,10-phenanthroline) $\text{Fe}^{\text{II}}$ perchlorate*

$\lambda_{\text{max}}$  (methanol) = 511 nm;  $\nu_{\text{C-N}}$  = 1078  $\text{cm}^{-1}$ ;  $^1\text{H}$  NMR (DMSO- $d_6$ , 600 MHz)  $\delta$  = 9.501 (d,  $J$  = 3.6 Hz,  $3 \times 1\text{H}$ ), 9.138 (m,  $3 \times 1\text{H}$ ), 9.048 (ddd,  $J$  = 8.1 Hz, 6.0 Hz, 4.6 Hz,  $3 \times 1\text{H}$ ), 7.891 (m,  $3 \times 4\text{H}$ ).

#### 2.3.2. *Tris(5-chloro-1,10-phenanthroline) $\text{Fe}^{\text{II}}$ perchlorate*

$\lambda_{\text{max}}$  (methanol) = 510 nm;  $\nu_{\text{C-N}}$  = 1080  $\text{cm}^{-1}$ ;  $^1\text{H}$  NMR (DMSO- $d_6$ , 600 MHz)  $\delta$  = 8.895 (dt,  $J$  = 5.1 Hz, 3.8 Hz,  $3 \times 1\text{H}$ ), 8.751 (m,  $3 \times 2\text{H}$ ), 7.774 (m,  $3 \times 4\text{H}$ ).

#### 2.3.3. *Tris(5,6-epoxy-5,6-dihydro-1,10-phenanthroline) $\text{Fe}^{\text{II}}$ perchlorate*

$\lambda_{\text{max}}$  (methanol) = 527 nm;  $\nu_{\text{C-N}}$  = 1066/1077  $\text{cm}^{-1}$ ;  $^1\text{H}$  NMR (DMSO- $d_6$ , 600 MHz)  $\delta$  = 8.595 (dd,  $J$  = 6 Hz, 4.8 Hz,  $3 \times 2\text{H}$ ), 7.548 (m,  $3 \times 4\text{H}$ ), 5.124 (m,  $3 \times 2\text{H}$ ).

#### 2.3.4. *Tris(2,2':6',2''-terpyridine) $\text{Fe}^{\text{II}}$ perchlorate*

$\lambda_{\text{max}}$  (methanol) = 551 nm;  $\nu_{\text{C-N}}$  = 1076  $\text{cm}^{-1}$ ;  $^1\text{H}$  NMR (DMSO- $d_6$ , 600 MHz)  $\delta$  = 9.261 (d,  $J$  = 8.1 Hz,  $2 \times 2\text{H}$ ), 8.833 (dd,  $J$  = 15.9 Hz, 7.9 Hz,  $2 \times 3\text{H}$ ), 8.009 (m,  $2 \times 2\text{H}$ ), 7.179 (ddd,  $J$  = 7.3 Hz, 5.7 Hz, 1.3 Hz,  $2 \times 2\text{H}$ ), 7.142 (d,  $J$  = 4.9 Hz,  $2 \times 2\text{H}$ ).

#### 2.3.5. *Tris(2,2'-dipyridyl) $\text{Fe}^{\text{II}}$ perchlorate*

$\lambda_{\text{max}}$  (methanol) = 520 nm;  $\nu_{\text{C-N}}$  = 1066/1077  $\text{cm}^{-1}$ ;  $^1\text{H}$  NMR (DMSO- $d_6$ , 600 MHz)  $\delta$  = 8.864 (d,  $J$  = 8.1 Hz,  $2 \times 2\text{H}$ ), 8.231 (td,  $J$  = 8.5 Hz, 1.3 Hz,  $2 \times 2\text{H}$ ), 7.530 (ddd,  $J$  = 7.2 Hz, 5.7 Hz, 1.2 Hz,  $2 \times 2\text{H}$ ), 7.395 (d,  $J$  = 5.3 Hz,  $2 \times 2\text{H}$ ).

#### 2.3.6. *Tris(1,10-phenanthroline) $\text{Fe}^{\text{II}}$ perchlorate*

$\lambda_{\text{max}}$  (methanol) = 509 nm;  $\nu_{\text{C-N}}$  = 1071  $\text{cm}^{-1}$ ;  $^1\text{H}$  NMR (DMSO- $d_6$ , 600 MHz)  $\delta$  = 8.401 (s, 2H), 8.813 (d,  $J$  = 1.2 Hz, 2H), 7.75 (dd,  $J$  = 8.1 Hz, 5.3 Hz, 2H), 7.708 (dd,  $J$  = 5.2 Hz, 1.2 Hz, 2H).

#### 2.3.7. *Tris(5-methyl-1,10-phenanthroline) $\text{Fe}^{\text{II}}$ perchlorate*

$\lambda_{\text{max}}$  (methanol) = 513 nm;  $\nu_{\text{C-N}}$  = 1081  $\text{cm}^{-1}$ ;  $^1\text{H}$  NMR (DMSO- $d_6$ , 600 MHz)  $\delta$  = 8.824 (m,  $3 \times 1\text{H}$ ), 8.676 (m,  $3 \times 1\text{H}$ ), 8.209 (d,  $J$  = 1.4 Hz,  $3 \times 1\text{H}$ ), 7.675 (m,  $3 \times 4\text{H}$ ), 2.898 (s,  $3 \times 3\text{H}$ ).

#### 2.3.8. *Tris(5,6-dimethyl-1,10-phenanthroline) $\text{Fe}^{\text{II}}$ perchlorate*

$\lambda_{\text{max}}$  (methanol) = 517 nm;  $\nu_{\text{C-N}}$  = 1077  $\text{cm}^{-1}$ ;  $^1\text{H}$  NMR (DMSO- $d_6$ , 600 MHz)  $\delta$  = 8.884 (d,  $J$  = 8.5 Hz,  $3 \times 2\text{H}$ ), 7.718 (dd,  $J$  = 8.5 Hz, 5.2 Hz,  $3 \times 2\text{H}$ ), 7.595 (d,  $J$  = 5.1 Hz,  $3 \times 2\text{H}$ ), 2.824 (s,  $3 \times 6\text{H}$ ).

#### 2.3.9. *Tris(4-methyl-1,10-phenanthroline) $\text{Fe}^{\text{II}}$ perchlorate*

$\lambda_{\text{max}}$  (methanol) = 510 nm;  $\nu_{\text{C-N}}$  = 1082  $\text{cm}^{-1}$ ;  $^1\text{H}$  NMR (DMSO- $d_6$ , 600 MHz)  $\delta$  = 8.790 (t,  $J$  = 6.8 Hz,  $3 \times 1\text{H}$ ), 8.471 (dd,  $J$  = 9.1 Hz, 2.6 Hz,  $3 \times 1\text{H}$ ), 8.406 (dd,  $J$  = 9.2 Hz, 2.6 Hz,  $3 \times 1\text{H}$ ), 7.716 (m,  $3 \times 2\text{H}$ ), 7.530 (m,  $3 \times 2\text{H}$ ), 2.879 (d,  $J$  = 3.3 Hz,  $3 \times 3\text{H}$ ).

#### 2.3.10. *Tris(5-amino-1,10-phenanthroline) $\text{Fe}^{\text{II}}$ perchlorate*

$\lambda_{\text{max}}$  (methanol) = 521 nm;  $\nu_{\text{C-N}}$  = 1066  $\text{cm}^{-1}$ ;  $^1\text{H}$  NMR (DMSO- $d_6$ , 600 MHz)  $\delta$  = 8.90 (td,  $J$  = 7.6 Hz, 3.9 Hz,  $3 \times 1\text{H}$ ), 8.31 (t,  $J$  = 8.5 Hz,  $3 \times 1\text{H}$ ), 7.72–7.57 (m,  $3 \times 2\text{H}$ ), 7.50–7.47 (m,  $3 \times 1\text{H}$ ), 7.22–7.13 (m,  $3 \times 1\text{H}$ ), 7.074 (d,  $J$  = 5 Hz,  $3 \times 1\text{H}$ ), 6.93 (d,  $J$  = 4.3 Hz,  $3 \times 2\text{H}$ ).

#### 2.3.11. *Tris(4,4'-dimethyl-2,2'-bipyridine) $\text{Fe}^{\text{II}}$ perchlorate*

$\lambda_{\text{max}}$  (methanol) = 527 nm;  $\nu_{\text{C-N}}$  = 1077/1091  $\text{cm}^{-1}$ ;  $^1\text{H}$  NMR (DMSO- $d_6$ , 600 MHz)  $\delta$  = 8.708 (s,  $3 \times 2\text{H}$ ), 7.35 (d,  $J$  = 5.8 Hz,  $3 \times 2\text{H}$ ), 7.196 (d,  $J$  = 5.8 Hz,  $3 \times 2\text{H}$ ), 2.516 (s,  $3 \times 6\text{H}$ ).

#### 2.3.12. *Tris(3,4,7,8-tetramethyl-1,10-phenanthroline) $\text{Fe}^{\text{II}}$ perchlorate*

$\lambda_{\text{max}}$  (methanol) = 510 nm;  $\nu_{\text{C-N}}$  = 1082  $\text{cm}^{-1}$ ;  $^1\text{H}$  NMR (DMSO- $d_6$ , 600 MHz)  $\delta$  = 8.493 (s,  $3 \times 2\text{H}$ ), 7.306 (s,  $3 \times 2\text{H}$ ), 2.790 (s,  $3 \times 6\text{H}$ ), 2.192 (s,  $3 \times 6\text{H}$ ).

#### 2.3.13. *Tris(4,4'-dimethoxy-2,2'-bipyridine) $\text{Fe}^{\text{II}}$ perchlorate*

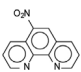
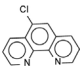
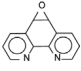
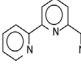
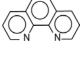


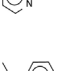
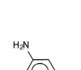
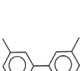
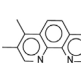
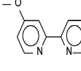
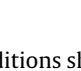
$\lambda_{\text{max}}$  (methanol) = 537 nm;  $\nu_{\text{C-N}}$  = 1081  $\text{cm}^{-1}$ ;  $^1\text{H}$  NMR (DMSO- $d_6$ , 600 MHz)  $\delta$  = 8.500 (s,  $3 \times 2\text{H}$ ), 7.17 (m,  $3 \times 4\text{H}$ ), 3.987 (s,  $3 \times 6\text{H}$ ).

### 2.4. Cyclic voltammetry

Electrochemical studies by means of cyclic voltammetry were performed on 0.002 mol  $\text{dm}^{-3}$  or saturated compound solutions in dry acetonitrile containing 0.1 mol  $\text{dm}^{-3}$  tetra-*n*-butylammonium hexafluorophosphate,  $[\text{N}^+(\text{Bu}_4)\text{N}][\text{PF}_6]$ , as supporting electrolyte and under a blanket of purified argon at 25 °C utilizing a BAS 100B/W electrochemical analyzer. A three-electrode cell, with a glassy carbon (surface area  $7.07 \times 10^{-6} \text{ m}^2$ ) working electrode, Pt auxiliary electrode and a  $\text{Ag}/\text{Ag}^+$  (0.010 mol  $\text{dm}^{-3}$   $\text{AgNO}_3$  in  $\text{CH}_3\text{CN}$ ) reference electrode [23], mounted on a Luggin capillary, was used [24]. Scan rates were 0.050–5.000  $\text{V s}^{-1}$ . Successive experiments

**Table 1**

Ligand structures of Fe<sup>II</sup> complexes [Fe(L<sub>3</sub>)]<sup>2+</sup>, formal reduction potentials, E<sup>0</sup> (exp) (V) arranged in decreasing order, E<sup>0</sup> (DFT) (V) calculated via linear correlation of experimental E<sup>0</sup> with DFT computed ionization potentials, and experimental and DFT absorbance maxima, λ<sub>max</sub> (nm), in gas phase and methanol.

	Fe <sup>II</sup> Complex Ligands L		E <sup>0</sup> (exp.) CH <sub>3</sub> CN	E <sup>0</sup> (DFT)	λ <sub>max</sub> (exp.) MeOH	λ <sub>max</sub> (DFT) Gas	λ <sub>max</sub> (DFT) MeOH
1	phen-NO <sub>2</sub>		0.894	0.899	511	545	–
2	phen-Cl		0.802	0.773	510	550	–
3	phen-epoxy		0.802	0.779	527	569	–
4	tpy-H		0.720	0.723	551	528	554
5	phen-H		0.698	0.745	509	546	566
6	bpy-H		0.682	0.678	520	563	576
7	phen-5Me		0.669	0.681	513	543	–
8	phen-Me <sub>2</sub>		0.640	0.660	517	539	–
9	phen-4Me		0.613	0.566	510	543	–
10	phen-NH <sub>2</sub>		0.585	0.568	521	541	–
11	bpy-Me <sub>2</sub>		0.523	0.524	527	579	–
12	phen-Me <sub>4</sub>		0.452	0.462	510	543	–
13	bpy-(OMe) <sub>2</sub>		0.363	0.362	537	628	–

under the same experimental conditions showed that all oxidation and formal reduction potentials were reproducible within 0.010 V. All cited potentials were referenced against the Fc/Fc<sup>+</sup> couple as suggested by IUPAC [25]. Ferrocene (Fc) exhibited peak separation, ΔE<sub>p</sub> = E<sub>pa</sub> – E<sub>pc</sub> = 0.069 V and i<sub>pc</sub>/i<sub>pa</sub> = 1.00 under our experimental conditions. E<sub>pa</sub> (E<sub>pc</sub>) = anodic (cathodic) peak potential and i<sub>pa</sub> (i<sub>pc</sub>) = anodic (cathodic) peak current. The formal reduction potential E<sup>0</sup> = (E<sub>p</sub> – E<sub>pc</sub>)/2 for an electrochemical reversible process. E<sup>0</sup> (Fc/Fc<sup>+</sup>) = 0.66(5) V vs SHE in [n(Bu<sub>4</sub>)N][PF<sub>6</sub>]/CH<sub>3</sub>CN [26].

## 2.5. DFT calculations

Density functional theory (DFT) calculations were performed with the ADF 2014 program [27] with the GGA functional BP86 [28,29]. Full geometry optimization with tight convergence criteria were done with the TZP basis set and a fine mesh for numerical integration. The closed shell Fe<sup>II</sup> complexes (q = 2, S = 0) were calculated spin restricted and the Fe<sup>I</sup> (q = 1 and S = 1/2) and Fe<sup>III</sup> (q = 3 and S = 1/2) complexes spin unrestricted.

Reliability of the DFT method was tested by comparing single crystal X-ray diffraction data [30] of  $[\text{Fe}^{\text{II}}(\text{phen})_3]^{2+}$  with geometrical parameters obtained by three different functionals, BP86 [28,29], OLYP [31–34] and B3LYP [35,36]. Bond lengths and angles around Fe centres were considered paramount. BP86 gave the best agreement with experimental structural data. The difference between calculated and average experimental Fe–N bond lengths was 0.005 Å. A difference between calculated and experimental metal–ligand bond lengths below a threshold of 0.02 Å are considered meaningless [37]. For all three functionals the S=0 ground state of  $[\text{Fe}^{\text{II}}(\text{phen})_3]^{2+}$  had the lowest energy.

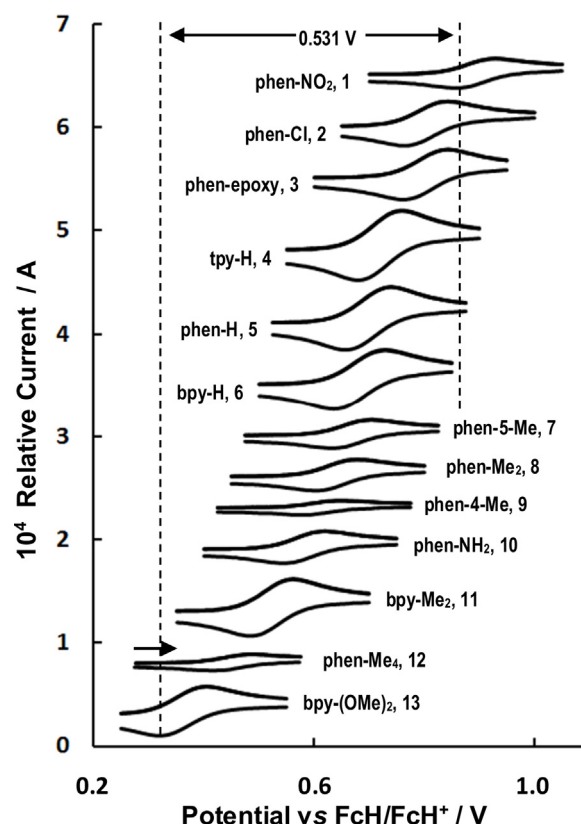
### 3. Results and discussion

Synthesis of the  $\text{Fe}^{\text{II}}$  complexes, being *tris*-coordinated with phenanthroline, allowing a neat crystalline product that is readily isolated after stirring a mixture of ligand and metal, may at first glance appear to be unproblematic. However, X-ray crystallography yields no reflections from ostensibly single crystals, while cyclic voltammetry persistently results in the  $\text{Fe}^{\text{II}} \rightarrow \text{Fe}^{\text{III}}$  oxidation wave being preceded by a smaller shoulder. On the other hand, performing the reaction in acidic medium as reported by Balakumar ensures a pure product, and was therefore the method of choice for the syntheses of all complexes in this study (see Table 1) [21,22].

As opposed to previous reports which compared redox properties amongst Fe–phenanthrolines where only similar substituents on the 4 and 7 phenanthroline positions were varied [19,20], the scope of the present study is, apart from its theoretical component, largely extended with regard to substitution pattern. Substituents were selected to vary from strongly electron withdrawing to electron donating. For the purpose of direct comparison, terpyridyl and bipyridyl ligands were also incorporated, ensuring experimental data for three of the most popular MLCT solar dye moieties to be acquired under similar conditions.

Due to its pronounced redox waves and electrochemical reversibility, iron was selected as first candidate amongst several related studies presently under investigation. Fig. 1 presents the  $\text{Fe}^{\text{II/III}}$  oxidation and reduction wave segments of the present series of complexes, obtained in acetonitrile at 25 °C as referenced against the ferrocene redox couple. The redox potential of unsubstituted  $[\text{Fe}^{\text{II}}(\text{phen})_3]^{2+}$  (5) here observed, agrees within 0.008 V with the value of 0.69 V reported elsewhere [19,20]. Formal reduction potentials of the three unsubstituted complexes;  $[\text{Fe}^{\text{II}}(\text{bpy})_3]^{2+}$  (6),  $[\text{Fe}^{\text{II}}(\text{phen})_3]^{2+}$  (5) and  $[\text{Fe}^{\text{II}}(\text{tpy})_2]^{2+}$  (4) lie close together, at 0.682, 0.698 and 0.720 V respectively, the overall variation being only 0.038 V, see Table 1. Of these, 4 resists oxidation more strongly, while 6 is most readily oxidized. The order and close proximity of these  $\text{Fe}^{\text{II/III}}$  formal reduction potential values are reflected in its first reduction potentials, at –1.784 (6), –1.768 (5) and –1.685 V (4) respectively, see Fig. 2.

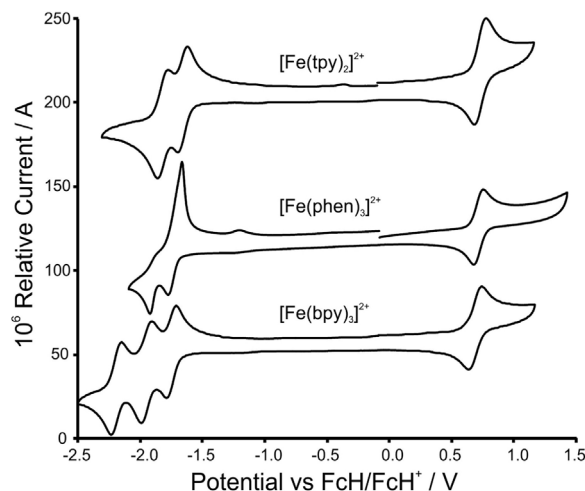
An overall formal reduction potential decrease of 0.531 V is seen for the entire series of Fe complexes, varying from 0.894 V where a nitro group is on the 5–phenanthroline position (1), to 0.363 V where two methoxy groups are on the *para*-pyridyl (13) positions. Clearly, whether substituents are on the inner phenanthroline ring or on the side rings, plays a significant role in the electrochemical tuning of these MLCT complexes, e.g. where the weak methyl electron donor is on the 5-phen position (7, inner ring)  $\text{Fe}^{\text{II}}$  oxidizes at 0.669 V, while when on the 4-phen position (9, outer ring) oxidation occurs more readily, namely at 0.613 V. In line with this observation, it is also seen that the effect of the strong amine electron donor on the 5-phen position (10) is much less than that of the multiple methyls on the outer rings (12). Amongst the phenanthroline sub-group in this study, the latter *tetra*-methyl



**Fig. 1.** Cyclic voltammograms of ca 0.002 mol dm<sup>−3</sup> or saturated solutions of 1–13 in  $\text{CH}_3\text{CN}/0.1 \text{ mol dm}^{-3} [\text{t}^{\text{Bu}}_4\text{N}][\text{PF}_6]$  on a glassy carbon-working electrode at a scan rate of 0.100 V s<sup>−1</sup>. Only  $\text{Fe}^{\text{II/III}}$  redox segments are indicated. Ligand L of the  $[\text{Fe}(\text{L}_3)]^{2+}$  complex is indicated on the graph. Scans were initiated in the positive direction as indicated by the arrow.

derivative is most readily oxidized. In general therefore, although being part of a delocalized fused ring system, the inductive effect as measured by corresponding  $\text{Fe}^{\text{II/III}}$  redox potentials, nevertheless significantly decreases over distance.

The ligand in this series that forms the complex that is most readily oxidized, is the *para*-dimethoxy substituted bipyridyl derivative, 13, with formal reduction potential of the complex



**Fig. 2.** Comparative wide scan cyclic voltammograms of ca 0.002 mol dm<sup>−3</sup> solutions of the indicated  $\text{Fe}^{\text{II}}$  complexes in  $\text{CH}_3\text{CN}/0.1 \text{ mol dm}^{-3} [\text{t}^{\text{Bu}}_4\text{N}][\text{PF}_6]$  on a glassy carbon-working electrode at a scan rate of 0.100 V s<sup>−1</sup>. Scans were initiated in the positive direction from −0.01 V.

being 0.363 V. This value compares closely with the analogue 4,7-dimethoxyphenanthroline derivative synthesized by Schmittle et al., who reported a formal reduction potential of 0.380 V [20]. These authors also synthesized phenanthrolines with similar amine substituents,  $N(\text{CH}_2\text{CH}_3)_2$  and  $\text{NH}(\text{CH}_2)_3\text{NH}_2$ , on the 4 and 7 phenanthroline positions, whereby the  $\text{Fe}^{\text{II/III}}$  formal reduction potentials were decreased to as much as  $-0.230$  V.

DFT calculations performed on complexes **1–13** ( $q = 2, 3$ ), gave geometry optimized electronic energies ( $E$ ) of each state which could directly or indirectly be used in correlations with experimentally obtained formal reduction potentials ( $E^0$ ). The most relevant computational descriptors that were considered [38], were computed HOMO (highest molecular orbital) energies ( $E_{\text{HOMO}}$ ), as well as ionization potentials ( $\text{IP} = E_{\text{complex}} - E_{\text{oxidized complex}}$ ).

Treatment of the entire series as a whole proved less than optimal, since, as was previously concluded, only closely related substances correlate linearly in this way [17]. By therefore considering the pyridyl sub-series apart from the phenanthrolines, a perfect correlation coefficient of 1.000 between IP and  $E^0$  came to the fore, see Fig. 3 and Table 2.  $R^2 = 0.954$  for the phenanthroline series.

Since the electron in the HOMO is removed during oxidation, correlation with HOMO energies usually also follow linear trends [17]. Present data yielded  $R^2 = 0.93$ , which is slightly worse than found for the ionization potential correlation. As discussed in the Introduction, our previous findings suggested comparison between experimentally measured potentials and computed HOMO or LUMO energies of compounds where substituents are varied only on similar positions, however, in this study phenanthroline substituents were varied in the widest possible way, e.g. not only different substituents, but different substituent quantities were involved, as well as on different positions. In view of these large substituent variations the slight worsening in correlation coefficient is thus expected.

The linear equations for trend lines as depicted in Fig. 3 are:

IP:

$$y = 3.90x + 9.44, R^2 = 1.000 \text{ (pyr. sub-series)}$$

$$y = 3.51x + 9.28, R^2 = 0.954 \text{ (phen. sub-series)}$$

$E_{\text{HOMO}}$ :

$$y = -3.31x - 7.64, R^2 = 0.926 \text{ (phen. sub-series)}$$

**Table 2**

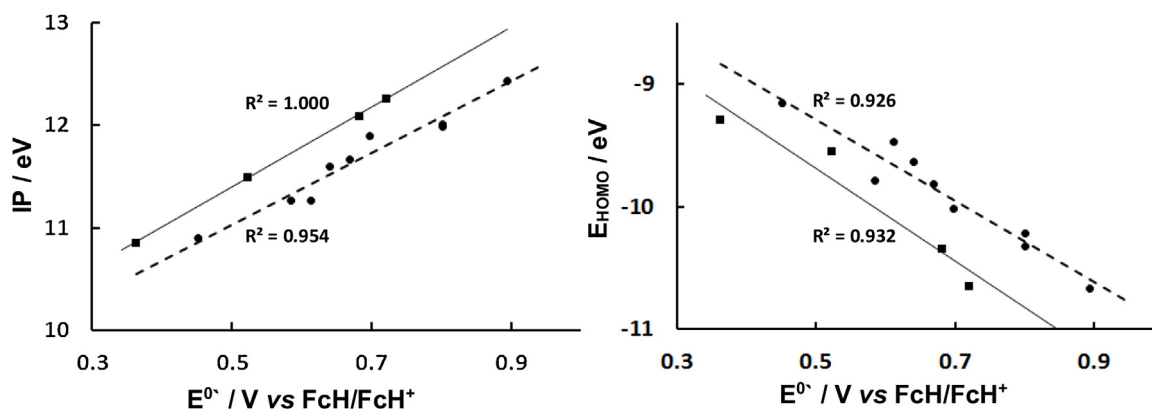
DFT computed ionization potentials (arranged in decreasing order) and HOMO energies of the Fe complex series  $[\text{Fe}(\text{L}_3)]^{2+}$ .

Fe complex ligand L	IP (eV)	$E_{\text{HOMO}}$ (eV)
phen-NO <sub>2</sub>	12.430	-10.669
phen-epoxy	12.372	-10.319
tpy-H	12.264	-10.647
bpy-H	12.091	-10.338
phen-Cl	11.987	-10.221
phen-H	11.890	-10.018
phen-5Me	11.665	-9.818
phen-Me <sub>2</sub>	11.592	-9.638
bpy-Me <sub>2</sub>	11.491	-9.549
phen-NH <sub>2</sub>	11.268	-9.786
phen-4Me	11.263	-9.477
phen-Me <sub>4</sub>	10.896	-9.160
bpy-(OMe) <sub>2</sub>	10.856	-9.291

$$y = -3.78x - 7.79, R^2 = 0.932 \text{ (pyr. sub-series)}$$

Utilizing the above linear equations and based only on theoretically computed  $E_{q=2}$ ,  $E_{q=3}$  and  $E_{q=1}$  values,  $E^0$  values of other related compounds may thus be predicted. These energies are readily obtainable directly from computation output files. As a test, the energies of three derivatives from the Schmittle group [20] were computed. Ionization potentials from these energies were calculated for the 4,7-(NO<sub>2</sub>)<sub>2</sub>-phenanthroline-Fe<sup>II</sup> electron-poor derivative, where  $E^0$  was determined to be 0.898 V. The related value for 4,7-(OCH<sub>3</sub>)<sub>2</sub>-phenanthroline-Fe<sup>II</sup> is 0.367 V, and for the electron-rich 4,7-(N(CH<sub>2</sub>CH<sub>3</sub>)<sub>2</sub>NO<sub>2</sub>)<sub>2</sub>-phenanthroline-Fe<sup>II</sup> it is  $-0.039$  V. Experimental  $E^0$  values reported by these authors were 0.890, 0.380 and  $-0.090$  V, which lies within 0.009, 0.013 and 0.041 V respectively from our theoretically predicted values. This corresponds to a correlation coefficient of almost unity.

With regard to dyes that may be employed in dye-sensitized solar cells, the ideal oxidation potential is determined by the chosen redox electrolyte. For the commonly used iodide/triiodide couple, the dye requires an oxidation potential around 0.4 to 0.5 V more positive than that of the electrolyte, since an overpotential is needed for rapid dye re-reduction after photochemical oxidation [39].  $E^0$  ( $\text{I}^3/\text{I}^-$ ) in acetonitrile is reported to be  $-0.276$  V vs ferrocene [40]. Based on this criterion alone, the Fe-phenanthroline and pyridyl species of this study thus all qualify as suitable dyes. It may be noted that derivitization is therefore not required, with the unsubstituted species having potentials at ca 0.7 V. Functionalization for the purpose of anchoring on e.g. a TiO<sub>2</sub> substrate should therefore also not pose a problem, in fact, the



**Fig. 3.** Linear correlation graphs of experimental formal reduction potentials ( $E^0$ ) versus corresponding calculated ionization potentials (IP, left) and HOMO energies ( $E_{\text{HOMO}}$ , right) of **1–13**. The trend corresponding to the Fe-phenanthroline sub-series is indicated by dashed lines, solid lines show the Fe-pyridyl sub-series.

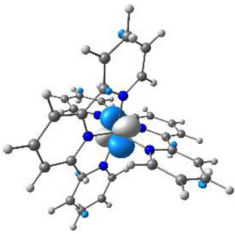
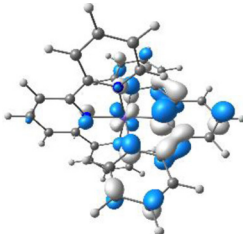
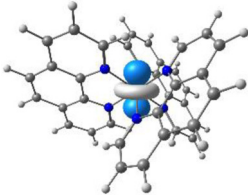
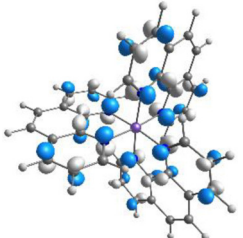
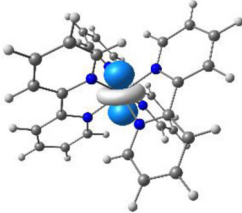
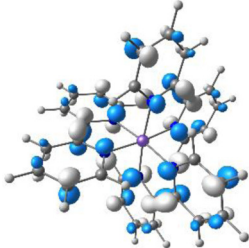
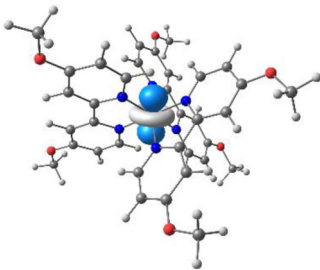
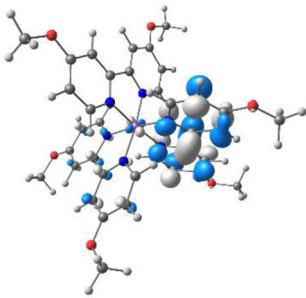
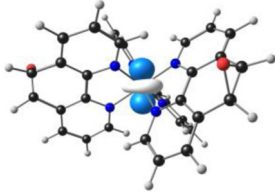
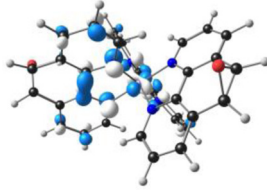
electron-withdrawing favoured –COOH anchor group is expected to only slightly increase  $E^{0'}$ .

Molecular orbital renderings which include examples of the HOMO and LUMO of selected complexes, are presented in Table 3. The photochemical metal-to-ligand charge transfer capacity is clearly illustrated, which implies that these complexes are suitable as charge transfer dyes. In all the other complexes, including those

not shown here (see Supporting Information), the HOMO is located mainly on the central metal, while directional transfer takes place during photochemical excitation, i.e. the charge being transferred to the empty LUMO which is completely or at least mostly located on the ligands.

Apart from desired electrochemical properties of potential dye molecules, photo-physical properties, amongst others, also need

**Table 3**  
HOMO and LUMO orbital renderings of selected  $\text{Fe}^{\text{II}}$  complexes  $[\text{Fe}(\text{L}_3)]^{2+}$ . (Complete series may be viewed in Supporting Information.).

$\text{Fe}^{\text{II}}$ Complex Ligands L	HOMO	LUMO
tpy-H (4)		
phen-H (5)		
bpy-H (6)		
bpy-OMe <sub>2</sub> (13)		
phen-epoxy (3)		



simultaneously be optimized. Of primary importance is that the absorbance spectrum of the dye overlap with the solar emission spectrum as completely as possible. The Fe complexes of the present series show particular promise, since the wavelengths of maximum absorbance lie immediately to the right of the solar maximum emission of about 490 nm. Also, the absorbance spectra are relatively wide (see spectra in Fig. 4), although not as wide as the solar emission spectrum, which very gradually fades into the deep infrared.

The Fe-phenanthroline complex, **5** absorbs at highest energy, namely 509 nm, and the Fe-terpyridyl complex at lowest energy, at 551 nm, which represents an overall spectral shift of only 42 nm, all other derivatives lying in between. Within the Fe-phenanthroline sub-series practically no spectral shift occurs as a result of widely differing electronically altered substituents, e.g. for nitro derivative, **1**,  $\lambda_{\text{max}}$  = 511 nm, while  $\lambda_{\text{max}}$  for the tetra-methyl compound, **12**, is 510 nm. Inclusion of extended aromatic systems or mixes of ligands being coordinated to the central metal are however expected to enhance absorbance band widths.

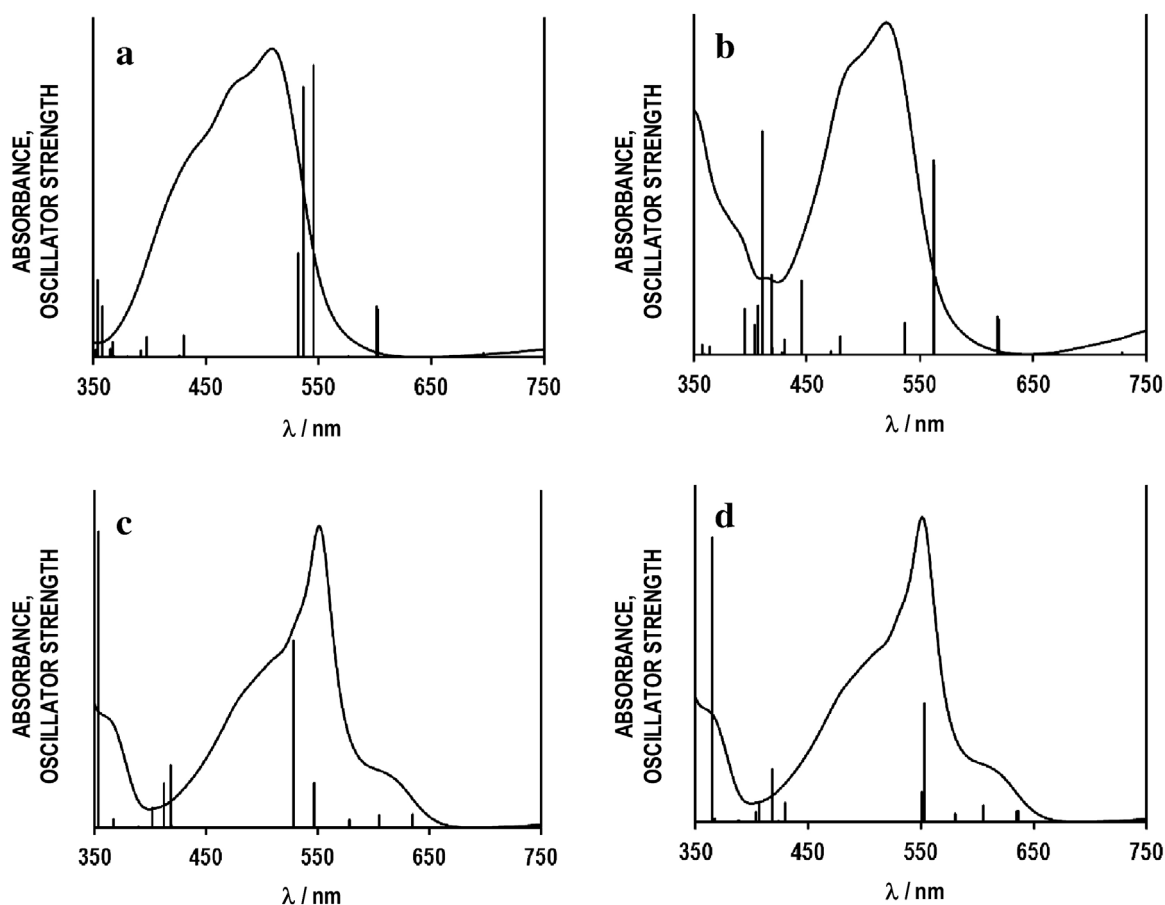
Fig. 4 also shows Time-Dependent DFT computed electronic oscillators for the three unsubstituted compounds: **4**, **5** and **6**. Apart from the Fe-terpyridyl compound, better simulation of experimental spectra were obtained when gas phase conditions were stipulated in computational input files. The general tendency was for calculations done in solvent environment, e.g. methanol, to yield redshifts in computed oscillators. For the unsubstituted Fe-phenanthroline, **5**, and Fe-bipyridyl, **6**, compounds the strongest gas phase calculated oscillators are about 40 nm higher than corresponding  $\lambda_{\text{max}}$  experimental values. Solvent calculations

resulted in an additional redshift of ca 20 nm, see Table 1. Solvent calculations for the Fe-terpyridyl compound, **4**, however, gave an almost perfect match; experimental  $\lambda_{\text{max}}$  being at 551 nm and the TDDFT value in MeOH at 554 nm (Figs. 4d). Also, both peaks at shorter wavelengths and those being responsible for minor shoulders, are in good agreement with experimental data.

#### 4. Conclusions

Comparison between experimental electrochemistry and spectroscopy results, and DFT computational data illustrates to a high level of confidence the reliability at which theoretical techniques may be used to simulate aspect of dye molecules with potential application in solar cells. Electrochemical redox potentials in the Fe-bipyridyl series here investigated can theoretically be predicted with almost 100% accuracy, the Fe-phenanthroline series at 95% confidence level. Theoretical molecular orbital renderings give upfront visual insight into the potential charge transfer characteristics of dye molecules, while TDDFT calculations of even large molecules like the present *tris*-coordinated Fe<sup>II</sup> complexes may be simulated fairly well, mostly to within 40 nm of experimental absorbance maxima. Enhancing computed spectra, by defining solvents, is dependent on the particular species under investigation.

The earth-abundant metal and ligands here investigated are of direct relevance to the Grätzel cell [41]. Theoretical methods that may be of considerable aid during the fast-track research and development of DSSC's were illustrated.



**Fig. 4.** TDDFT calculated electronic oscillators (bars) of (a)  $[\text{Fe}^{\text{II}}(\text{phen})_3]^{2+}$ , **5**, (b)  $[\text{Fe}^{\text{II}}(\text{bpy})_2]^{2+}$ , **6**, and (c)  $[\text{Fe}^{\text{II}}(\text{tpy})_2]^{2+}$ , **4**, all in gas phase, and (d)  $[\text{Fe}^{\text{II}}(\text{tpy})_2]^{2+}$  in methanol. Experimental UV-visible overlay spectra were acquired in methanol.

## Acknowledgements

This work has received support from the South African National Research Foundation and the Central Research Fund of the University of the Free State, Bloemfontein, South Africa. The High Performance Computing facility of the UFS is acknowledged for computer time.

## Appendix A. Supplementary data

Supplementary data associated with this article can be found, in the online version, at <http://dx.doi.org/10.1016/j.electacta.2016.09.034>.

## References

- [1] I.M. Kolthoff, V.A. Stenger, 2nd ed., *Volumetric Analysis*, vol.1, Interscience, New York, 1942, pp. 140.
- [2] P. George, D.H. Irvine, Electron-transfer reactions between metallic ions, coordination complexes and haemoglobin, *Journal of the Chemical Society* (1954) 587–593.
- [3] N. Robertson, Optimizing dyes for dye-sensitized solar cells, *Angewandte Chemie International* 45 (2006) 2338–2345.
- [4] J.E. Monat, J.K. McCusker, Highly Strained Iron(II) Polypyridines: Exploiting the Quintet Manifold To Extend the Lifetime of MLCT Excited States, *Journal of the American Chemical Society* 122 (2000) 4092.
- [5] S.-H. Hwang, C.N. Moorefield, P. Wang, F.R. Fronczek, B.H. Courtney, G.R. Newkome, Design, synthesis and photoelectrochemical properties of hexagonal metallomacrocycles based on triphenylamine, *Dalton Transactions* (2006) 3518–3522.
- [6] B. Bozic-Weber, E.C. Constable, C.E. Housecroft, Light harvesting with Earth abundant d-block metals: Development of sensitizers in dye-sensitized solar cells (DSCs), *Coordination Chemistry Reviews* 257 (2013) 3089–3106.
- [7] A. Kuhn, K.G. von Eschwege, J. Conradie, Reduction potentials of para-substituted nitrobenzenes – an infrared, nuclear magnetic resonance, and density functional theory study, *Journal of Physical Organic Chemistry* 25 (2011) 58–68.
- [8] A. Kuhn, K.G. von Eschwege, J. Conradie, Electrochemical and density functional theory modeled reduction of enolized 1,3-diketones, *Electrochimica Acta* 56 (2011) 6211–6218.
- [9] K.G. von Eschwege, Oxidation resilient dithiones – Synthesis, cyclic voltammetry and DFT perspectives, *Polyhedron* 39 (2012) 99–105.
- [10] J. Conradie, Density Functional Theory Calculations of Rh- $\beta$ -diketonato complexes, *Journal of the Chemical Society, Dalton Transactions* 44 (2015) 1503–1515.
- [11] M.M. Conradie, J. Conradie, Electrochemical behaviour of tris( $\beta$ -diketonato) iron(III) complexes: A DFT and experimental study, *Electrochimica Acta* 152 (2015) 512–519.
- [12] R. Freitag, J. Conradie, Electrochemical and Computational Chemistry Study of Mn( $\beta$ -diketonato)<sub>3</sub> complexes, *Electrochimica Acta* 158 (2015) 418–426.
- [13] R. Liu, J. Conradie, Tris( $\beta$ -diketonato)chromium(III) complexes: Effect of the  $\beta$ -diketonate ligand on the redox properties, *Electrochimica Acta* 185 (2015) 288–296.
- [14] J.J.C. Erasmus, J. Conradie, Chemical and electrochemical oxidation of [Rh( $\beta$ -diketonato)(CO)(P(OCH<sub>2</sub>)<sub>3</sub>CCH<sub>3</sub>)]: an experimental and DFT study, *Dalton Transactions* 42 (2013) 8655–8666.
- [15] A. Kuhn, J. Conradie, Electrochemical and DFT study of octahedral bis( $\beta$ -diketonato)-titanium(IV) complexes, *Inorg Chim Acta* 453 (2016) 247–256.
- [16] J. Conradie, Oxidation potential of [Rh( $\beta$ -diketonato)(P(OPh)<sub>3</sub>)<sub>2</sub>] complexes – relationships with experimental, electronic and calculated parameters, *Electrochimica Acta* 110 (2013) 718–725.
- [17] K.G. von Eschwege, J. Conradie, Redox potentials of ligands and complexes ?a DFT approach, *South African Journal of Chemistry* 64 (2011) 203–209.
- [18] T.B. Demissie, K. Ruud, J.H. Hansen, DFT as a Powerful Predictive Tool in Photoredox Catalysis: Redox Potentials and Mechanistic Analysis, *Organometallics* 34 (2015) 4218–4228.
- [19] M. Levis, U. Lüning, M. Müller, C. Wöhrle, Tris(1,10-phenanthroline)iron(II) Complexes. Influence of 4,7-Donor Substitution on the Redox Potential, *Zeitschrift für Naturforschung B* 49 (1994) 675–682.
- [20] M. Schmittel, H. Ammon, C. Wöhrle, Tris(1,10-phenanthroline)iron(II) Complexes – Broad Variation of the Redox Potential by 4,7-Substitution at the Phenanthroline Ligands, *Chemische Berichte* 128 (1995) 845–850.
- [21] P. Balakumar, S. Balakumar, P. Subramaniam, Application of the Marcus theory to the electron transfer reaction between benzylthioacetic acid and tris(1,10-phenanthroline)iron(III) perchlorate, *Reaction Kinetics, Mechanism, Catalysis* 107 (2012) 253–261.
- [22] A.A.G.A. Al Mahdi, M.A. Hussein, C.C. Joubert, J.C. Swarts, C.R. Dennis, A kinetic study of the oxidation of hydrazine by tris(1,10-phenanthroline)iron(III) in acidic medium, *Polyhedron* 81 (2014) 409–413.
- [23] D.T. Sawyer, J.L. Roberts Jr., *Experimental Electrochemistry for Chemists*, John Wiley & Sons, New York, 1974, pp. 54.
- [24] D.H. Evans, K.M. O'Connell, R.A. Peterson, M.J. Kelly, Cyclic Voltammetry, *Journal of Chemical Education* 60 (1983) 290–293.
- [25] G. Gritzner, J. Kuta, Recommendations on reporting electrode potentials in nonaqueous solvents, *Pure and Applied Chemistry* 56 (1984) 461–466.
- [26] A.J.L. Pombeiro, Electron-donor/acceptor properties of carbenes, carbenes, vinylidenes, allenylidenes and alkynyls as measured by electrochemical ligand parameters, *Journal of Organometallic Chemistry* 690 (2005) 6021–6040.
- [27] G. te Velde, F.M. Bickelhaupt, E.J. Baerends, C.F. Guerra, S.J.A. van Gisbergen, J.G. Snijders, T. Ziegler, Chemistry with ADF, *Journal of Computational Chemistry* 22 (2001) 931–967.
- [28] A.D. Becke, Density-functional exchange-energy approximation with correct asymptotic behavior, *Physical Reviews* 8 (1988) 3098–3100.
- [29] J.P. Perdew, Density-functional approximation for the correlation energy of the inhomogeneous electron gas, *Physical Reviews* 3 (1986) 8822–8824 Erratum: J.P. Perdew, *Physical Reviews*, B34 (1986), 7406.
- [30] Cambridge Structural Database, Version 5.36, November 2014 update, average values obtained from 3 crystals CSD reference codes: WEGRIK, WERLIO and TIMGIC.
- [31] N.C. Handy, A.J. Cohen, Left-right correlation energy, *Molecular Physics* 99 (2001) 403–412.
- [32] C. Lee, W. Yang, R.G. Parr, Development of the Colle-Salvetti correlation-energy formula into a functional of the electron density, *Physical Reviews B* 37 (1988) 785–789.
- [33] B.G. Johnson, P.M.W. Gill, J.A. Pople, The performance of a family of density functional methods, *Journal of Chemical Physics* 98 (1993) 5612–5626.
- [34] T.V. Russo, R.L. Martin, P.J. Hay, Density functional calculations on first-row transition metals, *Journal of Chemical Physics* 101 (1994) 7729–7737.
- [35] A.D. Becke, Densityfunctional thermochemistry. III. The role of exact exchange, *Journal of Chemical Physics* 98 (1993) 5648–5652.
- [36] P.J. Stephens, F.J. Devlin, C.F. Chabalowski, M.J. Frisch, Ab Initio Calculation of Vibrational Absorption and Circular Dichroism Spectra Using Density Functional Force Fields, *Journal of Physical Chemistry* 98 (1994) 11623–11627.
- [37] W.J. Hehre, A Guide to Molecular Mechanisms and Quantum Chemical Calculations, 181, Wavefunction Inc., 2003, pp. 153.
- [38] R.G. Parr, L. v. Szentpaly, S. Liu, Electrophilicity Index, *Journal of the American Chemical Society* 121 (1999) 1922–1924.
- [39] S.-W. Wang, K.-L. Wu, E. Ghadiri, M.G. Lobello, S.-T. Ho, Y. Chi, J.-E. Moser, F. De Angelis, M. Grätzel, M.K. Nazeeruddin, Engineering of thiocyanate-free Ru(II) sensitizers for high efficiency dye-sensitized solar cells, *Chemical Science* 4 (2013) 2423–2433.
- [40] G. Boschloo, A. Hagfeldt, Characteristics of the Iodide/Triiodide Redox Mediator in Dye-Sensitized Solar Cells, *Accounts of Chemical Research* 42 (2009) 1819–1826.
- [41] M. Grätzel, Solar energy conversion by dye-sensitized photovoltaic cells, *Inorganic Chemistry* 44 (2005) 6841–6851.

# Chapter 6

## Conclusions

---

The presented material illustrates the effectiveness of Density Functional Theory (DFT) calculations in the research of metal coordinated polypyridine complexes. The use of DFT calculations can minimize research time and cost in the experimental laboratory.

An electrochemical study of substituted polypyridine ligands and their octahedral cobalt(II) and iron(II) complexes, displayed redox peaks in acetonitrile as solvent as follows: the free, uncoordinated polypyridine ligands (1,10-phenanthroline, 2,2'-bipyridine and terpyridine and all derivatives) display their respective ligand reductions; the polypyridine-Fe(II) coordinated complexes displayed an Fe(II/III) redox couple as well as one to three coordinated ligand reduction events; and the polypyridine-Co(II) coordinated complexes displayed Co(II/III), Co(II/I) and coordinated ligand reduction peaks. From the results obtained it is shown that when the ligand is coordinated to a Co(II) metal center, the coordinated ligands experience reduction at potentials that are 0.5 V more positive than obtained for the uncoordinated ligand. When the ligand is coordinated to an Fe(II) metal center, the coordinated ligands experience reduction at potentials that are 0.8 V more positive than the reduction of the free ligand. The uncoordinated ligand displayed reduction peaks that are electrochemically and chemically irreversible while the organometallic polypyridine-metal(II) complexes, with the ligands coordinated to a metallic center, displayed ligand reduction peaks that are chemically and electrochemically reversible.

When the experimentally determined electrochemical and physical properties are related to Density Functional Theory (DFT) calculated energies, linear correlations are obtained with good  $R^2$  values in most cases. These linear correlations arise due to the high degree of electronic communication that exists between the metal centers and the coordinating polypyridine ligands. This illustrates that DFT could be used in research for the design of complexes that contain specific physical properties for any given potential use, before synthesis. The cost of any unsuccessful or unnecessary experiment is reduced due to the lower cost of calculations versus the cost of wet chemical methods. The time duration between conceptualization of an experiment and the delivery of results can also be shortened through the use of DFT if this is compared to the time needed for laboratory experiments. The DFT calculations also allow for the visualization of the geometries and electronic structure (such as the HOMO and LUMO orbitals) of the complexes being studied, displaying the unique properties



of the complexes as was observed in the case of the Co(II)- (Jahn-Teller distortion and locuses of electrochemical oxidation/reduction) and Fe(II)-polypyridines (locuses of electrochemical oxidation/reduction and spectroscopic properties).

Of note in the research conducted is the use of perchlorate as an anion (Chapter 4). Transition metal perchlorates are known to be potentially combustible (explosive), therefore there is a risk in the use of the mentioned anion. Consideration may be made in the use of a different anion eg. nitrate as in the case of the Co-polypyridine studies. It may even be of interest to investigate the use of the iodide anion, due to the fact that the iodide/triiodide couple is used within dye-sensitized solar cells, which would also allow for the introduction of less impurities (in this case the anion, if the iodide is not used) to the electrochemical system.

From all the results obtained in the presented material, most of the octahedral, polypyridine-Co(II) and -Fe(II) complexes possess the potential needed for dyes or mediators within dye-sensitized solar cells, namely 0.5 V less than the redox potential of the well-known iodide/triiodide mediator. However, the use of a specific redox couple as mediator in DSSC, also depends on the design of the specific cell.


# Appendix A

---


## **Author Copyright Permissions**


All copyright permissions of articles for use in a thesis/dissertation were requested on 23 January 2019 from Copyright Clearance Center.

**A1: Copyright Clearance Center Permission for 'Electrochemical and DFT study of the reduction of substituted phenanthrolines'.**



[Home](#)[Account Info](#)[Help](#)





**Title:** Electrochemical and DFT study of the reduction of substituted phenanthrolines

**Author:** Hendrik Ferreira, Marrigje M. Conradie, Karel G. von Eschwege, Jeanet Conradie

**Publication:** Polyhedron

**Publisher:** Elsevier

**Date:** 28 January 2017

© 2016 Elsevier Ltd. All rights reserved.

Logged in as:  
Hendrik Ferreira

[LOGOUT](#)

Please note that, as the author of this Elsevier article, you retain the right to include it in a thesis or dissertation, provided it is not published commercially. Permission is not required, but please ensure that you reference the journal as the original source. For more information on this and on your other retained rights, please visit: <https://www.elsevier.com/about/our-business/policies/copyright#Author-rights>

[BACK](#)[CLOSE WINDOW](#)

Copyright © 2019 Copyright Clearance Center, Inc. All Rights Reserved. [Privacy statement](#). [Terms and Conditions](#). Comments? We would like to hear from you. E-mail us at [customercare@copyright.com](mailto:customercare@copyright.com)

**A2: Copyright Clearance Center Permission for 'Electrochemical properties of a series of Co(II) complexes, containing substituted phenanthrolines'.**



[Home](#)[Account Info](#)[Help](#)





**Title:** Electrochemical properties of a series of Co(II) complexes, containing substituted phenanthrolines

**Author:** Hendrik Ferreira, Marrigje M. Conradie, Jeanet Conradie

**Publication:** Electrochimica Acta

**Publisher:** Elsevier

**Date:** 1 December 2018

© 2018 Elsevier Ltd. All rights reserved.

Logged in as:  
Hendrik Ferreira

[LOGOUT](#)

Please note that, as the author of this Elsevier article, you retain the right to include it in a thesis or dissertation, provided it is not published commercially. Permission is not required, but please ensure that you reference the journal as the original source. For more information on this and on your other retained rights, please visit: <https://www.elsevier.com/about/our-business/policies/copyright#Author-rights>

[BACK](#)[CLOSE WINDOW](#)

Copyright © 2019 Copyright Clearance Center, Inc. All Rights Reserved. [Privacy statement](#). [Terms and Conditions](#). Comments? We would like to hear from you. E-mail us at [customercare@copyright.com](mailto:customercare@copyright.com)

**A3: Copyright Clearance Center Permission for 'Electrochemical data of Co(II) complexes containing phenanthroline functionalized ligands'.**



RightsLink®

**Creative Commons Attribution License (CC BY)**

This article is available under the terms of the [Creative Commons Attribution License \(CC BY\)](#). You may copy and distribute the article, create extracts, abstracts and new works from the article, alter and revise the article, text or data mine the article and otherwise reuse the article commercially (including reuse and/or resale of the article) without permission from Elsevier. You must give appropriate credit to the original work, together with a link to the formal publication through the relevant DOI and a link to the Creative Commons user license above. You must indicate if any changes are made but not in any way that suggests the licensor endorses you or your use of the work.

Permission is not required for this type of reuse.

CLOSE WINDOW

Copyright © 2019 [Copyright Clearance Center, Inc.](#) All Rights Reserved.  
Comments? We would like to hear from you. E-mail us at [customercare@copyright.com](mailto:customercare@copyright.com)

**A4: Copyright Clearance Center Permission for Electrochemical and electronic properties of a series of substituted polypyridine ligands and their Co(II) complexes'.**



RightsLink®

Home

Account  
Info

Help



**Title:** Electrochemical and electronic properties of a series of substituted polypyridine ligands and their Co(II) complexes  
**Author:** Hendrik Ferreira, Marrigje M. Conradie, Jeanet Conradie

**Publication:** Inorganica Chimica Acta

**Publisher:** Elsevier

**Date:** 24 February 2019

© 2018 Elsevier B.V. All rights reserved.

Logged in as:  
Hendrik Ferreira

LOGOUT

Please note that, as the author of this Elsevier article, you retain the right to include it in a thesis or dissertation, provided it is not published commercially. Permission is not required, but please ensure that you reference the journal as the original source. For more information on this and on your other retained rights, please visit: <https://www.elsevier.com/about/our-business/policies/copyright#Author-rights>

BACK

CLOSE WINDOW

Copyright © 2019 [Copyright Clearance Center, Inc.](#) All Rights Reserved. [Privacy statement](#). [Terms and Conditions](#).  
Comments? We would like to hear from you. E-mail us at [customercare@copyright.com](mailto:customercare@copyright.com)



**A5: Copyright Clearance Center Permission for 'Cyclic voltammetry data of polypyridine ligands and Co(II)-polypyridine complexes'.**



RightsLink®

**Creative Commons Attribution License (CC BY)**

This article is available under the terms of the [Creative Commons Attribution License \(CC BY\)](#). You may copy and distribute the article, create extracts, abstracts and new works from the article, alter and revise the article, text or data mine the article and otherwise reuse the article commercially (including reuse and/or resale of the article) without permission from Elsevier. You must give appropriate credit to the original work, together with a link to the formal publication through the relevant DOI and a link to the Creative Commons user license above. You must indicate if any changes are made but not in any way that suggests the licensor endorses you or your use of the work.

Permission is not required for this type of reuse.

CLOSE WINDOW

Copyright © 2019 [Copyright Clearance Center, Inc.](#) All Rights Reserved.  
Comments? We would like to hear from you. E-mail us at [customercare@copyright.com](mailto:customercare@copyright.com)

**A6: Copyright Clearance Center Permission for 'Electronic properties of Fe charge transfer complexes - A combined experimental and theoretical approach'.**



RightsLink®

Home

Account  
Info

Help



**Title:** Electronic properties of Fe charge transfer complexes – A combined experimental and theoretical approach

**Author:** Hendrik Ferreira, Karel G. von Eschwege, Jeanet Conradie

**Publication:** Electrochimica Acta

**Publisher:** Elsevier

**Date:** 20 October 2016

© 2016 Elsevier Ltd. All rights reserved.

Logged in as:  
Hendrik Ferreira

LOGOUT

Please note that, as the author of this Elsevier article, you retain the right to include it in a thesis or dissertation, provided it is not published commercially. Permission is not required, but please ensure that you reference the journal as the original source. For more information on this and on your other retained rights, please visit: <https://www.elsevier.com/about/our-business/policies/copyright#Author-rights>

BACK

CLOSE WINDOW

Copyright © 2019 [Copyright Clearance Center, Inc.](#) All Rights Reserved. [Privacy statement](#), [Terms and Conditions](#).  
Comments? We would like to hear from you. E-mail us at [customercare@copyright.com](mailto:customercare@copyright.com)